THE ROLE OF RELAXIN IN LEFT VENTRICULAR FIBROSIS: ENDOGENOUS EXPRESSION AND THERAPEUTIC POTENTIAL

by

Jamie Lee Haney

B.S., Bioengineering, University of Pittsburgh, 2008

Submitted to the Graduate Faculty of

Swanson School of Engineering in partial fulfillment

of the requirements for the degree of

Doctor of Philosophy

University of Pittsburgh

2014

ProQuest LLC.
789 East Eisenhower Parkway
P.O. Box 1346
Ann Arbor, MI 48106 - 1346

UNIVERSITY OF PITTSBURGH

SWANSON SCHOOL OF ENGINEERING

This dissertation was presented

by

Jamie Lee Haney

It was defended on

November 11th, 2014

and approved by

Harvey S. Borovetz, Ph.D.
Distinguished Professor and Former Chair, Department of Bioengineering

Charles F. McTiernan, Ph.D.
Research Associate Professor, Department of Medicine

David S. Schwartzman, M.D.
Professor of Clinical and Translational Science, Department of Medicine

Yadong Wang, Ph.D.
William Kepler Whiteford Professor, Department of Bioengineering

Dissertation Director: Sanjeev G. Shroff, Ph.D.
Chair, Distinguished Professor, and Gerald McGinnis Chair, Department of Bioengineering

THE ROLE OF RELAXIN IN LEFT VENTRICULAR FIBROSIS: ENDOGENOUS EXPRESSION AND THERAPEUTIC POTENTIAL

Jamie Lee Haney, Ph.D.

University of Pittsburgh, 2014

Currently, there is a largely unmet need for therapeutic strategies to combat diastolic heart failure. The prevention and reversal of left ventricular (LV) fibrosis, a known contributor to diastolic dysfunction, may provide a solution for this clinical problem. Relaxin, via activation of its primary receptor RXFP-1, blocks collagen synthesis and enhances collagen degradation and thus, is a potent antifibrotic agent. The work presented here tested the hypotheses that the natural relaxin receptor-ligand system is upregulated in the fibrotic LV with diastolic dysfunction and exogenous relaxin administration can reverse LV fibrosis and restore diastolic function.

Several rat models of age- and hypertension-associated LV fibrosis were studied: young versus aged spontaneously hypertensive rats (SHR), normotensive Wistar-Kyoto rats (WKY) versus SHR, and control Sprague-Dawley (SD) rats versus renin overproducing transgenic (MREN) rats. An upregulation of the endogenous relaxin receptor-ligand system determined by quantitative real-time PCR was present in each of the fibrotic animal models, specifically a ~2-4.5 fold increase in mRNA expression of RXFP-1 and a tendency towards increased relaxin expression (~1.5 fold).

In the MREN rat model, this endogenous upregulation of the relaxin receptor-ligand system occurred in parallel with significantly elevated LV mRNA expression of known fibrotic biomarkers (TGFβ, BNP, and MMP2), suggesting an adaptive response. MREN rats also exhibited significant LV hypertrophy, fibrosis, and diastolic dysfunction (increased LV and

myocardial passive stiffness and slowed relaxation), while systolic function was unaltered. Administration of recombinant human relaxin (rhRLX, 0.5 mg/kg/day for 14 days) to MREN rats did not affect hypertension or hypertrophy. However, rhRLX administration significantly reversed mRNAs of fibrotic biomarkers and RXFP-1 and LV fibrosis in MREN rats. These changes were associated with significantly reduced passive stiffness and this beneficial effect was consistent even under the condition of stress (increased heart rate). In contrast, rhRLX administration did not alter LV relaxation.

We conclude that the endogenous LV relaxin receptor-ligand system exerts an adaptive response in a fibrotic environment. The ability of exogenous relaxin administration to reverse LV fibrosis and improve diastolic function may provide a novel strategy for treating diastolic heart failure.

TABLE OF CONTENTS

LIST OF TABLES

LIST OF FIGURES

ACKNOWLEDGEMENTS

I would like to thank my co-advisors, Dr. Sanjeev Shroff and Dr. David Schwartzman for their continued guidance and support throughout the process of this work. Despite all challenges or unexpected circumstances, you have encouraged me to be resourceful and helped me to establish an unwavering perseverance. I particularly appreciate the mentorship from Dr. Shroff as I pursued my professional development – you have always considered my best interests and inspired me to excel. I would also like to express gratitude towards the rest of my committee: Dr. Charlie McTiernan, Dr. Harvey Borovetz, and Dr. Yadong Wang, for their invaluable time and advice while completing this work of which I am very proud.

I owe everything I have learned about the methods and techniques I used to complete this work to my friends in the Cardiovascular Systems Laboratory (past and present): Caroline Evans, Steve Smith, and Jonathan Kirk. It has been an absolute pleasure working with you over the last 6 years and I will always hold you in the highest regard. And thank you to my undergraduate research assistants: Karuna, Casey, Sagar, and Riddhi, who have helped me with my experiments but more importantly, provided a refreshing reminder of the excitement of research.

I would like to thank the people who have helped me with the less glamorous aspects of animal research – Dave Fischer and Judy Thoma who expertly navigated me through everything surgical required for the animal experiments, Dr. Jasmina Varagic and Jessica VonCannon at

Wake Forest University for so generously contributing their time and efforts so that I could use the MREN rat model at Pitt. Above all, thank you to the rats, so many rats.

I would like to acknowledge the sources of funding that have supported me to complete my research and graduate tenure – the Swanson School of Engineering Department of Bioengineering, the McGinnis Chair Endowment, the National Institutes of Health, and the National Science Foundation.

Finally, I want to thank my family and friends who have given me their unconditional love and support. Mom, Jim, Carolyn, James, Alyssa, and Micky – you all make me so happy and proud on a daily basis. They say, "You can't pick your family", but in our case, I am glad that our parents picked each other. I love us. Aunt Annie, whether or not I like to admit it, you have been the driving force behind all of my most-prized academic accomplishments. "Thank you" is an understatement. I appreciate all my friends in Pittsburgh and in Bethlehem who have always bent an ear for me and expressed genuine (?) excitement about the research I was conducting. I especially appreciate Jon for his hugs when I was anxious, his pep talks when I felt defeated, and his unending confidence in me; you helped me reach the finish line.

Finally, I would like to take a moment to appreciate the most loyal and loving cheerleader in my life, my sister Micky. You are never far away when I need you and you always have a way of putting me at ease when I am stressed (sometimes the other way around). You are my best friend and I love you, you have no idea how much you inspire me. I would like to dedicate this work to the memory of our dad, Jim Haney. I hope that my small contributions can make an impact on improving heart disease outcomes for all the other dads out there.

1.0 INTRODUCTION

Heart failure is a serious epidemic affecting 5.1 million people in the United States, half of whom die within 5 years of diagnosis [1]. Heart failure occurs when the left ventricle (LV) is unable to adequately supply oxygenated blood to tissues of the body either by reduced pumping ability (systolic heart failure) or by impaired capacity for filling (diastolic heart failure), or both. The most commonly used determinant of systolic heart failure is reduced ejection fraction (measured by noninvasive echocardiography). However, nearly half of heart failure patients have preserved ejection fraction but severe diastolic dysfunction defined as increased LV passive stiffness and poor ventricular relaxation. This cohort seems to be increasing in number because of aging of the general population and increasing prevalence of pathological precursors to diastolic dysfunction, such as hypertension [2]. Despite therapeutic developments to improve systolic function, there is still a largely unmet need for effective therapy to improve diastolic function [3]. A primary cause of diastolic heart failure is hypertensive heart disease (HHD), which results in significant LV hypertrophy and fibrosis [4, 5]. While clinical evidence has shown that antifibrotic therapies hold the potential for improving diastolic function, there are currently no clinically available treatment options specific to LV fibrosis [6, 7].

1.1 LEFT VENTRICULAR FIBROSIS AND DIASTOLIC DYSFUNCTION

Heart tissue is made up of contractile cardiomyocytes, fibroblasts, vascular structures, and extracellular matrix proteins (primarily collagen) and its material properties and ability to function depend greatly on its compositional environment. The development of LV fibrosis occurs when mature, cross-linked collagen accumulates within the myocardium, causing compositional remodeling of the heart tissue. By mechanisms which remain unclear, the natural process of aging results in the loss of collagen regulation (accelerated synthesis outweighs degradation), and certain pathologies – such as hypertension – exacerbate this response. Hypertension contributes to LV fibrosis through mechanical and chemical mechanisms that ultimately result in diastolic dysfunction.

In response to hypertension, increases in cardiac mechanical work force compositional remodeling. Increased LV wall stress is compensated by an increase in the size of cardiomyocyte contractile units and LV wall thickness to improve contractile function of the LV against the elevated afterload. To prevent ventricular deformation (ie. dilation), collagen production is stimulated by activated fibroblasts to increase the tensile strength of the LV and transmit the contractile force from the cardiomyocytes to the entire ventricle [8]. When the LV is subjected to prolonged cardiac work, these physiological responses to hypertension can develop into pathological hypertrophy and LV fibrosis, the major contributors to diastolic dysfunction.

In addition to its mechanical contributions, hypertension stimulates cardiomyocyte hypertrophy and LV fibrosis through chemical means by inducing a systemic proinflammatory state that has downstream effects on myocardial structure and function. According to a recently proposed paradigm, hypertension (among other comorbidities of heart failure) induces a proinflammatory state that causes inflammation in the perivascular endothelium and reduces the

bioavailability and activity of important myocardial cytokines [9]. Reduced bioavailability of nitric oxide (NO), cyclic guanosine monophosphate (cGMP) content, and protein kinase G (PKG) activity results in cardiomyocyte hypertrophy and stiffness that disrupts their ability to actively relax to an unstressed length and force during diastole [8, 10]. Additionally, inflammatory cells and ventricular fibroblasts are known to release the profibrotic cytokine, transforming growth factor-beta (TGFβ), which activates the transition of fibroblasts to their high collagen-yielding myofibroblast form, upregulates the gene encoding for collagen production, and facilitates the cross-linking between mature collagen fibers, further driving LV fibrosis [11]. Mechanisms are naturally in place for collagen degradation where proteinases called MMPs break apart the collagen network and degrade the collagen fibers. This system is highly regulated and includes multiple MMPs with specific roles and inhibitors to the MMPs called TIMPs. In a fibrotic environment, however, collagen regulation is off balance in favor of collagen synthesis, mostly involving pathways downstream of TGFβ.

Together, LV fibrosis and structural and functional changes to cardiomyocytes lead to increased passive stiffness and impaired LV relaxation, which are hallmark of diastolic dysfunction. An overabundance of myocardial collagen and increased cross-linking between fibers has detrimental effects on LV passive stiffness properties that affect the end-diastolic pressure-volume relationship (EDPVR) [10]. In a hypertensive and fibrotic environment, molecular mechanisms are at play that act on cardiomyocyte cellular mechanics to delay active relaxation, and this is especially apparent at higher heart rates where the cardiac cycle time is shortened. By the mechanisms described here, it appears that blocking collagen production downstream of TGFβ and returning NO to the system may be most beneficial for preventing and reversing diastolic dysfunction. The active and passive components of diastolic dysfunction have

been studied in several animal models of hypertension and LV fibrosis to elucidate potential targets for therapeutic intervention.

1.1.1 Animal Models of Diastolic Dysfunction

The heterozygous transgenic (mREN2)27 rat (MREN), which exhibits an overactive renin-angiotensin system (RAS), is a model of severe hypertension and LV hypertrophy that has been shown to develop LV fibrosis as early as 8 weeks of age [12, 13]. The MREN model was created in 1990 by Mullins *et al.* by introducing the mouse REN-2 gene into the germline of normotensive Sprague-Dawley (SD) rats [12]. The overexpression of renin in this model drives the production of angiotensin-II (ATII) by the activated RAS, which results in LV hypertrophy and hypertension through vasoconstriction, fluid retention, and facilitation of catecholamine release [14]. Furthermore, diastolic dysfunction has been identified in this model compared to its species-background SD control as early as 12 weeks of age.

A long-standing and widely utilized animal model of hypertension, the spontaneously hypertensive rat (SHR), has been bred for a predisposition to hypertension. In this model, hypertension (defined as systolic blood pressures > 150 mmHg) develops after 14 weeks of age and, similar to human hypertension, develops more rapidly and severely in males [15]. As in diastolic heart failure, normal cardiac output is maintained in these animals presumably due to a compensated hypertrophic response that increases cardiac contractility [16, 17]. Compared to normotensive Wistar-Kyoto (WKY) control rats, adult SHR (~12 months of age) manifest diastolic dysfunction as impaired active relaxation as well as increased passive stiffness [17] which worsens as heart failure develops after 18 months of age [18]. The SHR model has been a major source of information for HHD and heart failure pathophysiology, but a common criticism

is the indeterminate origin of their hypertension and the advanced age required to manifest heart failure conditions. Particularly, comparing SHR to outbred normotensive WKY controls results in a wide variation in disease effects secondary to hypertension [19].

1.2 RELAXIN

An emerging player in diastolic heart failure research and antifibrotic collagen regulation is the naturally occurring peptide hormone relaxin [3, 20, 21]. Relaxin, once known as a pregnancy hormone, has shown promise as an antifibrotic hormone in multiple organ systems in both males and females [22-26]. Humans express three isoforms of relaxin: H1 and H2 relaxin have historically been associated with reproductive physiology while the gene for H3 relaxin has been localized to the brain and testis [27, 28]. In 2001, a study using human failing heart tissue showed that circulating serum levels as well as myocardial gene expression of H2 relaxin was significantly elevated, suggesting an involvement of the relaxin system in a situation of cardiac distress [29].

Rodents express two homologs of the three known human relaxin genes corresponding to H2 and H3 and termed relaxin-1 (Rln1) and relaxin-3 (Rln3), respectively. Relaxin-1 and relaxin-3 ligands bind with their primary G-protein coupled membrane receptor, RXFP-1, in multiple cell types leading to the stimulation of several downstream antifibrotic signaling pathways [30]. Mice lacking the Rln1 gene (Rln-/-) have demonstrated an age-dependent increase in lung [31], renal [32], and LV fibrosis [33]. *Du, et al.* provided evidence that relaxin-1 deficiency results in elevated myocardial collagen accumulation and impaired diastolic filling [33]. In rat ventricular fibroblasts, relaxin receptor-ligand binding has been associated with a reduction in profibrotic

cytokine release, inhibition of fibroblast to myofibroblast transformation, increases in expression and activity of collagen-degrading matrix metalloproteinases (MMPs) and decreases in expression of tissue inhibitors to MMPs (TIMPs), among other antifibrotic actions that control collagen turnover [23]. These studies support the necessity for a functioning endogenous relaxin receptor-ligand system as a regulator of collagen turnover and proper LV diastolic function.

1.3 MYOCARDIAL COLLAGEN REGULATION: A ROLE FOR RELAXIN

Several *in vitro* and *in vivo* studies have been reviewed which provide insight regarding the antifibrotic cellular mechanisms associated with relaxin [20, 27, 30, 34]. It has been postulated that relaxin ligands interact with RXFP-1 to antagonize fibrotic pathways by both inhibiting collagen synthesis and stimulating collagen degradation. The major contributor to fibrotic collagen accumulation is the transition of cardiac fibroblasts to their myofibroblast form that is facilitated by the cytokine TGFβ and its downstream Smad signaling cascade. The antifibrotic interference of relaxin receptor-ligand binding on this myofibroblast differentiation has been confirmed in several cell types and linked to simultaneous pathways in which collagen is degraded by activated MMPs [20].

In an early pioneer study by Samuel *et al*., rat ventricular fibroblasts were found to elicit a temporary and biphasic rise in cAMP upon relaxin stimulation [23] and since, this cAMP-mediated pathway has been the most extensively investigated for RXFP-1 signaling [34]. It has been reviewed that the initial phase of the biphasic cAMP accumulation observed upon receptor stimulation is a combination of GαS-mediated cAMP accumulation and $G\alpha_{OB}$-mediated cAMP inhibition. The second phase then occurs, involving downstream Gβγ, released from recruited

$G\alpha_{i3}$ proteins, to stimulate phosphatidylinositol 3 kinase (PI3K) and protein kinase C (PKC) activation [30]. Activated PKC is capable of translocating to the membrane of cardiac fibroblasts to activate adenylate cyclase (AC), which produces the second phase of cAMP accumulation. The primary effector of intracellular cAMP is activated protein kinase A (PKA), which phosphorylates signaling proteins involved with various gene transcription mechanisms including those related to fibrosis.

The MAPK pathway is another pathway activated by RXFP-1. In rat renal myofibroblasts there is a rapid and sustained increase in ERK1/2 phosphorylation that is associated with the anti-apoptotic action of relaxin in rat cardiomyocytes [35, 36]. Relaxin binding to RXFP-1 has also been associated with two other possible pathways that lead to increased nitric oxide (NO) synthesis [30, 36]. In one pathway, Akt is stimulated by activated PI3K and intracellular NO is produced by activated endothelial NO synthase (eNOS). In another, activated PKA can block gene transcription of NOSII which upregulates the inhibitor of NO synthase (iNOS) via nuclear transcription factors (IκB, NFκB) [37]. The importance of NO production in response to activated RXFP-1 was originally associated strictly with relaxin's known vasodilatory action but has since been implicated in the differentiation of renal myofibroblasts [36] and the upregulation of matrix metalloproteinases [38]. The work by Mookerjee *et al.* provided evidence that NO is involved in the nNOS–NO–cGMP pathway, which results in the inhibition of Smad2 phosphorylation and nuclear translocation (by formation of the Smad2/3 complex) that is necessary for TGFβ signaling. This in turn inhibits the TGFβ-mediated transition of cardiac fibroblasts to myofibroblasts and stunts collagen production. In 2012, Ahmad *et al.* showed that increased NO production may also drive the collagen degradation pathway by upregulation of

MMP-9 through the P13K, ERK1/2, and Akt pathways [39]. These collective findings were mapped out by Bathgate *et al.* and illustrated in **Figure 1**.

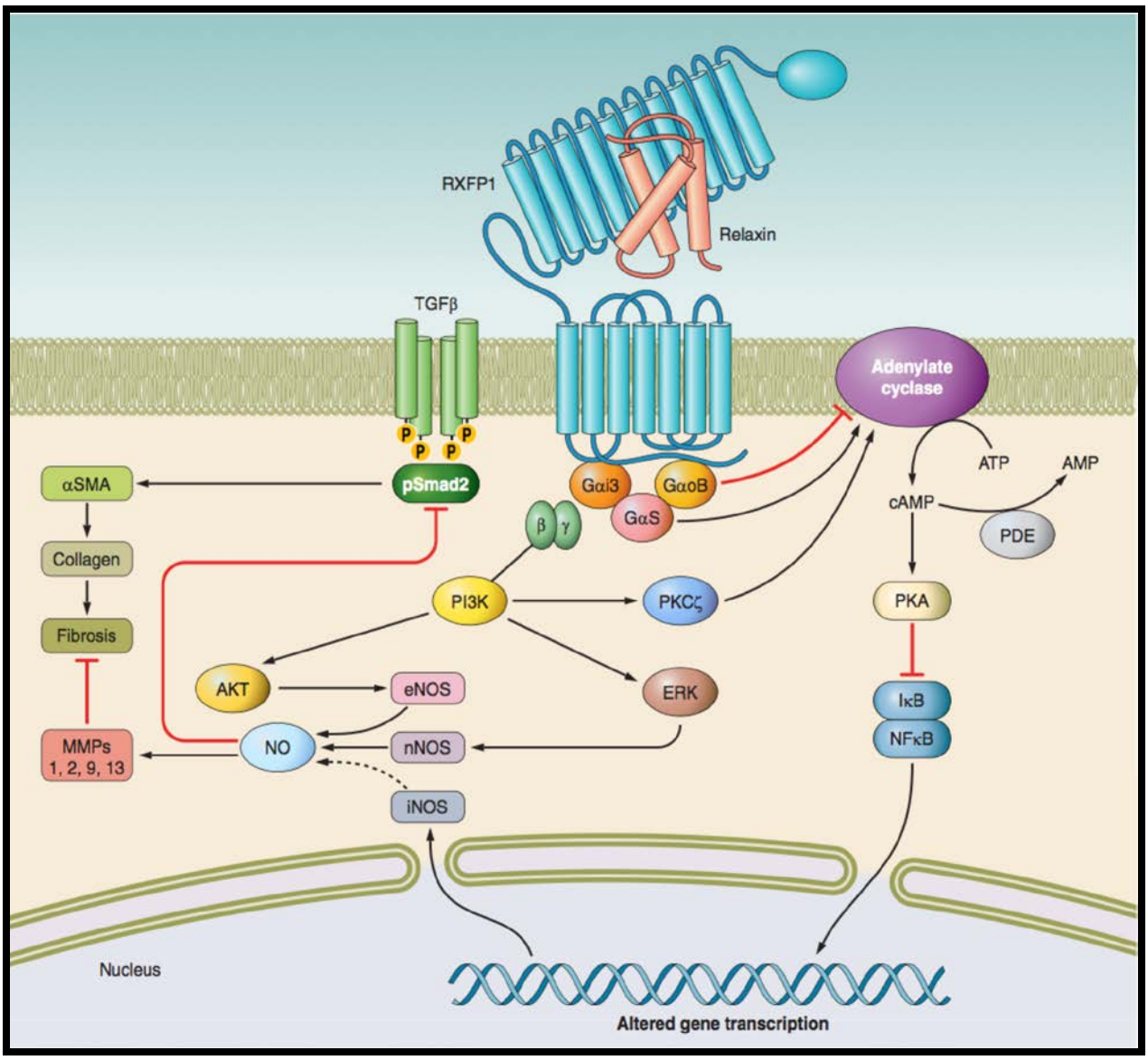

Figure 1. Antifibrotic pathways of relaxin [27]

1.4 EXOGENOUS RELAXIN AS AN ANTIFIBROTIC THERAPY

Recent suggestions that the endogenous relaxin receptor-ligand system behaves in a way to regulate collagen and reduce fibrosis targets this hormone as a potential therapy [40]. Administration of recombinant human relaxin (rhRLX) via osmotic minipump for 14 days reverses established LV fibrosis in several models of hypertension and heart failure, including SHR [41], transgenic MREN rats with experimental diabetes [42], mice overexpressing β2-adrenergic receptors (β2-TG) and hence developing fibrotic cardiomyopathy [23], and relaxin-1 deficient mice (Rln−/−) mice [23].

At the cellular level, it has been established *in vitro* that rat atrial and ventricular fibroblasts, which express the RXFP-1 receptor, show a reduced fibrotic phenotype in response to administration of rhRLX [23]. In this study, Samuel, *et al.* stimulated plated fibroblasts with profibrotic factors (TGFβ or ATII) and observed the expected transition of the fibroblasts to myofibroblasts accompanied by increased collagen synthesis and accumulation. When exogenous relaxin was added to the medium, the fibrotic phenotype was reversed; fibroblast proliferation and differentiation was reduced, collagen overexpression was decreased, and MMP expression was elevated. Additionally, a study by Hossain, *et al.* suggests that relaxin-3 may enhance the antifibrotic effects of exogenous relaxin through its action on the RXFP-1 receptor in rat ventricular fibroblasts [43]. Evidence from these *in vitro* studies confirm that the collagen regulation effect of exogenous relaxin administration involves both a decrease in collagen synthesis as well as an increase in degradation, but specifics surrounding this mechanism remain unclear.

When the antifibrotic potential of exogenous relaxin was tested at the cardiac tissue and whole animal levels of organization, true therapeutic potential became evident. Lekgabe, *et al.*

showed that excessive LV interstitial collagen deposition was reversed in adult SHR that had received 14 days of rhRLX administration [41]. Evidence is often incomplete or not available regarding effects of exogenous relaxin administration on functional outcomes in the LV relating to reduced active relaxation or passive stiffness. **Table 1** was adapted from Du, *et al.* as a review of the major findings and research gaps in recent exogenous relaxin administration studies [40].

Table 1. Functional effects of rhRLX administration in models of HHD and LV fibrosis

Model	**Fibrosis**	**Functional outcome(s)**	**Reference**
Isoproterenol-induced cardiac injury (rats)	Reduced	Improved ventricular contractility and lowered LV end-diastolic pressure	[44]
Myocardial infarction (mice)	Reduced scar density	Unchanged	Samuel CS, *et al.,* unpublished data
Fibrotic cardiomyopathy (β2-TG mice)	Reduced	Not determined	[23]
SHR (9 months old)	Reduced	Unchanged	[41]
SHR (18 months old)	Unchanged	Unchanged	Xu Q, *et al.,* unpublished data
Rln-/- mice	Reduced	Not determined	[23]
Diabetic MREN rats	Reduced	Partially improved LV diastolic function by echocardiography	[42]

Despite promising *in vitro* and *in vivo* evidence that rhRLX administration can prevent and reverse fibrotic collagen accumulation in established models of hypertension and LV fibrosis, there is a general lack of information towards relaxin's therapeutic potential to restore diastolic function in these models.

2.0 HYPOTHESES

The current understanding that relaxin binding and activating its primary receptor RXFP-1 has downstream effects to block collagen synthesis and stimulate collagen degradation suggests an antifibrotic mechanism for the endogenous relaxin receptor-ligand system. We postulate that this system is naturally adaptive in animal models of hypertension and aging with established LV fibrosis and diastolic dysfunction. Furthermore, we propose that exogenous administration of recombinant human relaxin (rhRLX) will therapeutically reverse established LV fibrosis and improve diastolic function. Based on these postulates, we developed the following specific aims to determine the role of relaxin in LV fibrosis and diastolic dysfunction focusing on endogenous expression of the relaxin receptor-ligand system and therapeutic effects of exogenous rhRLX administration.

3.0 SPECIFIC AIMS

Hypothesis 1. Endogenous relaxin receptor-ligand system expression is upregulated with LV fibrosis in animal models of hypertension and aging.

Specific Aim 1A. To quantify the mRNA expression of relaxin message (relaxin-1 and relaxin-3) and receptor (RXFP-1) in LV tissue from two rat models of hypertension-associated LV fibrosis: Transgenic MREN *vs.* normotensive SD controls and aged SHR *vs.* aged, normotensive WKY controls.

Specific Aim 1B. To quantify the mRNA expression of relaxin message (relaxin-1 and relaxin-3) and receptor (RXFP-1) in LV tissue from young SHR compared to aged SHR as a model of age-associated LV fibrosis.

Hypothesis 2. Exogenous administration of recombinant human relaxin (rhRLX) can inhibit and reverse LV fibrosis and restore diastolic function in hypertensive rats.

Specific Aim 2. To determine the effect of exogenous relaxin administration on established LV fibrosis and diastolic dysfunction in transgenic MREN rats compared to normotensive SD controls.

4.0 MATERIALS AND METHODS

4.1 ENDOGENOUS RELAXIN RECEPTOR-LIGAND EXPRESSION IN AN ENVIRONMENT OF FIBROSIS

Gene-level expression of endogenous relaxin peptides was measured by quantitative real-time PCR (qPCR). By this two-step method, LV tissue is purified to total RNA and reverse transcribed to complimentary DNA (cDNA) that is used as template material for amplification and quantification of genes of interest (GOI). For **Aims 1A and 1B**, gene expression of relaxin peptides from experimental fibrosis groups is expressed relative to healthy controls. The procedure for qPCR is also used for **Aim 2** where gene expression of fibrotic biomarkers from experimental treatment groups is expressed relative to healthy controls.

4.1.1 Animals

To understand the effects of aging and disease on the endogenous expression of relaxin peptides, three experimental models of hypertension- and aging-associated LV fibrosis were used and compared to their respective healthy controls. Pilot studies conducted in our lab demonstrated that gene expression of a known profibrotic biomarker (TGFβ) was significantly increased in hypertensive SHR compared with healthy WKY controls; we used the results of this study to determine the statistical power and sample size required for the following experiments. From this

pilot study, we determined that an effect size of 1.882 was reasonably likely to predict a difference in a sample of 16 (n=8 animals/group) when the difference exists in the population to 80% certainty. Based on this finding and in anticipation of pre-completion mortality rate within group of 20%, at least 6 rats per group was reasonable to support detection of significant differences at a *P*-value of 0.05.For hypertension-associated fibrosis, the mRen2(27) transgenic rat model (MREN, n=13) aged ~4 months was compared to species-background, age-matched Sprague-Dawley controls (SD, n=6). As a second model of hypertension-associated fibrosis, aged SHR (~12 months, n=11) were compared to sex- and age-matched, normotensive Wistar-Kyoto (WKY, n=9) controls. Young SHR (~4 months, n=8) were also compared to aged SHR as a model of age-associated fibrosis. All animals used in the study were male. Transgenic MREN rats were provided by Dr. Jasmina Varagic and the Hypertension and Vascular Research Center at Wake Forest University (Winston-Salem, NC), all other species were purchased from Charles River Laboratories (Wilmington, MA).

4.1.2 Isolation of Left Ventricular Total RNA

Total RNA was purified from frozen LV tissue using the miRNeasy Mini Kit (Qiagen, Inc., Valencia, CA). Briefly, 50 mg of tissue was isolated from frozen, basal LV cross-sections and submerged in lysis buffer (phenol/guanidine-based) and subjected to mechanical disruption with a Tissue Tearor homogenizer (BioSpec, Bartlesville, OK). Homogenized tissue lysate was centrifuged and the aqueous, RNA-containing partition was applied to an RNeasy Mini Spin Column where RNA binds to the membrane and other contaminants are washed away and discarded. After multiple washing steps, the total RNA was eluted with 50 µl of RNase-free water and the concentration was quantified using a spectrophotometer.

The total RNA eluent for each sample was diluted 1:20 in RNase-free water and absorbance at 260 nm wavelength (A_{260}) was measured using a Visible Spectrophotometer (Cole Parmer, Vernon Hills, IL). Wavelength correction was performed at 280 nm (A_{280}) and all samples were adjusted by a blank sample absorbance containing RNase-free water alone. To insure that the nucleic acid preparation was sufficiently free from protein contamination, all samples were required to satisfy $A_{260} > 0.15$ and RNA purity (A_{260} /A_{280}) > 1.8. These measurements were based on the report by Glasel *et al.* which describes that ratio values lower than 1.8 indicate the presence of protein, phenol, or other contaminants that absorb strongly near 280 nm [45]. Total RNA absorbance was converted to concentration by the equation: A_{260} reading of 1 = 44 μg/ml RNA based on the miRNeasy Handbook. Total RNA obtained by this method was used as template material for reverse transcription to cDNA used for qPCR experiments in **Aims 1A, 1B, and Aim 2**.

4.1.3 Reverse Transcription of RNA to Complimentary DNA

To prepare single-stranded cDNA suitable for qPCR experiments, the High Capacity Reverse Transcription cDNA Kit (Applied Biosystems Inc., Carlesbad, CA) was used. Based on the calculation of total RNA concentration explained in **Section 4.1.2**, a starting volume of RNA that corresponded to 1 μg was mixed with reverse transcription (RT) reaction master mix for a total volume of 20 μl. The components that made up the RT reaction master mix included: 10X RT Buffer, 10X RT Random Primers (to bind across the length of the RNA being transcribed), 25X dNTP Mix (containing 4 nucleotides: dATP, dCTP, dGTP, and dTTP), Multiscribe Reverse Transcriptase (a DNA polymerase), and RNase Inhibitor. The RT reaction was prepared in MicroAmp Fast Reaction Tubes (Applied Biosystems Inc., Carlesbad, CA) for thermal cycling

and long-term storage at -20°C. Each sample reaction went through thermal cycling in the PCRSprint Thermal Cycler (Cole Parmer, Vernon Hills, IL). The 4-step thermal cycling program included 10 min at 25°C, 120 min at 37°C, 5 sec at 85°C, and a final holding stage at 4°C.

4.1.4 Quantitative Real-Time PCR

The fundamental chemistry of real-time qPCR includes the repeat heating and cooling of DNA template material in the presence of gene-specific primers and DNA polymerase to produce double-stranded DNA (amplicons) that can be detected by fluorescent dye. With each heating and cooling cycle, the amount of template that incudes the gene of interest, and hence the fluorescent tag, is doubled and can be quantified in real-time.

To amplify and detect select gene targets, qPCR was performed using single-stranded cDNA templates created following the procedure in **Section 4.1.3**, SYBR Green Master Mix (Applied Biosystems Inc., Carlesbad, CA), and gene-specific Quantitect Primer Assays (Qiagen, Inc., Valencia, CA) for each gene of interest. The SYBR Green Master Mix contained SYBR GreenER dye which detects double-stranded DNA amplicon, AmpliTaq Gold DNA Polymerase, dNTP nucleotides including dUTP, and ROX passive reference dye. Quantitect Primer Assays including both forward and reverse primers for endogenous rat relaxin (relaxin-1, relaxin-3, and RXFP-1) and endogenous reference control gene (GAPDH) were used to make working qPCR mixes based on the experiments required for **Aims 1A, 1B, and Aim 2**. Detailed information regarding these primer assays can be seen in **Table 2.** All qPCR experiments were prepared in duplicate on MicroAmp Fast Optical 96-well Reaction Plates (Applied Biosystems Inc., Carlesbad, CA) and underwent 40 cycles of PCR cycling and optical LED recording using the StepOnePlus Real-Time PCR System (Applied Biosystems Inc., Carlesbad, CA).

Table 2. Gene-specific endogenous relaxin primer assays for qPCR experiments

qPCR Target	Gene of Interest	Animal	GenBank ID	Base Pairs	Amplicon Length	Dye Label	Qiagen Catalog Number
Endogenous control	GAPDH	Rat	NM_017008	1306	149 bp	SYBR	QT00199633
Relaxin-1	Rln1	Rat	NM_013413	800	101 bp	SYBR	QT00381444
Relaxin-3	Rln3	Rat	NM_170667	470	137 bp	SYBR	QT01796298
Relaxin receptor	Rxfp1	Rat	NM_201417	2277	94 bp	SYBR	QT00448371

The output from the real-time qPCR for each sample is the cycle number at which the SYBR fluorescence crosses a pre-defined threshold (C_T). To ensure that PCR results reflected the amplification of gene template and not artifact, we required that C_T values from usable data be less than 35 (i.e. gene amplification after cycles 35-40 was attributed to artifact). Results for each gene of interest (GOI) were normalized by the endogenous reference gene GAPDH ($\Delta C_T = C_{T,GOI} - C_{T,GAPDH}$) to correct for variations in starting template between samples. The comparative C_T method was used to express experimental data as fold change relative to healthy controls ($2^{-\Delta\Delta CT}$). The comparative C_T method comes from a derivation of the equation for exponential amplification by PCR and makes several assumptions, including that the efficiency of the PCR is close to 1 and the PCR efficiency of the target gene is similar to the endogenous control gene GAPDH [46]. To check that results from qPCR meet these assumptions, morphology of amplification plots and melting temperature curves were validated qualitatively.

4.2 ASSESSMENT OF LV FIBROSIS AND DIASTOLIC DYSFUNCTION IN RELAXIN-TREATED RATS

The MREN rat model is an established model of LV fibrosis at ~4 months age. To satisfy **Aim 2**, fibrosis in this model was measured at all levels of organization – from gene-level expression of profibrotic biomarkers, to tissue-level collagen area within the myocardium, to the whole-heart translation of fibrosis as diastolic dysfunction. To study the treatment effects of exogenous relaxin on established LV fibrosis, rhRLX was administered to the fibrotic MREN rat model and the degree of LV fibrosis and diastolic dysfunction was compared to vehicle-treated MREN rats as well as non-treated normotensive SD controls.

4.2.1 Animals

Male, transgenic MREN rats aged ~15 weeks were divided into two treatment groups: rhRLX-treated MREN (MREN-R, n=6-7) and VEH-treated MREN (MREN-V, n=5-12). Age-matched Sprague-Dawley rats were used as healthy controls (SD, n=6). Based on the analysis of power and sample size explained in **Section 4.1.1**, and in anticipation of pre-completion mortality rate within group of 20%, at least 6 rats per group was reasonable to support detection of significant differences at a *P*-value of 0.05.

4.2.2 Administration of Recombinant Human Relaxin (rhRLX)

At 15-16 weeks of age, animals were briefly anesthetized with isofluorane in preparation for subcutaneous minipump implantation surgery. Under sterile conditions, osmotic minipumps

(ALZET model 2ML2, Durect Corporation) containing either rhRLX (Novartis, Cambridge, MA) or VEH (20 mM sodium acetate, pH 5.0) were implanted subcutaneously in the peritoneal cavity. The 2ML2 osmotic minipumps were designed to administer drug-containing solution at an uninterrupted rate of 0.5 mg/kg/d for 14 days. Prior to implantation, the minipumps were primed for ~1 hour in sterile saline and weighed to ensure complete filling. At completion of treatment duration, the minipumps were removed from the animal, weighed, and aspirated for remaining solution. For all animals, <0.4 ml of solution remained in the minipump at the end of the treatment duration. To ensure proper administration of exogenous relaxin, circulating serum concentration of rhRLX was quantified by Quantikine rhRLX ELISA Assay (R&D Systems, Minneapolis, MN).

4.2.3 Experimental Design Overview

Upon completion of the treatment period, all animals underwent the same experimental protocol. First, body weights were recorded and blood pressures were taken by non-invasive tail blood pressure cuff. Animals were then euthanized and hearts were removed for functional testing by the isolated perfused heart method. After completion of functional trials (explained in **Section 4.2.7**), hearts were removed from the apparatus, left and right ventricles were separated and weighed, and LV cross-sections were prepared for subsequent histological and molecular testing.

4.2.4 Gene-Level Expression of Fibrosis

Basal LV cross-sections were fresh frozen in liquid nitrogen and stored at -80°C until processed for total RNA as described in **Section 4.1.2**. Total RNA was reverse transcribed to cDNA as

described in **Section 4.1.3**. Real-time qPCR was performed as described in **Section 4.1.4** using Quantitect Primer Assays (Qiagen, Valencia, CA) specific for fibrotic biomarker genes: transforming growth factor-beta (TGFβ), brain natriuretic peptide (BNP), and matrix-metalloproteinases (MMP2 and MMP9). Detailed information regarding these primer assays can be seen in **Table 3.**

Table 3. Gene-specific fibrotic biomarker primer assays qPCR experiments

qPCR Target	Gene of Interest	Animal	GenBank ID	Base Pairs	Amplicon Length	Dye Label	Qiagen Catalog Number
Endogenous control	GAPDH	Rat	NM_017008	1306	149 bp	SYBR	QT00199633
TGFβ-1	TGFβ	Rat	NM_021578	1482	145 bp	SYBR	QT00187796
BNP	BNP	Rat	NM_031545	628	94 bp	SYBR	QT00183225
MMP2	MMP2	Rat	NM_031054	3053	103 bp	SYBR	QT00996254
MMP9	MMP9	Rat	NM_031055	2986	149 bp	SYBR	QT00178290

As described in **Section 4.1.4**, the comparative C_T method was utilized to express the level of fibrotic mRNA expression in treatment groups (MREN-V and MREN-R) relative to non-treated healthy controls (SD).

4.2.5 Protein-Level Expression of Fibrosis

Interstitial and perivascular collagen content was measured by picrosirius red staining (PSR). When dissolved in saturated picric acid, sirius red dye aligns itself with collagen fibers and provides a visual, quantifiable distribution of collagen in tissue [47]. Combining brightfield microscopy (**Section 4.2.5.3**) and computational image analysis (**Section 4.2.5.4**), the amount

and spatial distribution of stained myocardial collagen was quantified for experimental groups (MREN-V and MREN-R) and compared to SD controls.

4.2.5.1 Left Ventricular Cross-Sections Apical cross-sections isolated from LV samples were fixed in 10% neutral buffered formalin for >48 hours. Tissue samples were embedded in paraffin blocks, cut into 6 μm sections, and plated on charged microscope slides for histological staining.

4.2.5.2 Picrosirius Red Staining The protocol for PSR staining of LV was adapted from that used by Dr. Joseph Janicki at the University of South Carolina; the detailed protocol can be found in **Appendix D**. Before staining, tissue slides were deparaffined and rehydrated along a decreasing ethanol gradient. Phosphomolybdic acid, 0.2% (PMA) was used as a background treatment to remove cytoplasmic staining to increase collagen-to-tissue contrast. Next, slides were submerged for 60 minutes in 0.1% PSR solution containing Sirius red dye (Direct Red 80, Sigma Aldrich, St. Louis, MO) in saturated picric acid. The dye was washed from the slides with hydrochloric acid (HCl), dehydrated along an ascending ethanol gradient, cleared with xylenes, and mounted with a glass coverslip.

4.2.5.3 Brightfield Microscopy Stained tissue slides were imaged on the Olympus Provis AX70 brightfield microscope (Olympus Center Valley, PA) in the University of Pittsburgh Center for Biological Imaging Lab. For each slide, one representative image was taken by a blinded operator at 10X magnification for the endocardium to mid-myocardium region as well as the mid-myocardium to epicardium region. For perivascular images, a representative ventricular

arteriole was chosen and focused at 20X. All images were manually focused, and set to the same exposure time and level of transmitted light.

4.2.5.4 Image Processing and Analysis Images were saved as .tif files and imported into a custom analysis program written in MATLAB (**Appendix F.1**). Briefly, the program processed the RGB images by separating out the green-filtered image which showed the highest contrast between collagen and tissue staining. Background correction to remove non-tissue regions (i.e. white space) was performed by thresholding. The corrected, green-filtered image was inverted so that all stained collagen appeared white across a varying dark gray – black background (**Figure 2**). A graphic-user interface was developed which prompted the blinded user to manually select three regions of positive collagen stain. The three selected intensity values were averaged (we required that the standard deviation between intensities <15%) and used as the threshold for collagen staining. All pixels greater than or equal to this threshold were counted and saved. A visual representation of the final collagen count was displayed to the user as a quality check. This method was used for all interstitial and perivascular collagen quantification. To determine the tissue area, ImageJ software (NIH, Bethesda, MD) was used which includes a powerful color thresholding tool [48]. Original images were sharpened and contrast was enhanced so that tissue could be computationally differentiated from background. The color thresholding slider was used to manually determine and save the amount of tissue positive pixels (**Figure 2C-D**). For calculating the collagen:total tissue area ratio, the number of pixels of positive collagen determined from MATLAB (**Figure 2E-F**) was divided by the number of pixels of tissue determined by ImageJ.

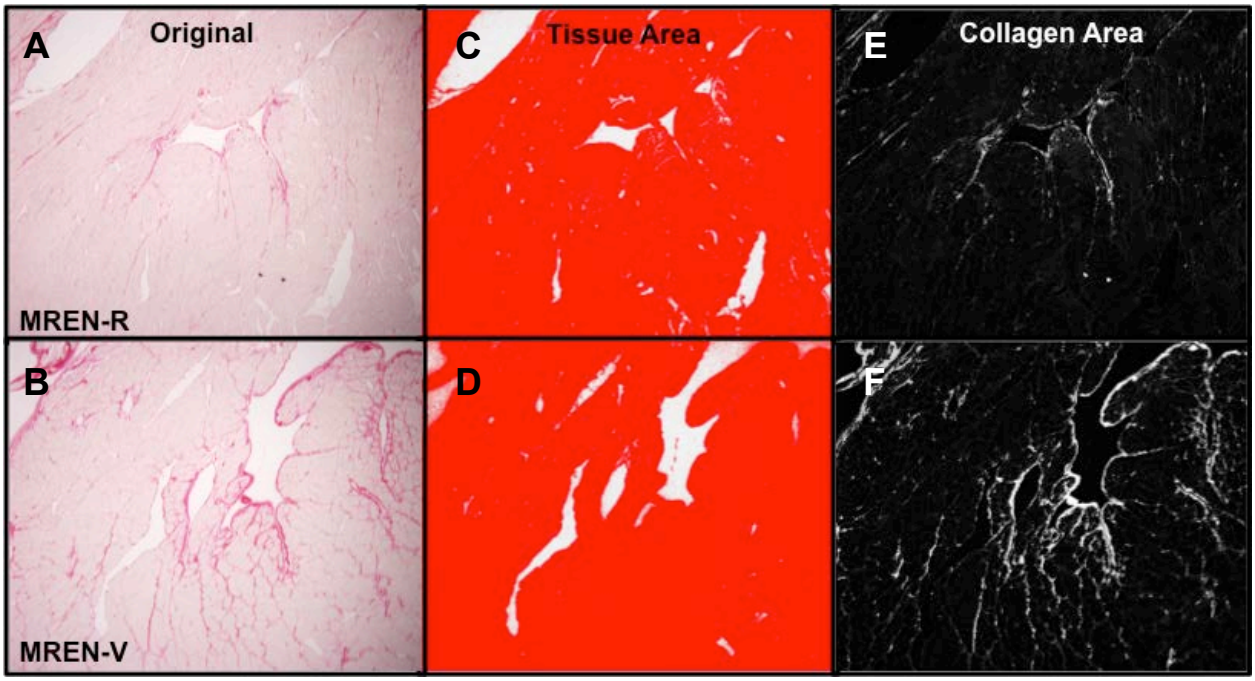

Figure 2. Image processing for collagen:total tissue area ratio calculation

Sample output from each phase of the computational quantification of tissue and interstitial collagen area in picrosirius red stained LV cross sections. Representations of the original image for MREN-R and MREN-V are shown in panels A and B, respectively. Panels C and D demonstrate the procedure for quantifying total tissue area by thresholding in ImageJ. Panels E and F represent the collagen area (white) which was determined by the custom MATLAB algorithm explained in previously.

To determine the lumen area of a given arteriole, the original image was opened with ImageJ and processed similarly as the interstitial images explained above. The freehand draw tool was used to trace the innermost luminal wall and the area of the trace was recorded (**Figure 3C-D**). For determining the collagen:lumen area ratio, the number of pixels of positive collagen determined from MATLAB (**Figure 3E-F**) was divided by the number of pixels of lumen area determined by ImageJ.

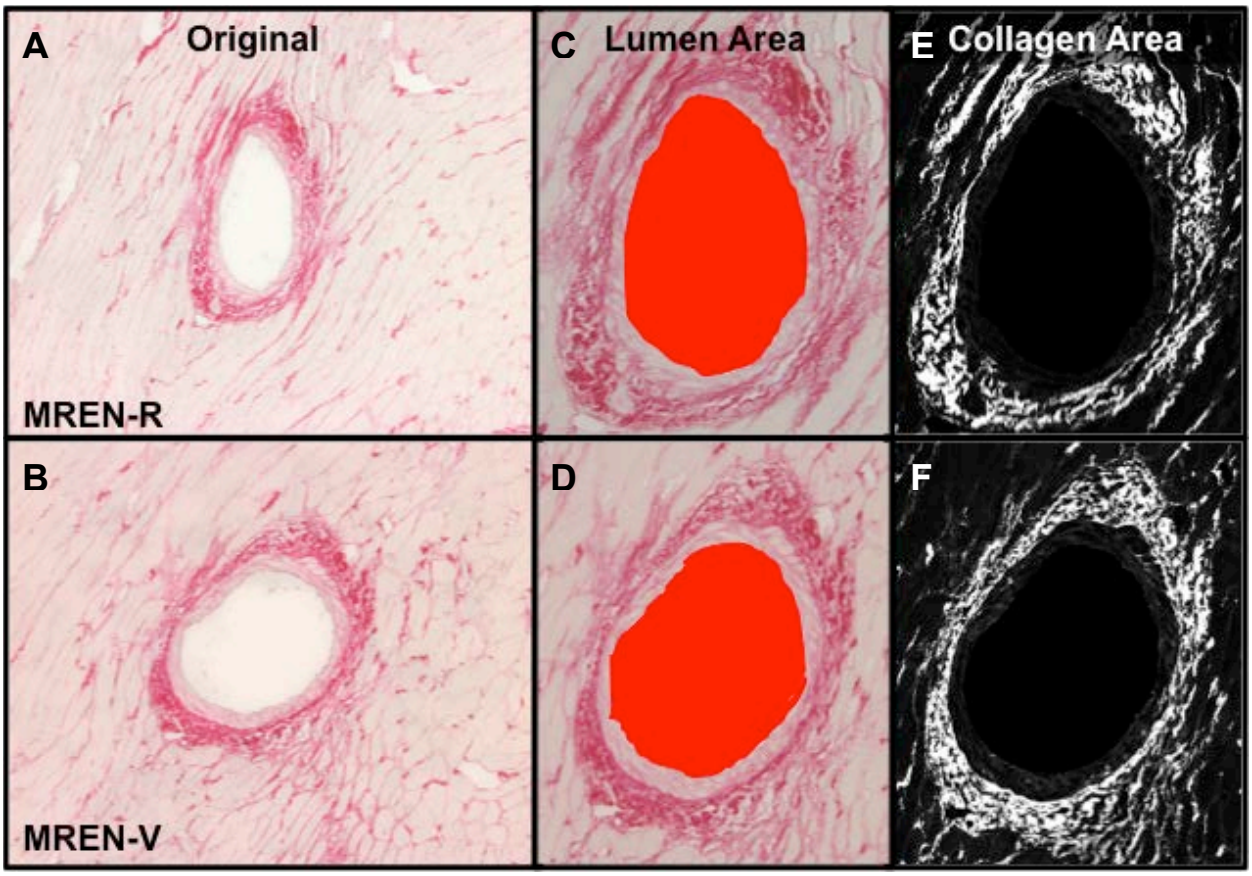

Figure 3. Image processing for perivascular collagen:lumen area ratio calculation

Sample output from each phase of the computational quantification of lumen and perivascular collagen area in picrosirius red stained LV cross sections. Representations of the original image for MREN-R and MREN-V are shown in panels A and B, respectively. Panels C and D demonstrate the procedure for quantifying lumen area (red) manually in ImageJ. Panels E and F represent the collagen area (white) which was determined by the custom MATLAB algorithm explained in previously.

4.2.6 Non-Invasive Blood Pressure Measurement

After the treatment period, awake animals were contained in a holding tube while repeat measurements of tail blood pressure were recorded on the CODA non-invasive blood pressure system (Kent Scientific, Torrington, CT). As part of the CODA system, an occlusion cuff was placed on the tail to occlude blood flow up to 250 mmHg while a distal differential pressure

transducer called the Volume Pressure Recording (VPR) sensor measured diastolic and systolic pressures as well as heart rate [49]. The occlusion cuff (OCC-L) and VPR sensor (VPR-L) underwent diagnostic testing before each experiment by pressure-hold testing with an allowable tolerance of <5% deviations in pressure over the length of the test. For each study pressure recording experiment, animals were maintained between 35-38°C by a heated stage and 10 acclimation cycles were conducted before data was recorded for use. At least 5 occlusion cycles were used for calculations of average diastolic, systolic, and mean pressure and heart rate for each animal.

4.2.7 Whole Heart-level Measurement of LV Function

The isolated perfused heart preparation, evolved from the technique originally described by Langendorff in 1898, is still a very powerful approach to measuring ventricular function [50]. By this method, the intact heart may remain viable outside of the circulation by retrograde perfusion through the coronary arteries so that *ex vivo* experimentation may be performed under highly controlled and repeatable conditions. A major advantage of this method is the ability to observe mechanical and material properties of the heart independent of influences from other organ systems, systemic circulation, or interferences from the central or autonomic nervous system. In our application, the relationship between volume step perturbations and simultaneous measurement of LV pressure provides the information necessary to determine the functional diastolic properties of active relaxation and passive stiffness.

4.2.7.1 Animal Preparation Following non-invasive blood pressure measurement, animals were anesthetized with an intraperitoneal injection of Euthasol (250 mg/kg, Henry-

Schein, Dublin, OH). Animals were then anticoagulated using 100 units of heparin, delivered via intramuscular injection, and the heart was excised by thoracotomy.

4.2.7.2 Isolated Perfused Heart Preparation Once the heart was excised from the animal, the aorta was quickly cannulated and retrograde aortic perfusion was started at a constant pressure of 75 – 90 mmHg using a perfusate solution (modified Krebs solution) consisting of (mM): NaCl 113, KCl 4.7, $MgSO_4$ 1.2, Na-EDTA 0.5, $NaHCO_3$ 28.0, Glucose 5.5, Pyruvate 5.0, $CaCl_2$ 2.5. The solution was oxygenated with 95% O_2 and 5% CO_2, maintained at 37°C, and pH adjusted to 7.4. The left and right atria were removed and a balloon made from high-density polyethylene (HDPE, from a plastic biohazard bag) was placed in the left ventricle through the mitral valve and secured with a suture though the LV apex. A catheter-tip pressure transducer (MPC-500, Millar Instruments, Houston, TX) was used to measure LV pressure as force generated on the balloon. The balloon volume was altered using a thumbscrew-controlled 500 µl microsyringe (Hamilton Gas Tight, Reno, NV). Platinum pacing electrodes were placed on the heart, which was then paced at an interbeat interval of 250 ms (240 bpm) using a Pace-1A cardiac stimulator (Radionics, Burlington, MA). Pressure data were digitized for later offline analysis at 1000 Hz based on the Nyquist-Shannon sampling theorem.

4.2.7.3 Frank-Starling Protocol Steady-state isovolumic LV pressure waveforms were recorded over a wide range of balloon volumes from an initial volume (V_0) corresponding to an end-diastolic pressure of 0 mmHg and increasing by manually-controlled 5±0.5 µl increments. The maximal left ventricular volume (V_{max}) corresponded to the volume that produced end-diastolic pressure greater than 25 mmHg.

4.2.7.4 Pacing Trials Diastolic dysfunction is typically more severe when the heart is subjected to stressors that increase the heart rate and shorten the interval for LV relaxation (i.e. exercise). Clinically, the symptoms of diastolic heart failure will often present in patients undergoing a stress test [2]. To test LV mechanical and material properties under stressed conditions, pacing trials were conducted at a shortened interbeat interval. Following the "baseline" Frank-Starling trials, the interbeat interval was reduced to 200 ms (300 bpm) and a "stressed" Frank-Starling trial was performed. The effect of stress was studied by comparing end-diastolic pressure-volume relationships (EDPVRs, defined in **Section 4.2.7.5**) from "baseline" trials to "stressed" trials across all treatment groups.

4.2.7.5 Analysis of Left Ventricular Function Left ventricular developed pressure (P_{dev}) was defined as the difference between peak end-systolic pressure and end-diastolic pressure (P_{ed}) [51]. Rates of pressure development (+dP/dt) and relaxation (-dP/dt) were calculated as positive and negative segments of the first derivative of the pressure waveform, respectively, and maximal rates of each were used to compare contractility ($+dP/dt_{max}$) and relaxation ($-dP/dt_{min}$). To account for differences in both left ventricular mass and volume, a thick walled spherical model of the LV (previously justified for appropriateness [52]) was used to convert pressures to developed or end-diastolic wall stress (σ) according to the following formula:

$$\sigma = \frac{P}{\left(1 + \frac{M}{\rho V}\right)^{\frac{2}{3}} - 1}$$

where M, ρ, and V are left ventricular muscle mass, muscle density (1.05 g/ml), and balloon volume, respectively [53, 54]. The relaxation time (T_{relax}) was defined as the time required for pressure to decay from 75% to 25% of the maximum. Similarly, the rise time (T_{rise}) was defined

as the time required for pressure to rise from 25% to 75% of the maximum [55]. Raw output data from a representative Frank-Starling trial can be seen in **Figure 4** which includes (clockwise from left) average pressure waveforms, developed pressure, rise time, rate of pressure development, rate of relaxation, relaxation time, end-diastolic pressure, and incremental volume steps.

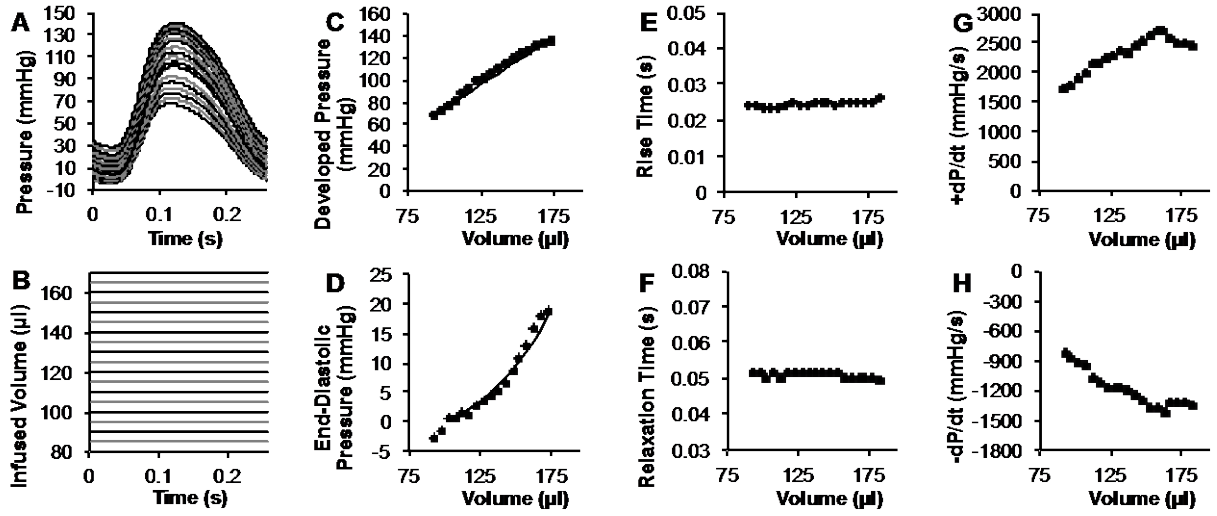

Figure 4. Sample output from isolated heart experiments

Averaged pressure waveforms (A), infused volume steps (B), developed pressure-volume relationship with linear fit (C), end-diastolic pressure-volume relationship with nonlinear fit (D), rise time (E), relaxation time (F), +dP/dt (G), and -dP/dt (H).

To measure contractile function from the Frank-Starling protocol, each volume step was normalized to V_0, and first-order linear regression was performed to determine the relationships between volume and peak pressure (PPVR) and developed pressure (DevPVR).

To calculate myocardial midwall strains, a spherical model of the LV was used to determine the LV chamber radius from the balloon volume at each volume increment (r_{LV}). Myocardial muscle density (1.05 g/ml) and ½ LV mass were used to estimate the volume of the

midwall myocardium (radius calculated from spherical assumption, r_{wall}). Together, these provided the midwall radius, $r_{mid} = r_{LV} + r_{wall}$. A reference radius value (r_0) was calculated from V_0 (initial volume corresponding to P_{ed}=0 mmHg) and used to calculate end-diastolic myocardial midwall strain by the following equation:

$$\varepsilon_{mid} = \frac{r_{mid} - r_0}{r_0}$$

To determine diastolic passive stiffness from the Frank-Starling protocol raw data, nonlinear regression was performed to determine the relationships between volume and end-diastolic pressure (EDPVR) according to the equation:

$$P_{ed} = A\left[e^{b(V-V_0)} - 1\right]$$

where A and b are coefficients determined by iterative curve fitting using a standard Levenberg-Marquardt least squares algorithm (nlinfit.m) in MATLAB. Details of the nonlinear curve fitting are expanded in **Appendix F**.

The relationship between end-diastolic stress and end-diastolic midwall strain was determined by fitting the nonlinear equation:

$$\varepsilon_{ed} = A\left[e^{b\sigma_{ed}} - 1\right]$$

where A and b are coefficients determined by iterative curve fitting using a standard Levenberg-Marquardt least squares algorithm (nlinfit.m, MATLAB). The exponential fit coefficient, b, is referred to as the stress-strain stiffness coefficient.

4.2.8 Heart Weights and Tibia Lengths

Upon completion of experimentation, the heart was removed from the isolated perfused heart setup, blotted to dry, and segmented into left and right ventricle sections. Sections were weighed

and fresh frozen in liquid nitrogen for use in compositional evaluation of fibrosis. The tibia length was measured and recorded for each animal for normalization of heart weights.

4.3 STATISTICAL ANALYSES

Data are presented as mean ± SEM and $P<0.05$ was deemed significant.

4.3.1 Expression of Endogenous Relaxin Receptor-Ligand System

Student's unpaired 't' test was used to compare the mean values of relative mRNA expression ($2^{-\Delta\Delta CT}$) of relaxin-1, relaxin-3, and RXFP-1 among all three fibrotic models: Young SHR *vs.* Aged SHR, Aged SHR *vs.* Aged WKY, and MREN *vs.* SD. Student's 't' test is based on the assumption that samples are normally distributed; hence, normality was confirmed in each data set by the Shapiro-Wilk test which tests the null-hypothesis that the data are normally distributed. A *P-value* >0.05 resulting from the Shapiro-Wilk test means that the null-hypothesis cannot be rejected and the sample set is normally distributed.

4.3.2 Assessment of LV Fibrosis and Cardiac Function

For all quantitative comparisons (fibrotic biomarker mRNA expression, picrosirius red staining, and functional data) single-factor ANOVA was used with three levels corresponding to the vehicle- and rhRLX-treated MREN rats and the SD controls. If a significant main effect was observed, then *post hoc* comparisons among groups were performed using Fisher's least

significant difference (LSD) test. As explained in **Section 4.3.1**, normality is also an assumption of ANOVA statistical testing and therefore normality was confirmed in each sample set by the Shapiro-Wilk test. ANOVA also assumes homogeneity of variances, so to confirm that this assumption was met, Levene's test was performed for each ANOVA test. Levene's test hypothesizes that the variances of all data sets are not equal, therefore a *P-value* <0.05 rejects this hypothesis and confirms homogeneity of variances.

4.3.3 Left Ventricular Function Relationships

Raw pressure or stress data were fitted by a built-in MATLAB function for iterative least squares regression (nlinfit.m) of the equations outlined in **Section 4.2.7.5**. Goodness of fit (R^2) was calculated as the ratio of the sum of squares of the regression (SSR) to the total sum of squares (SST) as outlined in the following equations.

$$SSE = \sum_{i-1}^{n} w_i \left(y_i - \hat{y}_i\right)^2$$

$$SSR = \sum_{i-1}^{n} w_i \left(\hat{y}_i - \bar{y}\right)^2$$

$$SST = \sum_{i-1}^{n} w_i \left(y_i - \bar{y}\right)^2$$

$$R - square = \frac{SSR}{SST} = 1 - \frac{SSE}{SST}$$

where w_i is a weighting factor which was not used. All fitted data were required to meet $R^2>0.8$ to be included in group comparison analyses.

Single-factor repeated measures ANOVA was used to compare mean values of pressure-volume or stress-strain relationships between vehicle- and rhRLX-treated MREN and SD controls. This method was also used to compare mean values of pressure-volume relationships at

different pacing durations (baseline *vs.* stressed). If significant main effects within variables or between variables occurred or if a significant interaction effect was observed, *post hoc* comparisons between groups were performed using Fisher's LSD test.

5.0 RESULTS

5.1 ENDOGENOUS RELAXIN RECEPTOR-LIGAND EXPRESSION IN AN ENVIRONMENT OF FIBROSIS

Specific Aim 1A. To quantify the mRNA expression of relaxin message (relaxin-1 and relaxin-3) and receptor (RXFP-1) in LV tissue from two rat models of hypertension-associated LV fibrosis: Transgenic MREN *vs.* SD controls and aged SHR *vs.* aged, normotensive WKY.

Specific Aim 1B. To quantify the mRNA expression of relaxin message (relaxin-1 and relaxin-3) and receptor (RXFP-1) in LV tissue from young SHR compared to aged SHR as a model of aging-associated LV fibrosis.

5.1.1 Endogenous Relaxin Expression in Transgenic MREN Rats

Transgenic MREN were compared to sex- and age-matched normotensive SD controls (**Table 4**). Fibrosis was confirmed in MREN at this age compared to SD controls by quantification of picrosirius red stained myocardial collagen:total tissue area (**Figure 5**). Relaxin message (relaxin-1 and relaxin-3) and receptor (RXFP-1) mRNA expression was quantified by real-time qPCR in LV tissue from the transgenic MREN rat and compared to SD controls (**Figure 6**). In this model of hypertension and fibrosis, the relative mRNA expression of relaxin-1 was elevated slightly, but not significantly, in MREN (1.59±0.57) *vs.* SD (1±0.24). Similarly, there was a

slight, non-significant increase in relative mRNA expression of relaxin-3 in MREN (1.15±0.17) *vs.* SD (1±0.19). The mRNA expression of receptor RXFP-1 was significantly upregulated in fibrotic MREN (4.48±0.87) *vs.* SD (1±0.23, *P=0.01*).

Table 4. General Characteristics of SD and MREN

Animals	**Age, m**	**BW, g**	**SBP, mmHg**	**HR, bpm**
SD (n=6)	4.3±0.05	552±35	153±4	371±12
MREN (n=5)	4.4±0.03	496±11	198±4*	396±19
BW indicates body weight; SBP, systolic blood pressure; HR, heart rate **P<0.05*				

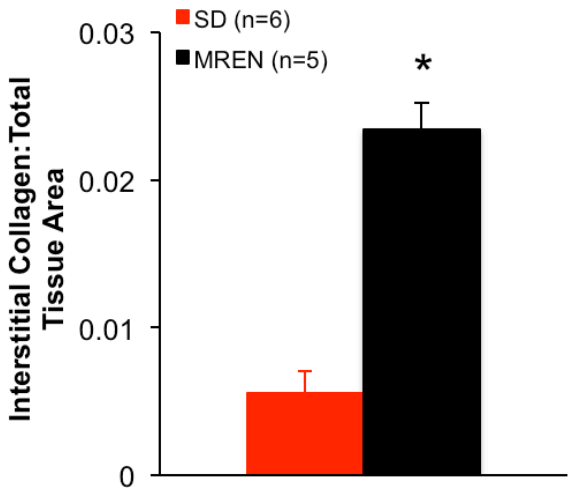

Figure 5. Tissue-level myocardial fibrosis in transgenic MREN *vs.* SD rats

Myocardial collagen was quantified by picrosirius red staining of LV cross-sections from MREN (n=5) and sex- and age-matched SD controls (n=6). Fibrosis was determined in MREN rats as significantly increased interstitial collagen:total tissue area compared to SD controls. **P<0.05* vs. SD by Student's t-test.

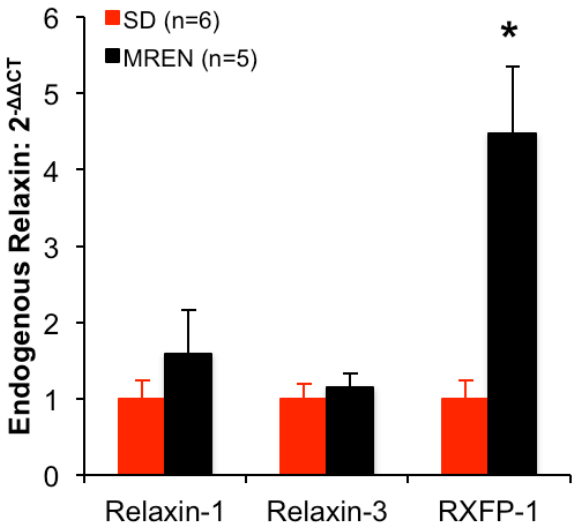

Figure 6. Endogenous relaxin expression in transgenic MREN *vs.* SD rats

Endogenous mRNA expression for relaxin message (relaxin-1 and relaxin-3) and receptor (RXFP-1) from LV tissue of MREN (n=5) were expressed relative to sex- and age-matched SD controls (n=6). Gene expression was quantified by real-time qPCR using specific primer assays for the genes of interest normalized by endogenous control gene, GAPDH. No significant differences exist between groups for relaxin message; however, RXFP-1 expression was significantly increased in MREN *vs.* SD. *$P<0.05$ vs. SD by Student's t-test.

5.1.2 Endogenous Relaxin Expression in Hypertensive SHR Rats

As a second model of hypertension-associated LV fibrosis, the aged SHR animal model was compared to sex- and age-matched normotensive Wistar-Kyoto (WKY) controls (**Table 5**). LV interstitial collagen was stained by immunohistochemistry using a primary antibody specific for collagen-1 (staining and quantification performed by Dr. Charles McTiernan). Myocardial fibrosis was confirmed in SHR compared to WKY controls as increased interstitial collagen:total tissue area (**Figure 7**). Gene expression of relaxin message (relaxin-1 and relaxin-3) and receptor (RXFP-1) was quantified in LV tissue from aged SHR and WKY controls (**Figure 8**). The relative mRNA expression of relaxin-1 was elevated slightly, but not significantly, in SHR (1.39±0.44) *vs.* WKY (1±0.46). Similarly, there was a slight, non-significant increase in relative

mRNA expression of relaxin-3 in aged SHR (1.57±0.36) *vs.* young SHR (1±0.16). Expression of the relaxin receptor RXFP-1 was elevated in LV tissue from the fibrotic SHR (2.02±0.46) *vs.* WKY (1±0.21), however this trend did not reach significance (*P=0.07*).

Table 5. General Characteristics of WKY and SHR

Animals	**Age, m**	**BW, g**	**SBP, mmHg**	**HR, bpm**
WKY (n=6)	11.8	432±9	153±6	344±18
SHR (n=15)	11.4	394±6*	190±5*	408±12
BW indicates body weight; SBP, systolic blood pressure; HR, heart rate **P<0.05*				

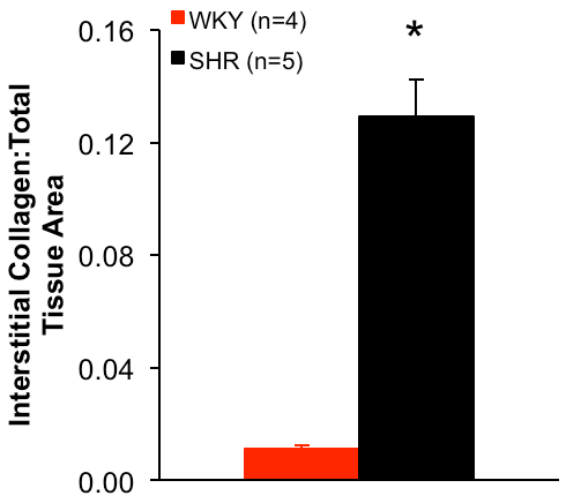

Figure 7. Tissue-level myocardial fibrosis in aged SHR *vs.* aged WKY rats

Myocardial collagen was quantified by immunohistochemical staining of LV cross-sections (primary antibody: anti-Collagen-1) from SHR (n=8) and sex- and age-matched WKY controls (n=6). Fibrosis was determined in SHR rats as significantly increased interstitial collagen:total tissue area compared to WKY controls. **P<0.05* vs. WKY by Student's t-test.

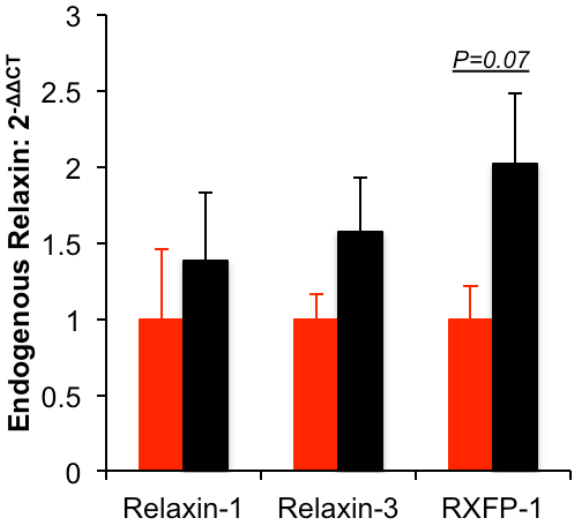

Figure 8. Endogenous relaxin expression in aged SHR *vs.* aged WKY rats

Endogenous mRNA expression for relaxin message (relaxin-1 and relaxin-3) and receptor (RXFP-1) from LV tissue of SHR (12 months, n=8) were expressed relative to sex- and age-matched WKY (12 months, n=6). Gene expression was quantified by real-time qPCR using specific primer assays for the genes of interest normalized by endogenous control gene, GAPDH. No significant differences exist between groups for relaxin message or receptor expression; however, RXFP-1 expression showed a trend of upregulated mRNA expression relative to WKY (*P=0.07*).

5.1.3 Endogenous Relaxin Expression in Age-Associated LV Fibrosis

We studied young SHR rats (~4 months) compared to aged SHR rats (~12 months) to represent a model of age-related fibrosis accelerated by hypertension (**Table 6**). Unfortunately we did not examine myocardial collagen to confirm fibrosis is this cohort, however we found that age was associated with an upregulation in the relaxin receptor-ligand system similar to the other models. Gene expression of relaxin message (relaxin-1 and relaxin-3) and receptor (RXFP-1) was quantified in LV tissue from aged SHR and presented relative to young SHR (**Figure 9**). The relative mRNA expression of relaxin-1 was elevated, but not significantly different, in aged SHR (1.92±0.73) *vs.* young SHR (1±0.12). Similarly, there was a slight, non-significant increase in

relative mRNA expression of relaxin-3 in aged SHR (1.25±0.29) *vs.* young SHR (1±0.03). The mRNA expression of relaxin receptor RXFP-1 was significantly upregulated in aged SHR (2.43±0.55) *vs.* young SHR (1±0.15, *P=0.04*).

Table 6. General Characteristics of young and aged SHR

Animals	**Age, m**	**BW, g**	**SBP, mmHg**	**HR, bpm**
YOUNG SHR (n=8)	4.6±1	346±5	124±3	308±2
AGED SHR (n=15)	11.4	394±6*	190±5*	408±12*
BW indicates body weight; SBP, systolic blood pressure; HR, heart rate **P<0.05*				

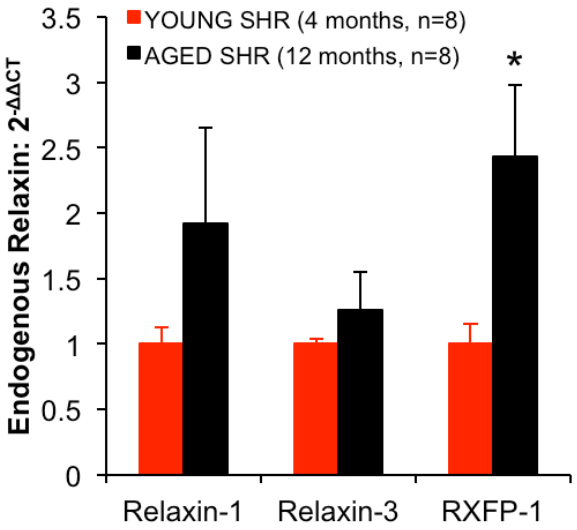

Figure 9. Endogenous relaxin expression in young SHR *vs.* aged SHR

Endogenous mRNA expression for relaxin message (relaxin-1 and relaxin-3) and receptor (RXFP-1) from LV tissue of aged SHR (12 months, n=8) expressed relative to young SHR (4 months, n=8). Gene expression was quantified by real-time qPCR using specific primer assays for the genes of interest normalized by endogenous control gene, GAPDH. No significant differences exist between groups for relaxin message; however, RXFP-1 expression was significantly increased in aged SHR *vs.* young SHR. **P<0.05* vs. young SHR by Student's t-test.

5.1.4 Summary

Quantitative real-time PCR was performed on LV tissue samples from three different known animal models of LV fibrosis. In each model, the relaxin receptor-ligand system showed a pattern of adaptive upregulation in response to a fibrotic environment. The relaxin message genes (relaxin-1 and relaxin-3) were slightly elevated in each model, however this trend never reached significance in any of the models. Interestingly, each model of LV fibrosis demonstrated a significant ~2-4.5-fold increase in the gene expression of the relaxin receptor RXFP-1. These data suggest, consistent with our hypothesis, that the relaxin system, at least in part, is naturally upregulated in the environment of fibrosis. Our next mission was to provide exogenous relaxin to the system to observe its therapeutic potential in this fibrotic environment.

5.2 ASSESSMENT OF LV FIBROSIS AND DIASTOLIC DYSFUNCTION IN RELAXIN-TREATED RATS

Specific Aim 2. To determine the effect of exogenous relaxin administration on established LV fibrosis and diastolic dysfunction in transgenic MREN rats compared to normotensive SD controls.

A preliminary assessment was performed in rhRLX- and vehicle-treated hypertensive SHR rats and compared to normotensive WKY control rats. Due to limited availability of SHR rats at the age which LV fibrosis becomes apparent, studies in this animal model were discontinued and replaced with the MREN rat model. Evidence of beneficial rhRLX

administration effects in aged SHR is presented in **Appendix A**, and while this study lacks evidence of functional improvements, compositional results tend to agree with the findings presented below in transgenic MREN rats.

5.2.1 Administration of rhRLX in Experimental Treatment Groups

Effective administration of exogenous relaxin was confirmed by rhRLX ELISA assay of blood serum with selective conjugate antibodies for recombinant human relaxin-2 (**Figure 10**). As expected, animals that had been administered rhRLX by osmotic minipump showed an average serum concentration of 112±24 ng/ml, comparable with dosages used in similar antifibrotic treatment studies [23, 43]. Animals that had received no treatment (SD) or vehicle treatment (MREN-V) had no detectable amounts of circulating rhRLX (0.51±0.05 and 0.36±0.99 ng/ml, respectively).

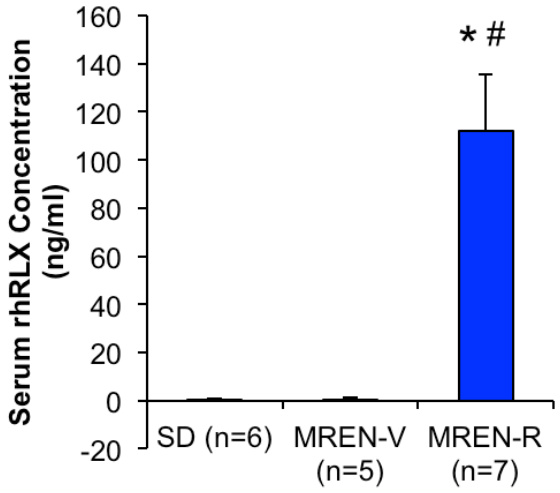

Figure 10. Circulating levels of rhRLX in experimental treatment groups

Blood serum was collected from all experimental treatment groups. MREN-R, which had received rhRLX by osmotic minipump for 14 days, had significantly elevated serum rhRLX concentration respective to non-treated SD and vehicle-treated MREN-V. *$P<0.001$ vs. SD, #$P<0.001$ vs. MREN-R by single-factor ANOVA with *post hoc* Fisher's LSD analysis.

5.2.2 Hypertension and Hypertrophy in rhRLX-Treated MREN Rats

It has been well reported that the upregulated renin-angiotensin system characteristic of the transgenic MREN rat model results in significant hypertension and LV hypertrophy [12, 14]. This pathological adaptation was confirmed in experimental MREN groups versus SD controls despite rhRLX or vehicle treatment. The blood pressure and heart rate measurements (**Figure 11**) were collected by serial non-invasive blood pressure tail-cuff cycles and averaged for each animal and across groups.

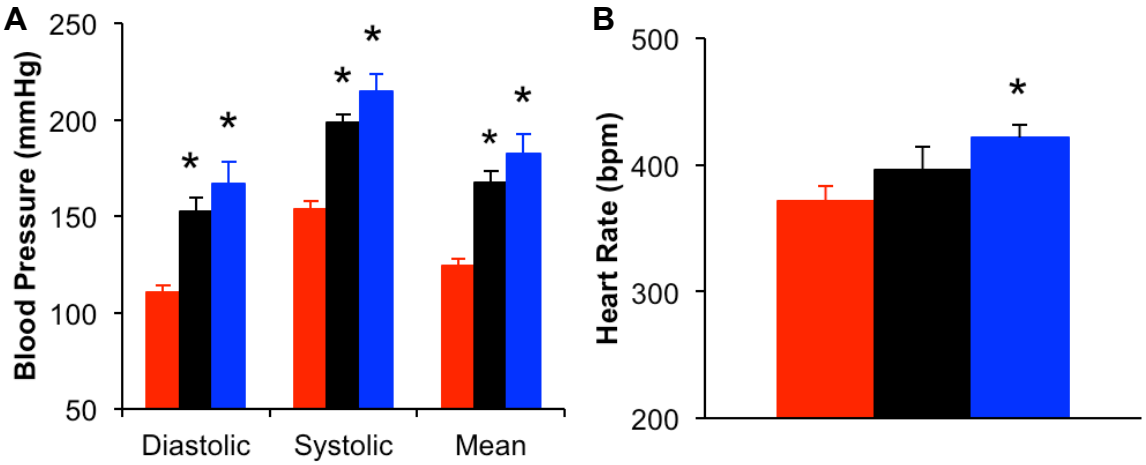

Figure 11. Hypertension and heart rate measurements in the MREN rat

There was a significant main effect of group for diastolic, systolic, and mean blood pressures with MREN-V and MREN-R demonstrating significant hypertension compared to SD controls (A). There was a significant increase in heart rate in MREN-R compared to the other two groups (B). *$P<0.05$ vs. SD by single-factor ANOVA with *post hoc* Fisher's LSD analysis

Hypertrophy was determined by whole heart and ventricle weights normalized by body weight or tibia length for each experimental treatment group (**Figure 12**). LV weights of MREN-V and MREN-R normalized by body weight (3.8±0.1 and 3.8±0.1, respectively) and tibia length (0.58±0.02 and 0.60±0.02, respectively) were significantly increased *vs.* LV weights of SD normalized by body weight (2.8±0.1, $P<0.001$) and tibia length (0.44±0.02, $P<0.001$). There was no significant difference between MREN treatment groups by Fisher's LSD *post hoc* analysis. RV weights of MREN-V and MREN-R normalized by body weight (0.64±0.02 and 0.64±0.04, respectively) did not differ from RV weights of SD normalized by body weight (0.76±0.05, $P=0.07$). There was a significant difference between RV weights normalized by tibia length for MREN-V (0.09±0.002) *vs.* RV weights normalized by tibia length from SD (0.12±0.007, $P=0.04$), this effect was not significant in MREN-R (0.10±0.002, $P=0.06$) compared to SD.

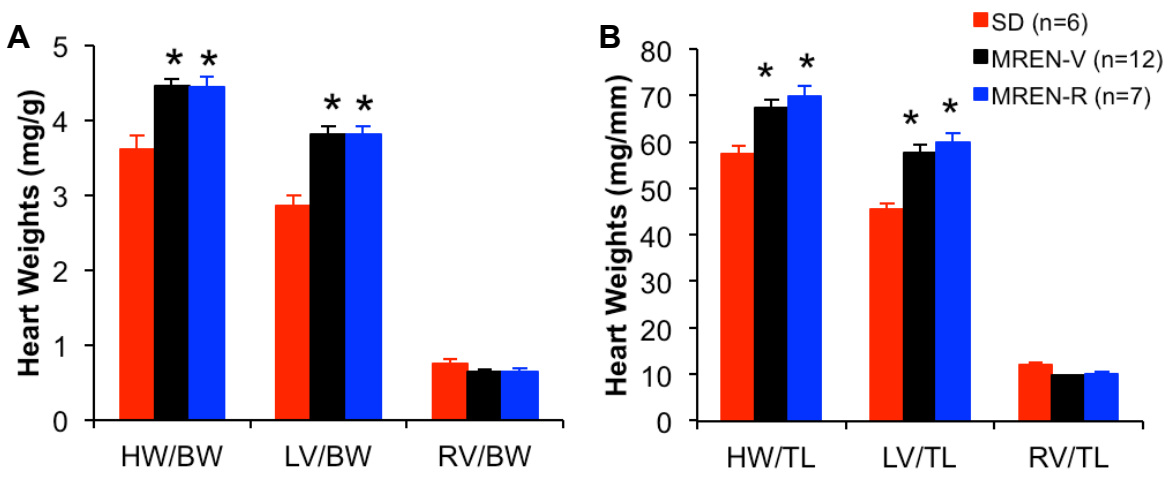

Figure 12. LV hypertrophy in the MREN rat

Left ventricular hypertrophy was evidenced in all MREN independent of treatment by significantly increased heart weights (HW) and LV weights when normalized by either (A) body weight (BW) or (B) tibia length (TL). There were no significant differences in normalized RV weight across all groups. *$P<0.001$ by single-factor ANOVA with Fisher's LSD *post hoc* to compare between MREN-V and MREN-R (no differences).

5.2.3 Gene-Level Expression of Fibrosis in Relaxin-Treated Rats

Gene-level indicators of an active fibrotic environment were measured by quantitative real-time PCR using targets specific for transforming growth factor-β (TGFβ), brain natriuretic peptide (BNP), and matrix metalloproteinases-2 and -9 (MMP2 and MMP9, **Figure 13**). As expected, LV tissue from MREN-V rats had significantly elevated mRNA expression of TGFβ (1.89±0.16 *vs.* 1±0.15, $P=0.001$), BNP (3.56±0.47 *vs.* 1±0.15, $P=0.001$), and MMP2 (2.60±0.24 *vs.* 1±0.19, $P<0.001$) versus SD controls, indicating active collagen turnover. Exogenous rhRLX treatment was able to significantly reduce this fibrotic expression for TGFβ (1.28±0.14, $P=0.01$) and MMP2 (1.44±0.13, $P<0.001$) versus MREN-V and showed no significant differences compared to SD controls. The elevated expression of BNP was not different between MREN-V and

MREN-R groups (3.56±0.47 *vs.* 3.01±0.50, respectively), suggesting that rhRLX administration has no effect on the upregulation of BNP in the MREN model of LV fibrosis. There were no differences in MMP9 expression across all experimental groups.

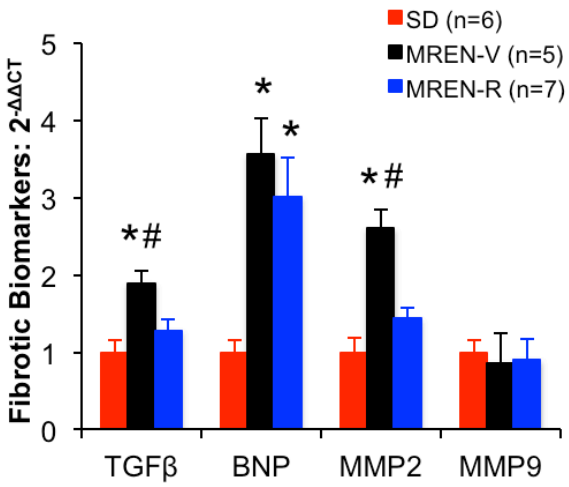

Figure 13. Expression of profibrotic biomarkers

Fibrotic biomarker mRNA expression for TGFβ, BNP, MMP2, and MMP9 from LV tissue of experimental treatment groups was expressed relative to SD controls. Gene expression was quantified by real-time qPCR using specific primer assays for the genes of interest normalized by endogenous control gene, GAPDH. MREN-V had significantly elevated expression of TGFβ and MMP2 versus SD, and MREN-R showed a significant reduction from the fibrotic response. Expression of BNP was significantly elevated in both MREN groups *vs.* SD controls, regardless of rhRLX administration. There were no significant differences in mRNA expression of MMP9 across all experimental groups. *$P<0.05$ vs. SD, $^{\#}P<0.05$ vs. MREN-R by single-factor ANOVA with Fisher's LSD *post hoc* analysis.

As described in **Section 5.1.3.**, endogenous relaxin message (relaxin-1 and relaxin-3) is slightly elevated and receptor (RXFP-1) is significantly elevated in fibrotic MREN-V versus SD controls. Administration of rhRLX attenuated this upregulation in MREN-R (**Figure 14**). Compared to MREN-V, MREN-R had reduced relaxin-1 mRNA expression (0.76±0.27 *vs.*

1.59±0.57, *P=0.13*), reduced relaxin-3 expression (0.71±0.11 *vs.* 1.15±0.17, *P=0.08*), and significantly reduced RXFP-1 expression (2.44±0.67 *vs.* 4.48±0.87, *P=0.03*).

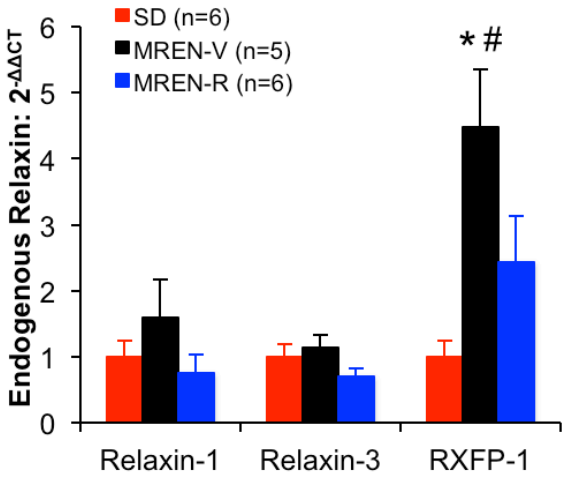

Figure 14. Endogenous relaxin expression in rhRLX-treated MREN

Expression of endogenous relaxin-1, relaxin-3, and RXFP-1 from experimental treatment groups was expressed relative to SD controls. Gene expression was quantified by real-time qPCR using specific primer assays for the genes of interest normalized by endogenous control gene, GAPDH. MREN-V had significantly elevated expression of RXFP-1 *vs.* SD controls that was significantly attenuated by rhRLX treatment in MREN-R. $*P<0.05$ vs. SD, $^{\#}P<0.05$ vs. MREN-R by single-factor ANOVA with Fisher's LSD *post hoc* analysis.

5.2.4 Interstitial and Perivascular Fibrosis in Relaxin-Treated Rats

To measure LV fibrosis on the protein-level, tissue sections were stained by picrosirius red (PSR) dye, imaged, quantified, and compared across experimental groups. Tissue samples were divided by region to specifically focus on interstitial collagen in the epicardial region (**Figure 15A,D,G**) and endocardial region (**Figure 15B,E,H**) separately. Arterioles to represent perivascular collagen were chosen based on morphology of the vessel and location within the endocardial region (**Figure 15C,F,I**).

In the outer epicardial region, no significant differences in collagen protein:total tissue area were detected across the groups (**Figure 16A**). In the MREN-V group, the epicardial collagen ratio was moderately increased (0.01±0.002) when compared to SD and MREN-R (0.007±0.002 and 0.008±0.002, respectively). However, the inner endocardial regions of MREN-V were significantly more collagen-rich than SD controls (0.023±0.003 *vs.* 0.006±0.001, *P<0.001*) suggesting a spatial disparity of fibrotic collagen deposition (**Figure 16B**). This interstitial fibrosis in the endocardial region was significantly reduced in MREN-R versus MREN-V (0.01±0.001 *vs.* 0.023±0.003, *P=0.003*) to where it was not statistically different from SD controls.

Perivascular collagen was also quantified and normalized to arteriolar lumen area as a measure of protein-level fibrosis (**Figure 16C**). Similar to the interstitial collagen deposition, MREN-V demonstrated significantly increased perivascular collagen versus SD controls (0.91±0.11 *vs.* 0.58±0.06, *P=0.032*) and rhRLX administration was able to significantly reverse this fibrosis (0.37±0.06 *vs.* 0.91±0.11, *P=0.001*) to levels not statistically different from SD controls.

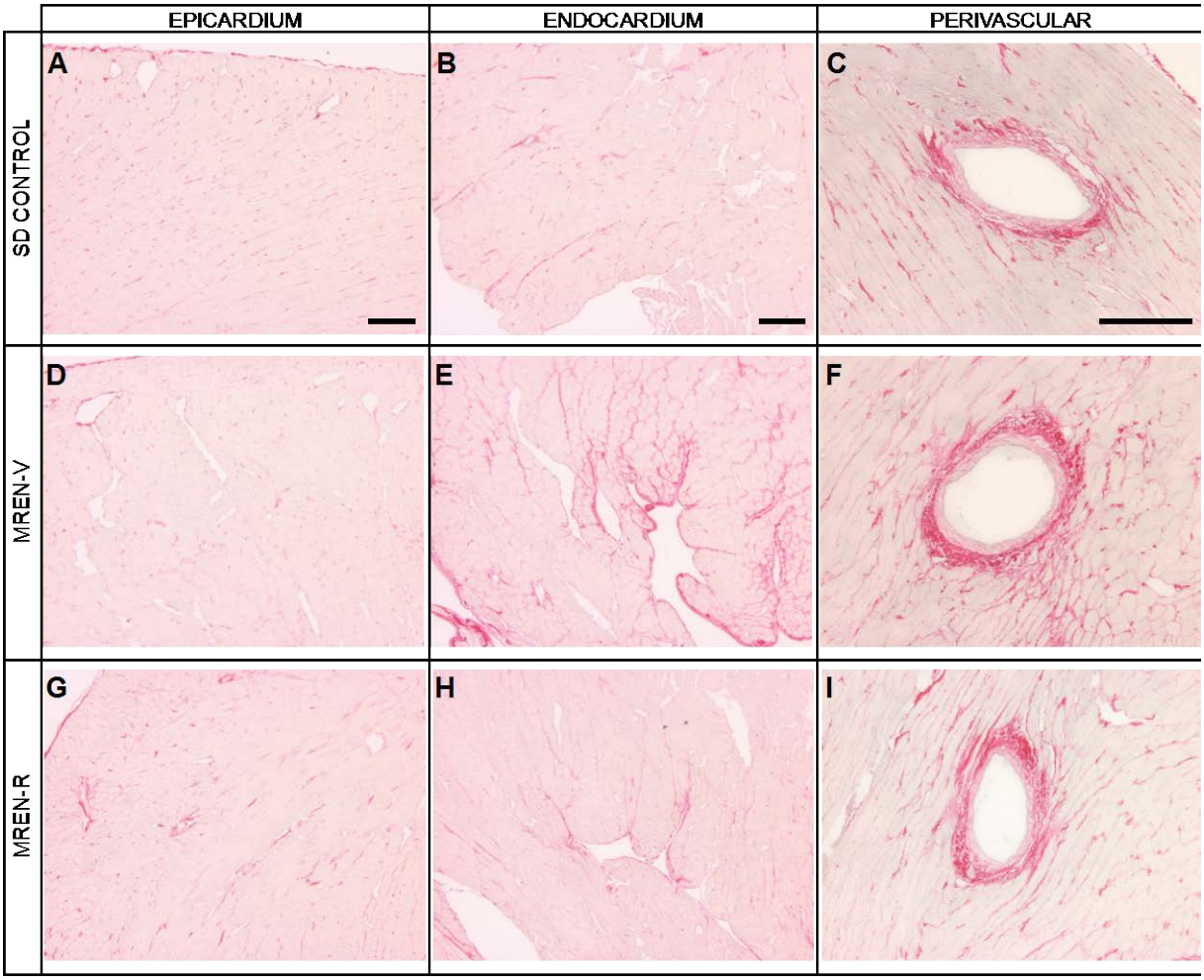

Figure 15. Picrosirius red staining

Epicardial (A,D,G) and endocardial (B,E,H) regions of PSR-stained LV cross-sections were imaged at 10X magnification and arterioles (C,F,I) were focused at 20X magnification for interstitial and perivascular collagen, respectively. Qualitatively, MREN-V appear to have increased collagen in the endocardium and perivascular regions when compared to MREN-R and SD controls.

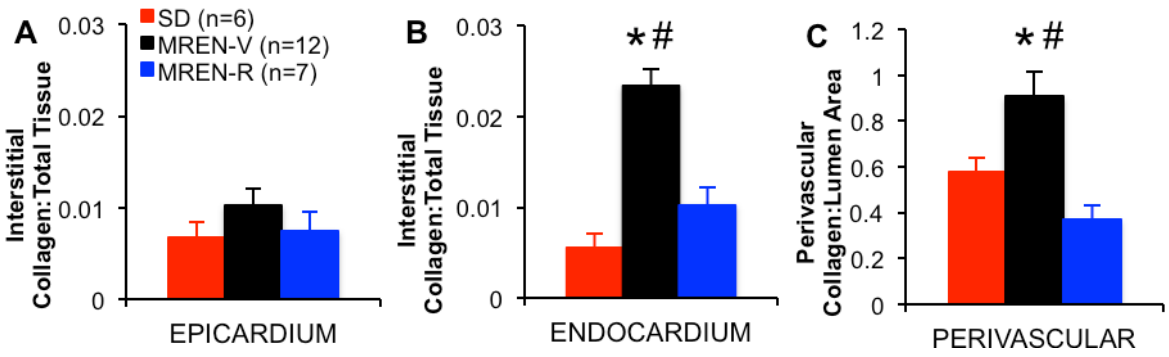

Figure 16. Regional quantification of picrosirius red staining

Images were processed computationally and interstitial and perivascular collagen was quantified for each of the experimental groups. There was no difference in interstitial collagen at the level of the LV epicardium (A) across the groups. However, at the endocardial (B) and perivascular (C) levels, MREN-V were significantly more collagen-rich compared to both SD controls and rhRLX administration reduced this fibrotic phenotype in MREN-R. $*P<0.05$ vs. SD, $^{\#}P<0.05$ vs. MREN-R by single-factor ANOVA with Fisher's LSD *post hoc* analysis.

5.2.5 Contractility Parameters in Relaxin-Treated Rats

The isolated perfused heart experiments produced raw LV pressure waveforms at varying balloon volumes based on the Frank-Starling protocol. Contractility was determined based on peak and developed pressures and corresponding stresses, the rates of pressure development, and the rise time.

Peak pressure, or maximum pressure, was plotted against incremental volume steps and fitted with a linear relationship defined in **Section 4.2.7.5** to determine the peak pressure-volume relationship (PPVR) for each experimental group. There was a significant difference in V_{max} across the groups with MREN-V and MREN-R reaching significantly higher maximum volumes (184±3 and 188±5, respectively) compared to SD controls (136±13). Hence, for comparative purposes, the PPVR was plotted using a normalized volume (V/V_0). There were no significant differences in PPVR across all experimental groups (**Figure 17**) though the PPVR was elevated

slightly in MREN-R versus MREN-V and SD controls, though this increase did not reach statistical significance (*P=0.265*).

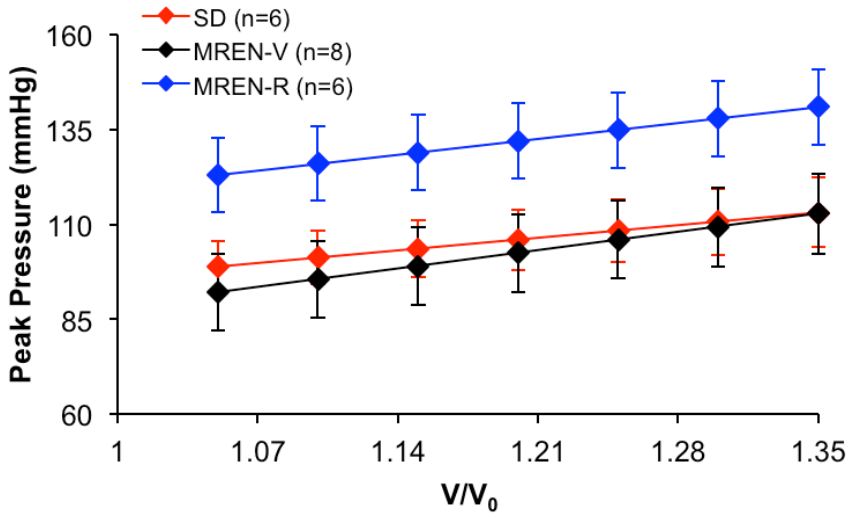

Figure 17. Peak-pressure volume relationships in MREN rat

Contractile function, determined by PPVR, tended to be higher in MREN-R *vs.* MREN-V and SD controls, though no significant main effects were observed by single-factor repeated-measures ANOVA.

Similar to the PPVR, the developed pressure was fitted with a linear relationship defined in **Section 4.2.7.5**. This relationship, the developed pressure-volume relationship (DevPVR), was not significantly different between all experimental groups by repeated-measures ANOVA (*P=0.285*).

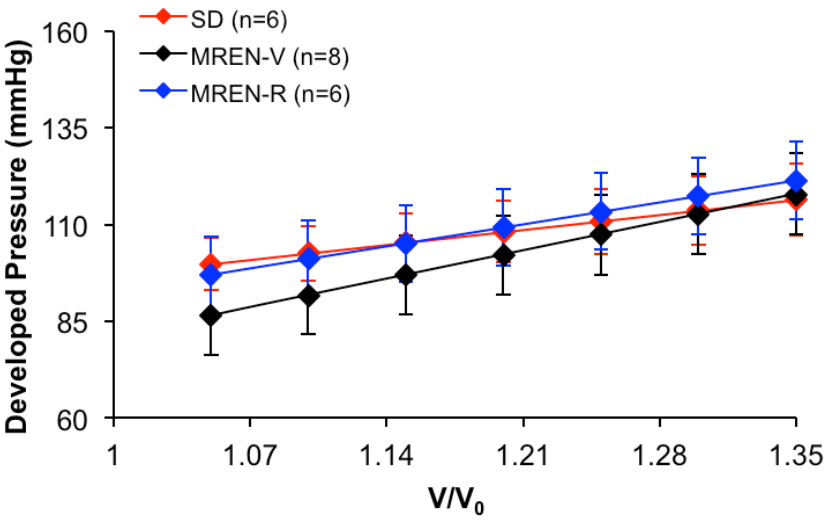

Figure 18. Developed-pressure volume relationships

Contractile function, determined by DevPVR and plotted against normalized volume, was not significantly different across all experimental groups by repeated-measures ANOVA.

End-diastolic myocardial midwall strain was calculated using a reference radius corresponding to the initial volume where P_{ed}=0 mmHg (V_0). Developed stress was calculated from developed pressure, volume, and LV weight following **Section 4.2.7.5**. Raw developed stress was plotted against end-diastolic midwall strain and fitted with a linear relationship defined in **Section 4.2.7.5** (**Figure 19**). This relationship, the developed stress-midwall strain relationship, was not distinguishable across all groups (*P=0.465*).

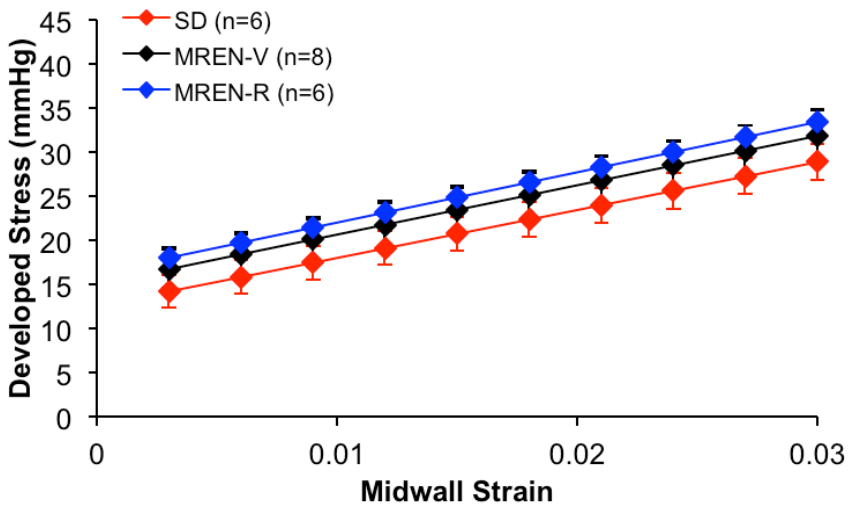

Figure 19. Developed stress-midwall strain relationships

Developed stress-midwall strain relationships were determined for each experimental group by fitting data by first-order linear regression. Midwall strains were calculated using a reference strain based on LV initial volume (V_0). There were no significant differences across all groups by repeated measures ANOVA.

The rate of pressure development (+dP/dt) was calculated for each cardiac cycle along incremental volume steps and the maximum rates ($+dP/dt_{max}$) are presented for each experimental group in **Figure 20**. The maximal rate of pressure development was significantly reduced in MREN-V versus SD controls (2602±198 *vs.* 3564±78 mmHg/s, *P=0.001*) but no differences existed between MREN-R and the two groups (3011±143 mmHg/s).

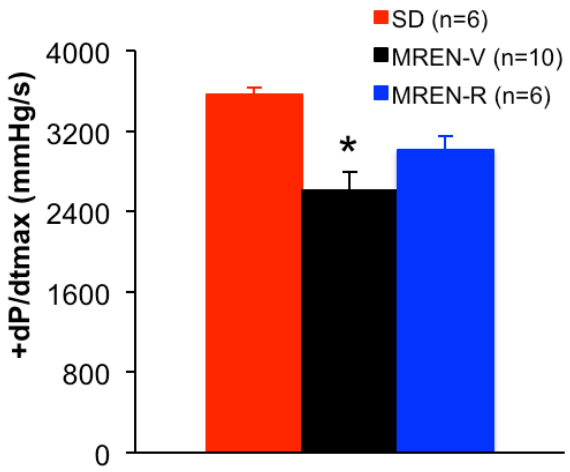

Figure 20. Maximal rate of pressure development

Contractility as measured by maximum rate of pressure ($+dP/dt_{max}$) development was significantly blunted in MREN-V compared to SD controls. There was no significant effect of rhRLX administration. *$P<0.05$ vs. SD controls by single-factor ANOVA with Fisher's LSD *post hoc* analysis.

Rise time was also calculated for each cardiac cycle and averaged across incremental volume steps. Rise time was not significantly different between any of the treatment groups (**Figure 21**), though MREN-V was slightly increased (0.024±0.006 s) compared to SD controls (0.022±0.004 s) and MREN-R (0.022±0.006 s).

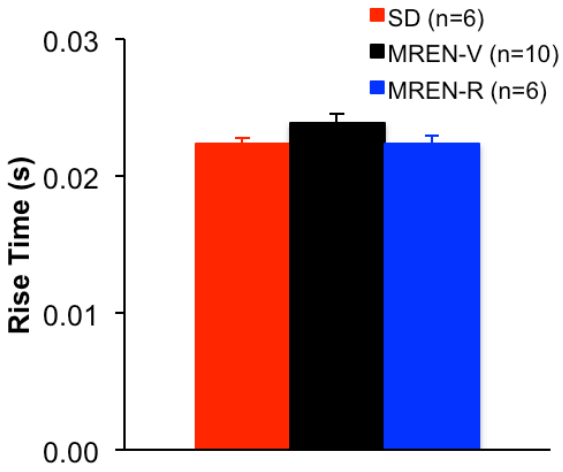

Figure 21. Rise time

Contractility as measured by the time required for pressure to rise from 25% to 75% of the maximum (rise time) was not significantly different across all experimental groups, despite a modest increase in MREN-V.

5.2.6 Diastolic Function in Relaxin-Treated Rats

The volume where P_{ed}=0 mmHg (V_0) provides information about the chamber dilation between experimental groups (**Figure 22**). Compared to SD controls, V_0 was significantly increased in MREN-R (115±0.03 *vs.* 56±0.02 µl, *P<0.001*) and MREN-V (113±0.02 *vs.* 56±0.02 µl, *P<0.001*). Hence, for comparative purposes, all pressure-volume relationships were plotted against normalized volumes (V/V_0). LV passive stiffness was evaluated for each experimental group by the following relationships: end-diastolic pressure-volume relationship (EDPVR, **Figure 23**), stiffness coefficient (dP_{ed}/dV)-end-diastolic pressure relationship (dP_{ed}/dV-P_{ed}, **Figure 24**), and end-diastolic stress-midwall strain relationship (**Figure 25**).

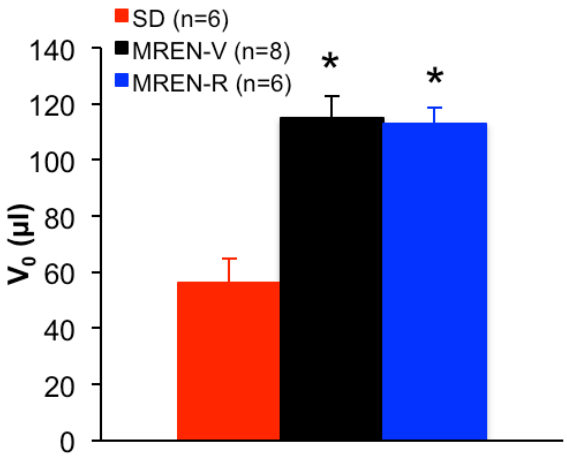

Figure 22. V_0 values for all experimental groups

Initial volume where P_{ed}=0 mmHg (V_0) was determined for each group by interpolation of raw pressure-volume step data. Both MREN experimental groups had increased V_0 compared to SD controls, regardless of rhRLX administration. *$P<0.001$ vs. SD controls by single-factor ANOVA with Fisher's LSD *post hoc* analysis.

EDPVR was calculated by non-linear curve fitting of raw end-diastolic pressures at increasing volume increment steps as described in **Section 4.2.7.5**. By comparison of EDPVR, LV from MREN-V were significantly stiffer *vs.* SD controls ($P<0.001$) and rhRLX administration was able to significantly reverse this stiffness ($P=0.005$) to levels not different from controls ($P=0.284$). Similarly, the relationship between stiffness coefficient (dP_{ed}/dV) and end-diastolic pressure demonstrated significantly stiffer MREN-V compared to SD controls ($P<0.001$) and MREN-R ($P=0.001$) with no significant difference between rhRLX-treated MREN-R and SD controls ($P=0.578$). Finally, the relationship between end-diastolic stress and myocardial midwall strain was determined to account for differences in ventricular size and chamber mass across experimental groups. End-diastolic midwall strain was calculated using a reference radius corresponding to an initial LV volume where P_{ed}=0 mmHg (V_0). The averaged end-diastolic stress-midwall strain relationship was significantly elevated in MREN-V versus SD

controls (*P=0.02*) and rhRLX administration was able to significantly reverse the stiffness (*P=0.03*) to levels not different from controls (*P=0.821*).

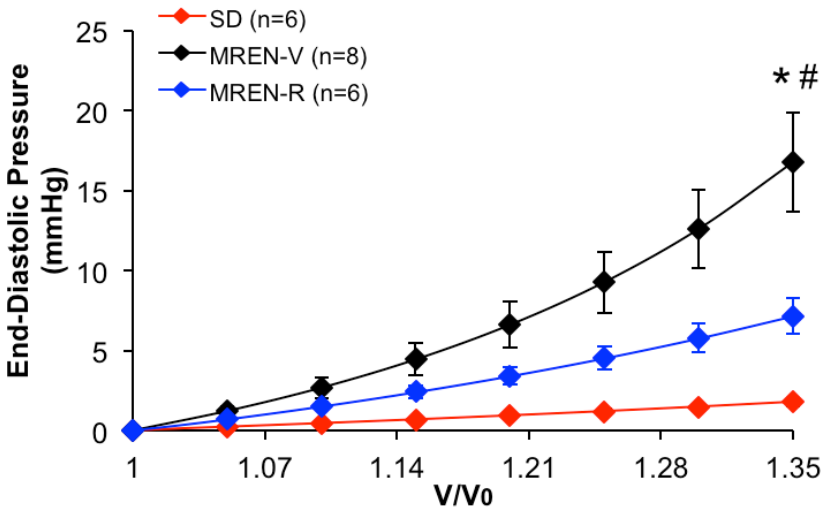

Figure 23. End-diastolic pressure-volume relationships

End-diastolic pressure-volume relationships (EDPVR) were obtained for each group by non-linear curve fitting using an exponential model of end-diastolic pressure as a function of LV volume. Results were averaged within experimental groups and plotted against normalized volume (V/V_0). MREN-V had significantly stiffer LV as evidenced by an upward shift in EDPVR *vs.* SD controls. This stiffness was significantly reduced by rhRLX administration in MREN-R. $^{*}P<0.05$ vs. SD, $^{\#}P<0.05$ vs. MREN-R by repeated-measures ANOVA with *post hoc* analysis by Fisher's LSD test.

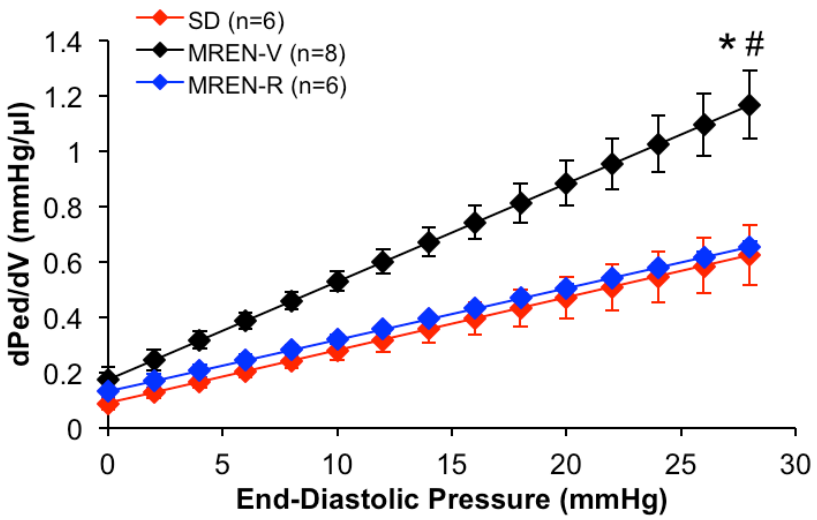

Figure 24. End-diastolic stiffness coefficient-pressure relationship

As a measure of LV passive stiffness, the end-diastolic stiffness coefficient (dP_{ed}/dV) was plotted against end-diastolic pressure (P_{ed}) for each experimental group. MREN-V had significantly stiffer LV as evidenced by increased dP_{ed}/dV *vs.* SD controls over the range of end-diastolic pressures. This stiffness was significantly reduced by rhRLX administration in MREN-R. $^{*}P<0.05$ vs. SD, $^{\#}P<0.05$ vs. MREN-R by repeated-measures ANOVA with *post hoc* analysis by Fisher's LSD test.

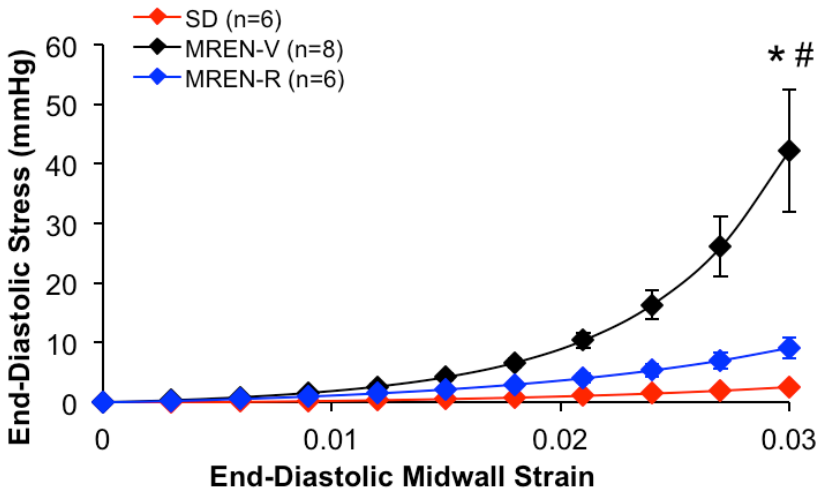

Figure 25. End-diastolic stress-midwall strain relationship

End-diastolic stress-midwall strain relationships were determined for each experimental group by non-linear regression. End-diastolic midwall strains were calculated using a reference strain based on LV initial volume (V_0 corresponding to a volume where P_{ED}=0). There was a significant increase in passive LV stiffness in MREN-V *vs.* SD controls that was normalized with rhRLX treatment in MREN-R. $^{*}P<0.05$ vs. SD, $^{\#}P<0.05$ vs. MREN-R by repeated-measures ANOVA with *post hoc* analysis by Fisher's LSD.

The exponential stiffness coefficient from the end-diastolic stress-midwall strain relationship was determined by iterative curve fitting (**Figure 26**). There was a significant main effect of treatment (*P=0.008*) and *post hoc* analysis showed that MREN-V had significantly increased stress-strain coefficients versus SD controls (133±18 *vs.* 72±9, *P=0.006*) and MREN-R (133±18 *vs.* 77±6, *P=0.01*). There were no differences between SD and MREN-R.

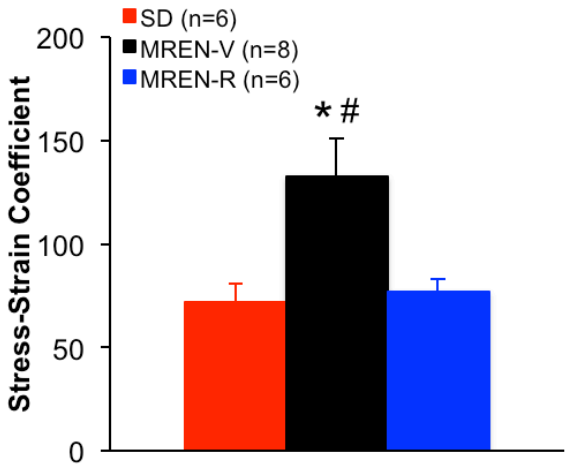

Figure 26. End-diastolic stress-strain stiffness coefficient

The coefficient of end-diastolic stiffness was determined by non-linear curve fitting of the exponential model of end-diastolic stress-midwall strain. LV from the MREN-V group had significantly increased stiffness *vs.* SD controls and this stiffness was reduced with rhRLX-treatment in MREN-R. $*P<0.05$ vs. SD, $^{\#}P<0.05$ vs. MREN-R by single-factor ANOVA with *post hoc* analysis by Fisher's LSD.

The rate of pressure relaxation (-dP/dt) was calculated for each cardiac cycle along incremental volume steps and the maximum relaxation rates ($-dP/dt_{min}$) are presented for each experimental group in **Figure 27**. The maximal rate of pressure relaxation was significantly blunted compared to SD controls in both MREN-V (1305±84 *vs.* 1925±74 mmHg/s, $P<0.001$) and MREN-R (1487±75 *vs.* 1925±74 mmHg/s, $P=0.01$).

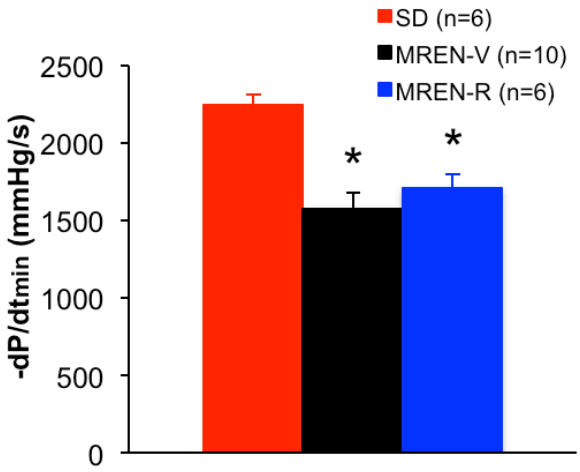

Figure 27. Maximal rate of pressure relaxation

Maximal rate of pressure relaxation ($-dP/dt_{min}$) was blunted in MREN-V and MREN-R compared to SD controls. There was no significant effect of rhRLX-treatment between the experimental groups; however, modest improvements in relaxation were present in MREN-R. *$P<0.05$ vs. SD controls by single-factor ANOVA with Fisher's LSD *post hoc* analysis.

Relaxation time was also calculated for each cardiac cycle and averaged across incremental volume steps. Compared to SD controls, relaxation time (**Figure 28**) was significantly slower in both MREN-V (0.048±0.001 *vs.* 0.041±0.001 s, $P=0.001$) and MREN-R (0.048±0.001 *vs.* 0.041±0.001 s, $P=0.003$).

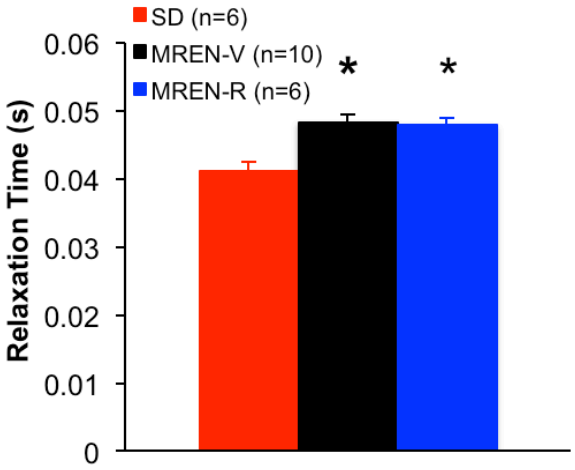

Figure 28. Relaxation time

Relaxation as measured by the time required for pressure to fall from 75% to 25% of the maximum (relaxation time) was significantly elongated for both MREN groups *vs.* SD controls, despite rhRLX administration. *$P<0.05$ vs. SD by single-factor ANOVA with Fisher's LSD *post hoc* analysis.

To test diastolic function under stressed conditions, cardiac pacing was increased and a final Frank-Starling protocol was run. LV passive stiffness increased in each experimental group under the stressed condition versus baseline based on the upward shifted EDPVR (**Figure 29A-C**). The difference between the EDPVRs of the stressed and baseline conditions (ΔEDP) revealed that the beneficial effect of rhRLX administration to improve diastolic passive stiffness persisted despite the stress perturbation (**Figure 29D**).

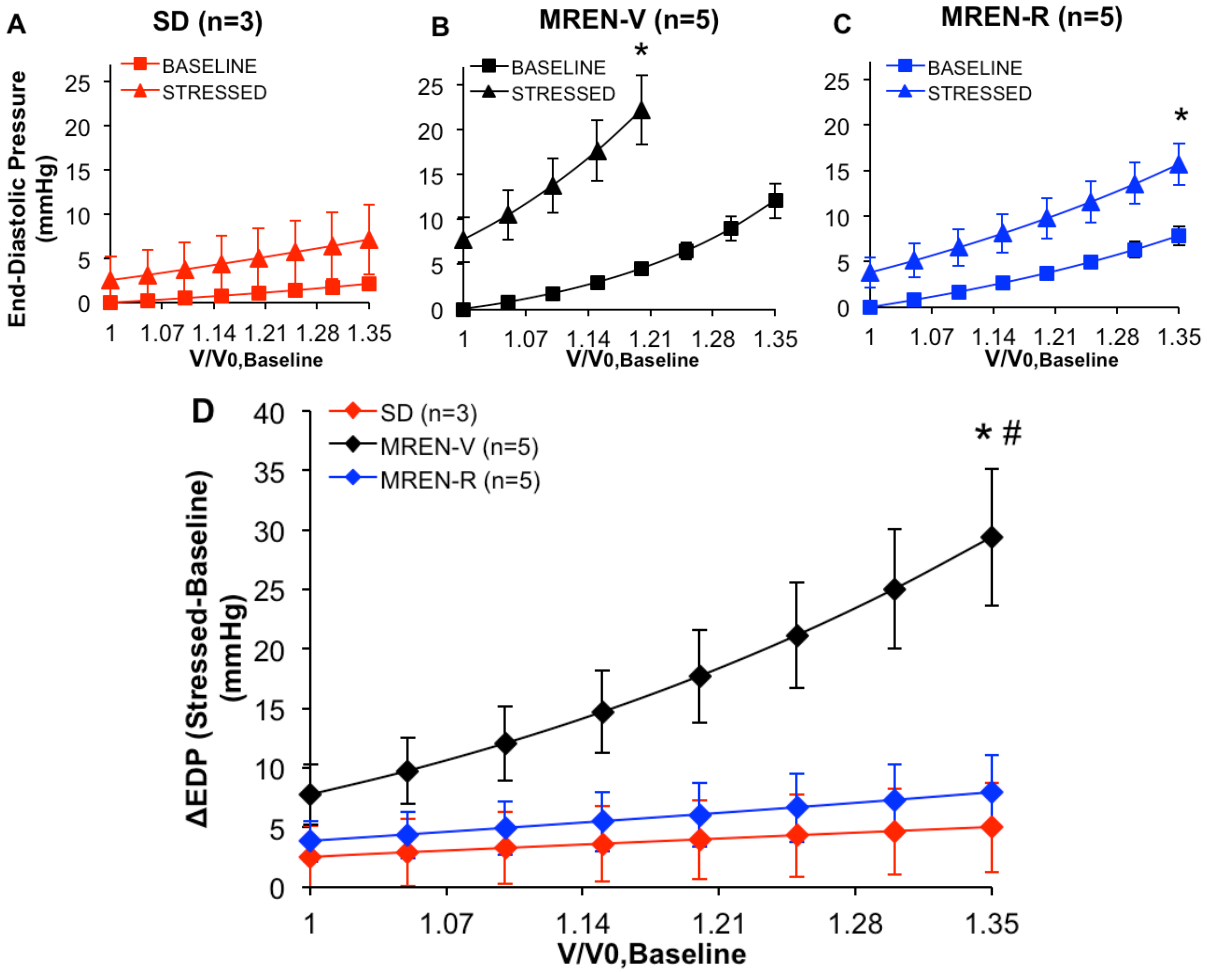

Figure 29. End-diastolic function in pacing studies

Diastolic function was observed under stressed conditions (increased pacing) and EDPVRs were compared between baseline and stressed condition for each experimental group (A-C). The difference in end-diastolic pressure from each condition (ΔEDP) was plotted for all groups against normalized volume. *$P<0.05$ vs. SD, $^{\#}P<0.05$ vs. MREN-R by repeated-measures ANOVA with *post hoc* analysis by Fisher's LSD.

5.2.7 Summary

Here we have shown that 14 days of exogenous rhRLX administration is capable of reversing LV fibrosis on both the gene- and protein-levels in the MREN rat model. We have shown that endogenous relaxin expression responds in a compensatory manner in an active fibrotic

environment, similar to the other biomarkers presented. As such, the reversal of LV fibrosis by rhRLX administration also normalized the endogenous expression of RXFP-1 and reduced the expression of relaxin-1 and relaxin-3. While exogenous relaxin administration had no significant effect on contractile function in the MREN model, the reversal of LV fibrosis was associated with a reduction in diastolic passive stiffness as evidenced by a significant downward shift of the EDPVR and stress-strain relationship compared to MREN-V. In contrast to the improvements in passive stiffness, rhRLX administration had no effect on LV diastolic relaxation in MREN.

6.0 DISCUSSION

6.1 ENDOGENOUS RELAXIN IN AN ENVIRONMENT OF FIBROSIS

Gene expression patterns of relaxin family peptides and their respective receptors have been studied in several different animal models by several different methods over the last two decades [27]. The primary relaxin receptor, RXFP-1, is the only receptor to date that has been localized in heart tissue and has the ability to bind both rat relaxin isoforms (relaxin-1 and relaxin-3) as well as human relaxin-2. For this reason, the mRNA expression of the RXFP-1 receptor and its two primary ligands, relaxin-1 and relaxin-3, was quantified in LV tissue from aged SHR and transgenic MREN rats to characterize the response of the endogenous relaxin receptor-ligand system in an environment of LV fibrosis.

Both hypertension- and age-associated models of LV fibrosis presented a similar trend: a ~1.5-fold, non-significant increase in relaxin message (both relaxin-1 and relaxin-3) and a ~2-4.5-fold, significant increase in mRNA expression for the relaxin receptor RXFP-1 compared to respective controls. Previous studies with genetically modified mouse models have shown that deficiency of relaxin (message and/or receptor knock-out) leads to fibrosis [23, 40, 56]. Here we show a compensatory response in which the endogenous relaxin receptor-ligand system is upregulated in an environment of established fibrosis, at least at the level of gene expression. Together, these findings clearly demonstrate that relaxin plays a role in the homeostasis of

fibrosis. In a healthy setting it acts to regulate collagen and when fibrosis sets in it adapts in attempt to fight back. However, the adaptive response is not powerful enough to prevent or reverse fibrotic collagen accumulation.

There are few comparable studies available that consider endogenous relaxin receptor-ligand expression in an environment of established fibrosis. However, when considering precursors to fibrosis – either acute or chronic stressors – an adaptive response of the endogenous relaxin receptor-ligand system in the direction of a compensatory mechanism has been observed which agrees with our findings. Dschietzig *et al.* showed that an acute increase in LV end-diastolic pressure from 5 to 25 mmHg in male Wistar rats for two hours correlated with elevated mRNA expression of relaxin-1 in LV tissue [29]. Furthermore, they correlated increased circulating plasma levels of human relaxin to severe congestive heart failure (CHF) in human patients; this, they predicted, was indicative of a compensatory mechanism in which the relaxin system is upregulated in the failing heart.

6.1.1 Relaxin Isoforms in the Rat Left Ventricle

The current understanding is that endogenous relaxin message is expressed in heart tissue and works locally as a ligand to RXFP-1 to facilitate cardiovascular adaptations to fibrosis [27]. However, there is not yet a definitive characterization of which isoforms of relaxin exist in rat left atria and/or ventricles and how they are distributed. There is gene-level evidence that the relaxin-3 isoform is expressed in rat atria and ventricles, and this mRNA expression is upregulated with cardiac remodeling after myocardial infarction [57]. This study by Kompa *et al.* also concluded by RT-PCR that relaxin-1 is not expressed in rat atria or ventricles, which contradicts previous observations. In 1995, Gunnersen *et al.* demonstrated by Northern blot that

relaxin-1 is expressed in rat heart tissue, though there was no separation between atria and ventricles and the expression was lower than that in other organ systems such as reproductive tissues and brain [58]. It must also be noted, that this review of previous findings comes from reports utilizing different qualitative or quantitative techniques and the gene targets were not always characterized for cross-reactivity between different relaxin isoforms [27].

The Quantitect gene primers used for endogenous relaxin receptor-ligand expression experiments described herein are commercially-available and bioinformatically validated based on the GenBank NCBI reference sequences for rat relaxin-1 (NM_013413.1), relaxin-3 (NM_170667.2), and RXFP-1 (NM_201417.1). Visual inspection of amplification plots and melting temperature curves was performed after each experiment to validate primer specificity and to ensure no primer-dimer formation (indicated by single representative peaks for each primer assay, explained in **Section 4.1.4.**). To our knowledge, the results presented here represent the first conclusive evidence that relaxin message (relaxin-1 and relaxin-3) and receptor (RXFP-1) are expressed locally in male rat LV tissue and this system is upregulated in the environment of LV fibrosis.

6.1.2 Adaptive Upregulation of Endogenous Relaxin in Hypertension-Associated Fibrosis

We looked at the transgenic hypertensive MREN rat compared to its age-matched, species-background Sprague-Dawley controls as a model of hypertension-associated LV fibrosis. The genetic manipulation in MREN rats allowed for the development of severe hypertension and LV fibrosis at a young age and we found that in this model of fibrosis, there tended to be minor increases in relaxin-1 and relaxin-3 compared to SD with only the 4.5-fold increase in RXFP-1 in MREN reaching significance. These results confirmed for us that the relaxin receptor-ligand

system is upregulated in the fibrotic LV of MREN rats compared to their normotensive controls, at least regarding the RXFP-1 receptor. Next we wanted to see if this was a generalized phenomenon by testing a second model of hypertension-associated LV fibrosis. We continued the study with the aged, hypertensive SHR compared to age-matched, normotensive WKY rats to provide a second model of hypertension-associated fibrosis. We confirmed that SHR had significantly higher blood pressures and significantly increased myocardial collagen compared to the WKY controls, confirming LV fibrosis in this model. As we saw in the MREN model, this LV fibrosis in SHR was associated with elevations in the endogenous mRNA expression of the relaxin receptor-ligand system, though in this case, the effect did not reach statistical significance. The increased mRNA expression for RXFP-1 was more dramatic in the MREN model compared to the SHR model of fibrosis, though both were elevated above their respective controls. This finding suggests a mechanism for relaxin receptor-ligand system upregulation that is independent of hypertension. Instead, we suspect that contributions from the fibrotic environment trigger the expression of endogenous relaxin receptor-ligand expression and Pinto *et al.* concluded that at the same age, MREN demonstrate significantly more severe LV hypertrophy, fibrosis, and impaired diastolic function (reduced $-dP/dt_{min}$) compared to SHR [13].

Despite the lack of statistical significance in mRNA expression of the relaxin receptor-ligand system in SHR compared to WKY, this data, in addition to the results from the MREN model allowed us to conclude that there are trends towards an upregulation of the relaxin receptor-ligand system in a setting of fibrosis. Consequently, we wanted to test if this trend would also present in a condition of aging, which is known to naturally contribute to fibrosis.

6.1.3 Adaptive Upregulation of Endogenous Relaxin in Aging-Associated Fibrosis

We studied young SHR rats (~4 months) compared to aged SHR rats (~12 months) to represent a model of age-related fibrosis accelerated by hypertension. Unfortunately we did not examine myocardial collagen to confirm fibrosis is this cohort, however we found that aging was associated with an upregulation in the relaxin receptor-ligand system similar to the other models. Our results showed a modest increase in relaxin-1 and relaxin-3 expression, as seen before, suggesting that relaxin production is not impaired as a function of aging. Instead, the relaxin receptor RXFP-1 seems to be adaptive in this model of aging-associated LV fibrosis as evidenced by the significant 2.5-fold increase in mRNA expression in LV tissue from aged SHR versus young SHR.

6.1.4 Relaxin: A Natural Player in Cardiac Fibrosis

While significant research has gone into understanding the antifibrotic actions downstream of relaxin receptor-ligand binding, mostly involving NO-mediated mechanisms, limited information is available regarding regulators of endogenous relaxin expression. Most recently, Moore *et al*. made substantial progress to elucidate mechanisms of heart failure that contribute to RXFP-1 expression. Using rat cardiomyocytes, they found that RXFP-1 expression was upregulated 2-3-fold after stimulation by alpha-adrenergic receptor agonists (α-AR) and this response was inhibited by beta-adrenergic receptor agonists (β-AR). They suggested a potential connection to current heart failure therapies that utilize β-AR blockers; speculating that in heart failure, where circulating levels of norepinephrine (a non-specific adrenergic receptor agonist) are known to be elevated [59], β-AR blockers might act to disinhibit the upregulation of endogenous RXFP-1 and

downstream antifibrotic effects. Furthermore, Moore *et al.* showed that the α-AR-mediated RXFP-1 upregulation was abolished by selectively inhibiting the PKC or ERK signaling pathways, suggesting their involvement in the mechanism of RXFP-1 regulation [60]. Since both of these pathways are activated downstream of RXFP-1 activation, this finding could indicate a potential positive feedback mechanism. Further studies are required, possibly involving gene silencing or targeted inactivation of players in the fibrosis pathway, to elucidate the molecular mechanisms and pathological significance of the regulation of the endogenous relaxin receptor-ligand system.

6.2 EXOGENOUS RELAXIN ADMINISTRATION REVERSES LV FIBROSIS AND IMPROVES DIASTOLIC FUNCTION

Previous treatment studies have shown that exogenous relaxin administration has the ability to reverse established fibrosis and repair diastolic dysfunction *in vitro* [23] and at least partially *in vivo* (**Table 1**). Our work has confirmed that 14 days of rhRLX administration is capable of significantly improving diastolic function at the whole organ level, presumably through the reversal of LV fibrosis by NO-mediated mechanisms. We first confirmed that the MREN rats exhibit significant hypertension and hypertrophy, and administration of rhRLX had no effect on these precursors to diastolic dysfunction. Hence, we wanted to assess the presence and expression patterns of gene-level biomarkers of fibrosis in MREN rats and how administration of rhRLX may interfere at the level of mRNA expression.

6.2.1 Gene-Level Regulation of Fibrotic Biomarkers

The significant upregulation of the profibrotic cytokine TGFβ in MREN-V was consistent with other studies in this model [61]. As detailed in **Section 1.3**, TGFβ plays a major role in collagen synthesis by activating the Smad signaling pathway that results in profibrotic gene transcription and fibroblast to myofibroblast transition. Administration of rhRLX was capable of reversing the profibrotic upregulation of TGFβ in MREN-R to baseline levels not different from SD controls. The inhibition of collagen synthesis via TGFβ regulation has been confirmed in other rhRLX-treatment studies [23, 26, 62] and in the MREN model, specifically [42, 61]. While no assays were performed to quantify collagen synthesis directly, it has been shown that rat TGFβ-treated fibroblasts have significantly increased protein-level expression of α-SMA which facilitates myofibroblast transition, and administration of rhRLX recovers this profibrotic response to baseline levels of non-treated cells [23]. Furthermore, Samuel *et al.* showed in their 2008 study utilizing the MREN rat model that diabetic (streptozotocin-treated) MREN rats treated with rhRLX had significantly reduced α-SMA compared with vehicle-treated MREN and this was associated with a significant reduction in cardiac collagen concentration [42].

Brain natriuretic peptide (BNP) is locally expressed by the ventricles in conditions of cardiac overload and is known to act as a natural diuretic in response to an overactive renin-angiotensin system. With respect to fibrosis, BNP has been identified as a bioactive signaling molecule that activates downstream pathways of collagen turnover, including the matrix metalloproteinases (MMPs) [63]. It is likely that the upregulation of BNP expression in LV from both MREN-V and MREN-R is related to their genotype of an overactive RAS, and less to do with fibrosis mechanisms.

While the biological role of MMPs is to degrade mature collagen networks, a pillar of diastolic heart failure is the excessive turnover of collagen, with both synthesis and degradation mechanisms activated [4]. Fibrotic overexpression of MMP-2 was present in the MREN-V model, and as in the aged SHR model [62], this phenotype was reversed by rhRLX administration and normalized to baseline levels. There were no detectable differences in the expression of MMP-9 across all groups. These results conflict with previous *in vitro* experiments that report an increase in MMP-2 and MMP-9 gene expression and activity in TGFβ-treated fibroblasts after receiving rhRLX treatment. Because of the gene-level evidence that administration of rhRLX inhibits TGFβ production and does not increase MMP expression, it seems that the antifibrotic effects of relaxin are targeted to collagen synthesis and less involved with degradation pathways. A better understanding of the degradation mechanisms involved with the reversal of fibrosis by administration of rhRLX will require a broader examination of the gene- and protein-level expression and activity of multiple MMPs and of their endogenous inhibitors (tissue inhibitors of metalloproteinases, TIMPs).

In agreement with our findings that endogenous relaxin receptor-ligand expression is upregulated in a fibrotic environment (**Section 6.1**), the reversal of LV fibrosis by administration of rhRLX also normalized the endogenous expression of RXFP-1 and reduced the expression of relaxin-1 and relaxin-3. Since the regulatory mechanisms that govern endogenous relaxin receptor-ligand system expression are still widely disputed, we can only speculate that profibrotic pathways (possibly involving TGFβ) may contribute to adaptive upregulation of the endogenous relaxin receptor-ligand system and by eliminating this stimulus, administration of rhRLX restores the endogenous relaxin system to baseline levels for healthy collagen regulation.

6.2.2 Reversal of Interstitial and Perivascular Fibrosis

Pronounced LV interstitial and perivascular fibrosis is hallmark of the hypertensive MREN model [13, 42, 64-66]. Here, we have confirmed that 14 days of rhRLX administration is capable of reversing both interstitial and perivascular fibrosis in MREN, as shown previously [42], and we have expanded on this finding to include an element of regional dependence of collagen accumulation in this model.

Perivascular fibrosis has long been associated with the progression of HHD to diastolic dysfunction because of the perivascular inflammation that occurs in response to the pressure-overloaded LV. In the early stages of HHD, LV fibrosis is mainly observed in the perivascular space where the vascular endothelium is in contact with profibrotic cytokines (like TGFβ) and extends radially outward to the interstitial space [8]. For these reasons, perivascular fibrosis in the MREN model has been used as an indicator of a fibrotic phenotype [65, 66] and was consistent in our results. The concept of a collagen gradient in the radial direction from the blood-contacting endothelium outward can be adapted from the vasculature to explain the heterogeneity of collagen deposition in the LV endocardium versus the epicardium. The chemical influences occurring at the LV endothelium may work alone or in concert with mechanical influences of the endocardium itself which is known to behave as a stiffer material than epicardium [67], to promote the region-dependent progression of fibrosis within the myocardial interstitium. Having confirmed that the MREN rat model demonstrates the precursors to diastolic dysfunction – hypertension, hypertrophy, and fibrosis measured at the gene- and tissue-level – and administration of rhRLX was capable of removing the insult of fibrosis, we predicted that MREN would demonstrate impaired LV function and the effects of relaxin would carry through to therapeutically improve this condition.

6.2.3 Left Ventricular Contractility

Exogenous relaxin administration had no significant effect on contractile function in the MREN model. While some previous *in vitro* and *in vivo* studies in rodents suggest a positive inotropic effect in the atria [57], this response was not present in larger animals or humans, nor has a direct effect been confirmed in ventricular tissue [68]. More importantly, we were interested in how diastolic dysfunction would manifest in the fibrotic MREN rats and what effect administration of rhRLX would have on diastolic passive stiffness and LV relaxation.

6.2.4 Improvements to Diastolic Function

The significant reduction in profibrotic gene expression and tissue-level interstitial and perivascular collagen within the LV endocardium after administration of rhRLX was associated with a significant improvement in diastolic function. These compositional level improvements that translate to reduced passive stiffness are due to the increase in nitric oxide (NO)-dependent collagen turnover which occurs downstream of relaxin receptor-ligand binding [27, 30, 36]. The production of NO in response to activated RXFP-1 prevents myofibroblast transition [36] and indirectly upregulates collagen degradation [38] to remodel the myocardial collagen network of cross-linked fibers that contributes to passive stiffness. Evidence of reduced LV passive stiffness after administration of rhRLX was observed in MREN-R as a significant downward shift in slope of the EDPVR compared to MREN-V. This reduction was further validated by the dP_{ed}/dV-P_{ed} relationship which showed that at the same end-diastolic pressures, MREN-R had significantly reduced stiffness coefficients. The downward shifted slope of the end-diastolic stress-midwall strain relationship provided evidence that administration of rhRLX also improved the material

stiffness of the myocardium, most likely due to reduced cardiomyocyte stiffness in response to increased bioavailability of NO.

Diastolic function is defined by both properties of passive stiffness and relaxation. We expected that both properties would be improved in LV treated with rhRLX because of the significant collagen remodeling in the endocardium and increased availability of NO. However, our results showed that rhRLX administration had no effect on LV relaxation in MREN. The maximal rate of pressure relaxation ($-dP/dt_{min}$) was significantly blunted in MREN-V and could not be recovered by rhRLX administration in MREN-R. The relaxation time was also significantly prolonged in both MREN groups versus SD controls with no improvement from rhRLX administration. Hypertension is associated with elevated reactive oxygen species (ROS) that in the presence of increased NO from rhRLX administration may form peroxynitrite (ONOO-). High levels of peroxynitrite have been shown to slow diastolic relaxation by modifying myocardial protein structure and function, particularly affecting Ca^{2+} reuptake by the sarcoplasmic reticulum [9]. Therefore, we suspect that while diastolic passive stiffness is improved by relaxin's NO-mediated reduction in myocardial collagen, the adverse pathways involving ONOO- may still be at play preventing an improvement in relaxation.

Despite the persistent relaxation dysfunction, we conducted a final experiment to test the effect of administration of rhRLX under cardiac stress, which is a clinical problem from patients with diastolic heart failure. We increased the pacing during the Frank-Starling protocol to simulate increased heart rate as a condition of cardiac stress. By examination of the EDPVR, passive stiffness was slightly elevated in the SD controls consistent with what is seen clinically. The fibrotic MREN-V rats had a much more dramatic response to the elevated heart rate and passive stiffness was significantly increased, which would pose a danger for patients in diastolic

heart failure. Administration of rhRLX to MREN-R effectively reduced this passive stiffness (evidenced by a significant reduction in ΔEDP-volume relationship) and these rats were significantly less affected by the cardiac stress condition compared to MREN-V that had not received treatment, which is an important clinically relevant finding.

6.2.5 Targeted Effects of Relaxin to Fibrotic Environment

A major therapeutic advantage of exogenous relaxin therapy is the ability of the hormone to selectively prevent and reverse a fibrotic phenotype without damaging baseline collagen levels. While fibrotic dysregulation of collagen is detrimental to proper cardiac function, healthy collagen turnover is responsible for many structural and mechanical properties of the myocardium. Disease-targeted effects of rhRLX administration have been observed in models of renal [25, 26], lung [26], and cardiac [62] fibrosis. For these reasons, we omitted the treatment control group (SD-R) from our analysis of exogenous relaxin administration. We have previously confirmed that rhRLX administration elicits no unwanted treatment effects in a similar normotensive rat model (Wistar-Hannover, WHAN). These data are presented in **Appendix C**.

6.2.6 Study Limitations

One of the major findings of this work is that administration of exogenous relaxin is capable of reducing myocardial collagen, and we attribute this to mechanisms associated with collagen synthesis downstream of TGFβ. However, no assays beyond the gene-level mRNA expression of TGFβ were performed to confirm this conclusion. Previously, the MREN rat was studied as a

model of diabetic cardiomyopathy (streptozotocin-treated) and exogenous relaxin was administered for 14 days following the same methods used here [42]. In this study, the reversal of interstitial fibrosis by relaxin was associated with reduced protein-level expression of alpha-smooth muscle actin (αSMA), which is commonly used as an indicator of fibroblast to myofibroblast transition and hence collagen synthesis. Because of this previous report, we did not include this assay as part of our experimental design.

We found that the MREN rat model did not have increased contractility despite its hypertensive and hypertrophic state, like we expected (**Section 5.2.5**). The nature of the isolated, perfused heart protocol requires the assessment of cardiac function outside of known contributors to contractility like the sympathetic nervous system. This is a limitation that might have led to the unexpected results we observed; however, since the scope of this work did not require a complete assessment of contractile function, we did not include further analysis. To assess the contractile function and kinetics of contraction in the MREN model, future studies could be designed which involve the conductance catheter method that measures LV systolic and diastolic function *in vivo* or the cardiomyocytes could be isolated and tested for contractile force using methods described in **Section 8.2**.

We acknowledge that the systemic delivery of exogenous rhRLX may not be optimal since high dosages are required to achieve therapeutic antifibrotic effects. For the purposes of this work, we implemented a dosage and treatment duration for administration of rhRLX which was shown previously to be therapeutic [21, 25, 40-42, 62] and validated by our own preliminary studies (**Appendix B**). However, the half-life of recombinant human relaxin-2 is relatively short and clearance through the kidneys can occur in as little as 5 hours (in non-pregnant rabbits [69]), therefore continued systemic infusion of rhRLX is necessary for therapeutic reversal of fibrosis

but may have off-target effects. This speaks to the development of a localized delivery scheme and future studies are currently being considered which include localized infusion of exogenous rhRLX in the pericardial space.

Finally, it is acknowledged that myocardial collagen plays an important role in healthy heart function; it provides structural support and prevents excessive chamber dilation (or myocyte stretch). Therefore, theoretically, reducing collagen may have adverse consequences. While we provide evidence that 14 days of rhRLX administration is effective for reversing interstitial and perivascular fibrosis and providing functional improvements during diastole, we did not include specific *in vivo* experiments to confirm that administration of relaxin has no detrimental effects on the structural integrity of the LV. We have, however, shown that administration of relaxin has no effect on LV dilation under *ex vivo* conditions since there are no differences between V_0 (**Figure 22**) or V_{max} between MREN rats treated with rhRLX or vehicle treatment (V_{max}: 184±3 and 188±5 μl, respectively). We also conducted a study in normotensive Wistar-Hannover rats and confirmed that administration of rhRLX has no collagen-reducing effects in healthy tissue (**Appendix C**). Thus, relaxin-induced reduction in collagen concentration appears to be selective ("intelligent"): it reduces collagen only when there is fibrosis. Furthermore, there is no evidence of any adverse effects of relaxin treatment on ventricular structure. Additional studies are necessary to identify mechanisms underlying this "intelligent" antifibrotic effect of relaxin.

7.0 TAKE HOME MESSAGES

Endogenous mRNA expression of the relaxin receptor-ligand was measured in three models of aging and hypertension to detect the natural response of the relaxin system to an environment of fibrosis. The aged SHR model and the transgenic MREN model both represent severe hypertension and LV hypertrophy that progresses toward heart failure in a similar fashion to that seen in humans [15, 16, 70]. In all models, evidence of modest upregulation of relaxin-1 and relaxin-3 and significant upregulation of RXFP-1 was detected in LV from the fibrotic group. This finding confirms a natural adaptive response of the relaxin system in failing heart tissue, yet this compensatory mechanism is not sufficient to reverse the fibrotic phenotype in these animal models. Administering exogenous relaxin treatment for 14 days can reverse the fibrotic phenotype and improve diastolic passive stiffness. These findings may contribute to a clinically relevant strategy for treating diastolic heart failure.

8.0 FUTURE DIRECTIONS

The topics and findings discussed herein present several opportunities for future studies addressing the antifibrotic effects downstream of relaxin receptor-ligand binding to improve diastolic function. Specifically, we have reviewed that exogenous relaxin binding its primary receptor RXFP-1 acts to regulate collagen synthesis, presumably through mechanisms involving NO. Therefore, future efforts focusing on NO upregulation may be as effective, or more effective, for achieving the therapeutic effects seen in the exogenous relaxin administration studies. Similarly, combination therapies may also be considered which include known anti-hypertensive drugs or anti-inflammatories in addition to antifibrotic relaxin to improve diastolic function by both reducing passive stiffness and improving ventricular relaxation. It will also be beneficial to study the functional effects of such therapies zoomed in to the level of cardiomyocyte and myofilament dynamics. Potential strategies for developing these future studies are considered below.

8.1 COMBINATION THERAPIES

It has been shown that relaxin binding to its primary receptor RXFP-1 initiates a signaling cascade that results in the upregulation of NO production that has downstream antifibrotic effects (**Figure 1**). Therefore, the question presents, "Why not simply upregulate NO production as a

therapeutic approach?" This is a reasonable consideration, and will likely be addressed as further studies implementing antifibrotic approaches against diastolic dysfunction are developed. Below, we propose a few possible therapeutic strategies and their implications in models of diastolic heart failure.

8.1.1 Exogenous Relaxin and Anti-Hypertensive Medication

As described in **Section 1.1**, hypertension is the primary precursor to diastolic dysfunction since it provides stimuli for increasing hypertrophy (elevated afterload) and fibrosis (increased TGFβ and production and cross-linking of myocardial collagen). Therefore, it seems logical that including anti-hypertensive medication along with antifibrotic relaxin may improve diastolic function by reducing the precursors to diastolic function.

There are currently several anti-hypertensive drugs available clinically which serve to reduce blood pressure by different pathways. Diuretics (many involving vasodilatory properties) help the kidneys eliminate excess salt and water from the body's tissues and blood. ACE inhibitors inhibit the activation of angiotensin-converting enzyme (ACE), an enzyme responsible for the conversion of angiotensin I into angiotensin II, a potent vasoconstrictor. Similar to ACE inhibitors, angiotensin II receptor blockers (ARBs) work by antagonizing the activation of angiotensin receptors. Diuretics, ACE inhibitors, and ARBs may be beneficial for reducing the mechanical work of the heart and thereby removing the stimuli that increase hypertrophy and TGFβ production that contribute to fibrosis and diastolic dysfunction. However, these therapies do little to reverse already established fibrosis and diastolic dysfunction. Hence, harnessing the anti-hypertensive effects of these drugs, in concert with relaxin's ability to reverse fibrosis and

restore proper collagen regulation, may be an effective strategy for improving diastolic heart failure.

8.1.2 Exogenous Relaxin and Anti-Inflammatory Medication

The newly proposed paradigm that hypertension leads to a systemic proinflammatory state which increases ROS and ONOO-, in addition to other profibrotic mechanisms, introduces another potential target for intervention. Furthermore, we attributed the lack of improvement to ventricular relaxation after exogenous relaxin administration to the persistence of ONOO- disabling proper cardiomyocyte relaxation. To improve this condition, research has focused on the use of substances with antioxidative properties such as statins and resveratrol. It may be that including an anti-inflammatory to improve ventricular relaxation in addition to the reversal of fibrosis by exogenous relaxin administration would provide solutions to both impaired relaxation and increased passive stiffness seen in diastolic heart failure.

From **Figure 1**, which was developed as a compilation of many previous studies elucidating the effects downstream of relaxin receptor-ligand binding, we know that the antifibrotic effects of relaxin are attributed mainly to the upregulation of NO production in target tissues. For this reason, we acknowledge that a more appropriate therapeutic approach for reversing the diastolic dysfunction that occurs from increased LV fibrosis may be to focus on NO specifically, and how it can be delivered or upregulated clinically. Sildenafil is a drug that increases NO production by blocking the destruction of NO-producing cGMP by PDE-5. A recent study showed that sildenafil was not able to increase levels of cGMP or improve LV diastolic function, likely because of the reduced bioavailability of NO in heart failure [71]; therefore one could imagine that supplementing the sildenafil-treated system with NO through

exogenous relaxin administration could symbiotically improve diastolic dysfunction by improving ventricular relaxation.

8.2 FUNCTIONAL STUDIES AT THE LEVEL OF CARDIOMYOCYTES

Some questions still remain after completion of **Aim 2**. Mainly, is the reversal of LV passive stiffness that we see after administration of relaxin attributable to the reduction in myocardial collagen, or are there underlying mechanisms at play regarding the stiffness and relaxation properties of the cardiomyocytes? Future studies may be developed to address these questions and provide further detail to the implementation of exogenous relaxin as a therapy for diastolic heart failure.

The functional experiments that we performed provided information about LV contractile and diastolic function in response to administration of relaxin. As explained in **Section 1.1**, the LV is a composite structure that is made up contractile cardiomyocytes, cardiac fibroblasts and extracellular matrix proteins. Therefore, as an addendum to the functional experiments performed on the isolated, perfused heart, we could zoom in to the level of cardiac muscle fibers and cardiomyocytes dissected from animals that have been treated with exogenous relaxin to observe cellular properties of contraction, as well as passive stiffness and relaxation. Isolated fibers are typically representative of the intact myocardium in measurements of cardiac mechanics yet are free from connective tissue and endothelium, which cause significant modification of tissue viscoelastic and contractile properties [72]. Therefore, they are very useful, and sometimes superior, tools for investigating cellular mechanisms of the LV. Recently, researchers have questioned whether the increased myocardial passive stiffness seen in diastolic

heart failure is attributable completely to increased myocardial collagen, or if subcellular contributions involving titin may be responsible.

Cardiomyocyte stiffness is partially dependent on distensibility of the giant cytoskeletal protein titin, which spans half the length of the sarcomere from the Z disk to the M line. Titin functions as a bidirectional spring responsible for early diastolic recoil and late diastolic relaxation of cardiomyocytes [73]. To test the separate influences of titin and collagen in diastolic dysfunction and how administration of relaxin may be beneficial, studies could be designed to disable titin in an environment of fibrosis. For example, a study conducted by Chung *et al.* tested the passive force-length relations of skinned fibers before and after KI/KCl administration. KI/KCl extracts thick and thin filaments leaving titin unanchored and therefore measurements after this perturbation relate to the elasticity of the extracellular matrix alone. By subtracting this relation from the baseline passive force-length relation before KI/KCl administration, the elasticity attributable to titin can be calculated [74]. Borrowing this method, cardiomyocytes isolated from rhRLX-treated animals (or isolated cardiomyocytes pretreated with exogenous relaxin *in vitro*) would provide information about how administration of relaxin reduces passive stiffness – either through mechanisms involving titin or through regulation of collagen at the tissue level. These experiments will provide further understanding of the mechanisms of relaxin's antifibrotic actions and how it can therapeutically improve diastolic heart failure.

APPENDIX A

EXOGENOUS RELAXIN ADMINISTRATION IN SHR RAT MODEL

This preliminary study was designed to test the compositional (gene- and protein-level indices of LV fibrosis) and functional changes that occur after 14 days of rhRLX administration in the SHR rat model of hypertension. SHR rats aged ~12 months were administered rhRLX (SHR-R, n=14) or vehicle (SHR-V, n=5) by subcutaneous osmotic minipump for 14 days (0.5 mg/kg/day) and effective administration was measured by rhRLX ELISA Assay (**Figure 30**). Hypertension was confirmed in the SHR groups by noninvasive blood pressure tail-cuff (**Table 7**). Sex- and age-matched WKY rats were used as normotensive controls (n=4). Animals were sacrificed at several different experimental end-points and data was shared among collaborative research groups. Gene-level mRNA expression of known profibrotic biomarkers (TGFβ, BNP, MMP2, MMP9) was performed by qPCR. Interstitial LV fibrosis was determined by immunohistochemistry using a primary antibody against collagen-1 protein in frozen LV tissue samples and quantified by image analysis. All qPCR and immunohistochemistry assays in this preliminary study were performed by Wenyu Xiang under the guidance of Dr. Charlie McTiernan. Indices of LV function (systolic and diastolic properties) were measured by the pressure-volume admittance

catheter method performed by Jeff Baust of Dr. Hunter Champion's lab with assistance from Jamie Haney. Data compilation and analysis of findings was performed by Jamie Haney.

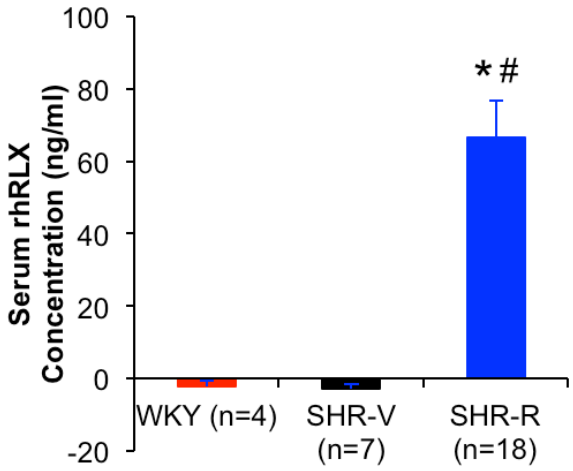

Figure 30. Circulating levels of rhRLX in SHR rat model

Blood serum was collected from all experimental treatment groups. SHR-R, which had received rhRLX by osmotic minipump for 14 days, had significantly elevated serum rhRLX concentration respective to vehicle-treated WKY and vehicle-treated SHR-V. *$P<0.001$ vs. WKY, #$P<0.001$ vs. SHR-R by single-factor ANOVA with *post hoc* Fisher's LSD analysis.

Table 7. Hypertension in the SHR rat

		WKY (n=4)	SHR-V (n=4)	SHR-R (n=14)	*P-value*
	AGE (w)	50.6 ± 0.0	47.9 ± 0.5	50.0 ± 0.9	*NS*
	BODY WEIGHT (g)	436 ± 6	370 ± 3	384 ± 9	<0.01*
HYPERTENSION	DIASTOLIC BP (mmHg)	107 ± 14	147 ± 20	158 ± 6	<0.01*
HYPERTENSION	SYSTOLIC BP (mmHg)	167 ± 15	199 ± 17	204 ± 6	<0.01*
HYPERTENSION	MEAN BP (mmHg)	126 ± 14	164 ± 19	173 ± 6	<0.01*

Data are mean ± SEM. As expected, the well-documented SHR rat model demonstrated significant hypertension versus age- and sex-matched WKY controls rats. Hypertension was not affected by 14 days of rhRLX administration, as there were no statistical differences between SHR-V and SHR-R. *$P<0.01$ represents SHR-V vs. WKY by single-factor ANOVA with Fisher's LSD *post hoc* analysis.

When compared to WKY controls, SHR-V showed upregulated mRNA expression of all known biomarkers of fibrosis: TGF-β, BNP, MMP2, and MMP9. After rhRLX administration, this fibrotic phenotype was reversed significantly to baseline levels (**Figure 31**).

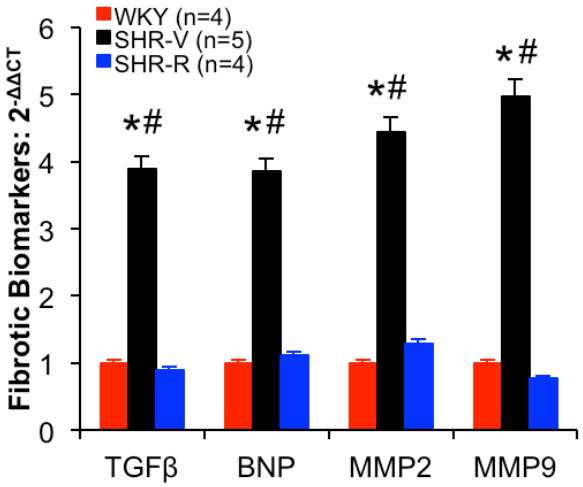

Figure 31. Fibrotic biomarker expression in rhRLX-treated SHR

Fibrotic biomarker mRNA expression for TGFβ, BNP, MMP2, and MMP9 from LV tissue of experimental treatment groups was expressed relative to WKY controls. Gene expression was quantified by real-time qPCR using specific primer assays for the genes of interest normalized by endogenous control gene, GAPDH. SHR-V had significantly elevated expression of all biomarkers versus WKY, and SHR-R showed a significant reduction from the fibrotic response. $*P<0.05$ vs. WKY, $^{\#}P<0.05$ vs. SHR-R by single-factor ANOVA with Fisher's LSD *post hoc* analysis.

Interstitial collagen was measured by immunohistochemistry in frozen endocardial LV samples from all experimental groups. Exogenous relaxin administration significantly reduced LV collagen area fraction (displayed in **Figure 32** as percentage of total tissue area) in SHR-R when compared to SHR-V (2.9% vs. 15.1%, $P<0.05$). LV fibrosis was unaffected by rhRLX administration in normotensive WKY-R compared to WKY-V rats (1.1% vs. 0.73%, $P=0.31$), hence vehicle-treated WKY are used as the control group. **Figure 32** also includes the qualitative

immunostaining of a representative SHR-R and SHR-V samples illustrating the positively stained collagen fraction in red, cytoplasmic staining in green, and nuclear stain in blue.

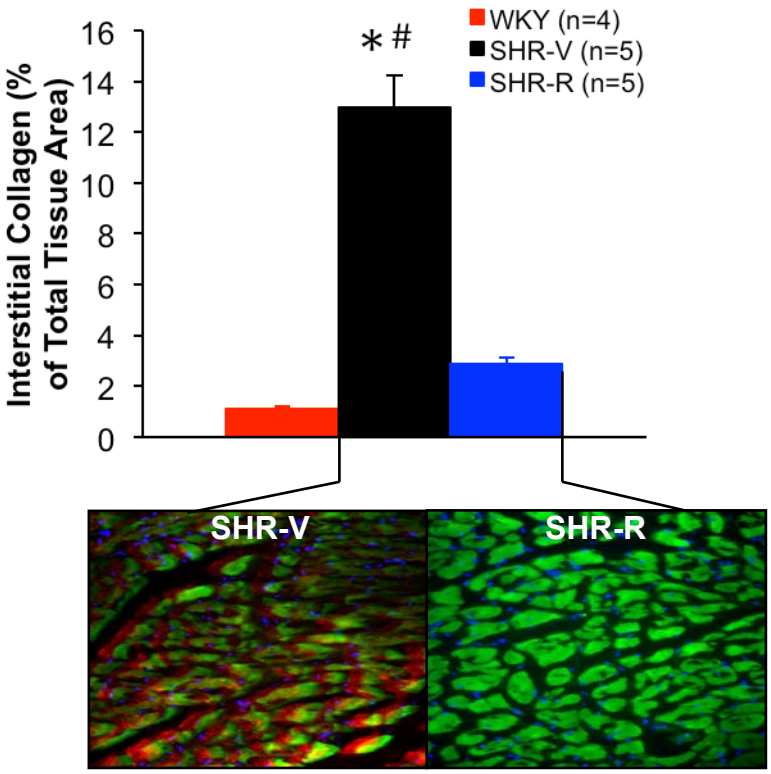

Figure 32. Tissue-level LV fibrosis in rhRLX-treated SHR

Interstitial LV collagen antibody expression (as percentage of total tissue area) was significantly higher in SHR-V compared to WKY. Relaxin administration was able to reverse this expression in SHR-R to where it was not significantly different from WKY. *$P<0.05$ vs. WKY and $^{\#}P<0.05$ vs. SHR-R by single-factor ANOVA with Fisher's LSD *post hoc* analysis.

Although rhRLX administration to SHR-R was able to significantly reverse LV fibrosis on the compositional level, there was no conclusive evidence for functional improvements. There were no significant differences in kinetic indices of contractility ($+dP/dt_{max}$ and rise time) across all experimental groups (**Figure 33**).

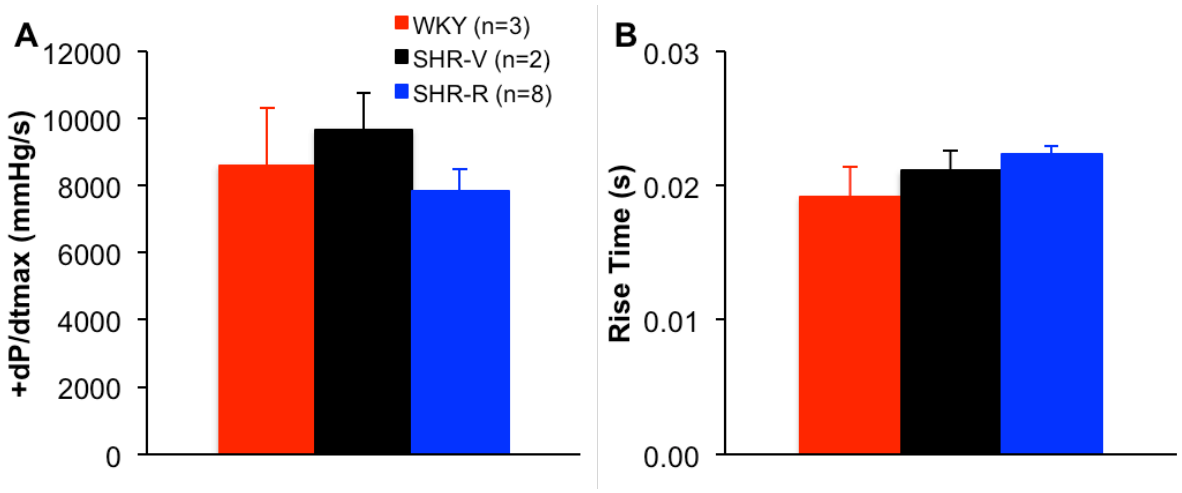

Figure 33. Kinetic properties of contraction in rhRLX-treated SHR

Maximal rate of pressure development ($+dP/dt_{max}$, A) and rise time (B) were determined by pressure-volume admittance catheter. There were no significant differences in either contractile property between the SHR-V and SHR-R (*P>0.05* by single-factor ANOVA).

Similar to contractility indices, rhRLX administration did not significantly affect LV diastolic function. Relaxation ($-dP/dt_{min}$ and relaxation time, **Figure 34**) was measured by the pressure-volume admittance catheter method and passive stiffness was determined by analysis of end-diastolic pressure-volume relationship (EDPVR, **Figure 35**).

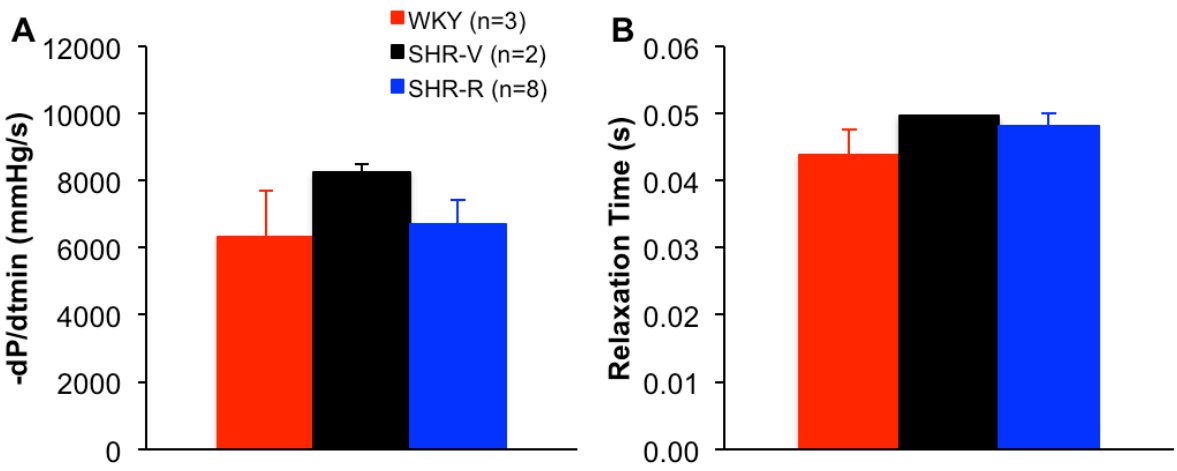

Figure 34. Kinetic properties of relaxation in rhRLX-treated SHR

Maximal rate of pressure relaxation ($-dP/dt_{min}$, A) and relaxation time (B) were determined by pressure-volume admittance catheter. There were no significant differences in either relaxation property between the SHR-V and SHR-R (*P>0.05* by single-factor ANOVA).

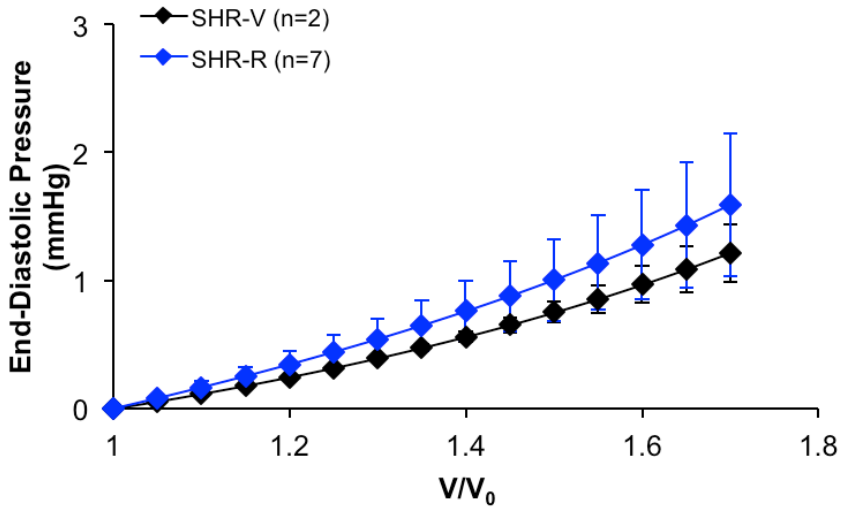

Figure 35. EDPVR in rhRLX-treated SHR

End-diastolic pressure-volume relationships (EDPVR) were obtained for SHR-V and SHR-R by non-linear curve fitting using an exponential model of end-diastolic pressure as a function of LV volume. Results were averaged within experimental groups and plotted against normalized volume (V/V_0). There were no significant differences between groups by repeated-measures ANOVA.

Results from this preliminary work provided evidence that exogenous rhRLX administration is capable of reducing established LV fibrosis on the compositional level by reversing upregulated mRNA expression of fibrotic biomarkers and reducing interstitial collagen area fraction. However, no significant functional improvements were observed following rhRLX administration. This was most likely due to small sample sizes due to limited availability of aged rats and complications with the pressure-volume admittance catheter method. The strong antifibrotic response seen in SHR-R provided rationale for continuing the study of exogenous rhRLX administration using a different model of LV fibrosis and diastolic dysfunction (ie. transgenic MREN rat model) and alternate methods for functional measurements (ie. isolated perfused heart method and Frank-Starling protocol).

APPENDIX B

ANTIFIBROTIC EFFECTS OF EXOGENOUS RELAXIN AS A FUNCTION OF TREATMENT DURATION

As a supplement to the preliminary study in **Appendix A**, we set out to determine how the antifibrotic effects of administration of exogenous relaxin would present at longer treatment durations. Previously, we have shown that 14 days of exogenous rhRLX administration is capable of eliciting a molecular and compositional rectification from fibrosis in SHR. Interestingly, this effect did not translate to functional changes as assessed through pressure-volume relationships. The goal of this series of experiments was to investigate whether or not a functional change from rhRLX may occur with longer treatment duration.

SHR rats aged ~12 months were administered rhRLX for either two- (SHR-R-2wk, n=4) or four-weeks (SHR-R-4wk, n=4) or vehicle (SHR-V, n=2) by subcutaneous osmotic minipump (0.5 mg/kg/day). Age- and sex-matched WKY rats were used as healthy controls (WKY, n=4). Gene-level mRNA expression of known profibrotic biomarkers (TGFβ, BNP, MMP2, MMP9) was performed by qPCR. Interstitial LV fibrosis was determined by immunohistochemistry using a primary antibody against collagen-1 protein in frozen LV tissue samples and quantified by image analysis. All qPCR and immunohistochemistry assays in this study were performed by

Wenyu Xiang under the guidance of Dr. Charlie McTiernan. Functional parameters of end-diastolic pressure and volume were determined by echocardiography (W. Xiang) in anesthetized animals. Data compilation and analysis of findings was performed by Jamie Haney.

When compared to WKY controls, SHR-V showed upregulated mRNA expression of all known biomarkers of fibrosis: TGF-β, BNP, MMP2, and MMP9. After both rhRLX administration treatment durations, this fibrotic phenotype was reversed significantly to baseline levels (**Figure 36**). Interestingly, prolonged administration of rhRLX did not down-regulate the mRNA expression of these biomarkers of fibrosis past a baseline that was comparable to WKY and there were no differences between the SHR-R-2wk and SHR-R-4wk experimental groups.

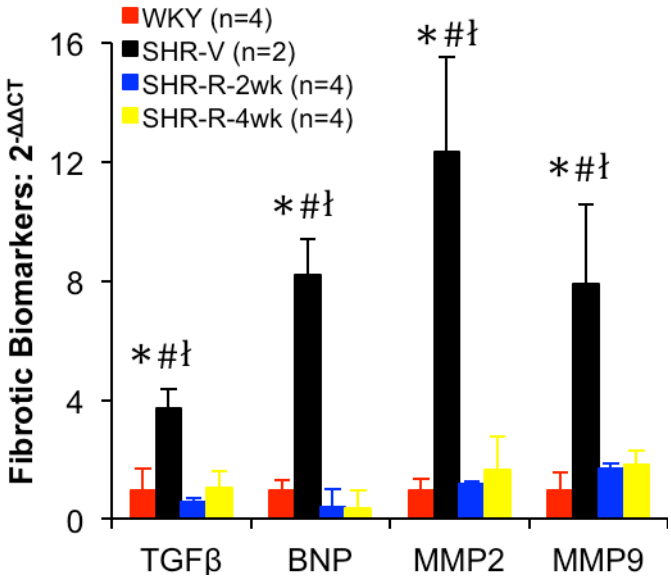

Figure 36. Gene-level fibrosis in SHR after variable rhRLX treatment durations

Fibrotic biomarker mRNA expression for TGFβ, BNP, MMP2, and MMP9 from LV tissue of experimental treatment groups was expressed relative to WKY controls. Gene expression was quantified by real-time qPCR using specific primer assays for the genes of interest normalized by endogenous control gene, GAPDH. SHR-V had significantly elevated expression of all biomarkers versus WKY, and administration of rhRLX showed a significant reduction from the fibrotic response in both SHR-R-2wk and SHR-R-4wk groups. *$P<0.01$ vs. WKY, $^{\#}P<0.01$ vs. SHR-R-2wk, $^{ł}P<0.01$ vs. SHR-R-4wk by single-factor ANOVA with Fisher's LSD *post hoc* analysis.

Interstitial collagen was measured by immunohistochemistry in frozen endocardial LV samples from all experimental groups. Exogenous relaxin administration significantly reduced LV collagen area fraction to a similar extent regardless of treatment duration (displayed in **Figure 37** as a ratio to total tissue area). This result suggests that 14 days of administration of rhRLX is capable of fully reversing fibrotic collagen deposition and prolonged treatment does not lead to continued collagen degradation past healthy levels (i.e. there were no significant differences between either rhRLX treatment group and healthy WKY controls).

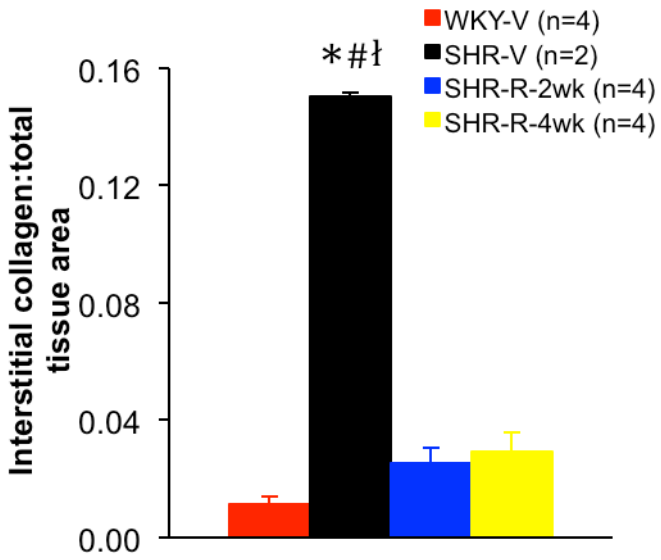

Figure 37. Tissue-level fibrosis in SHR after variable rhRLX treatment durations

Interstitial LV collagen antibody expression (as ratio to total tissue area) was significantly higher in SHR-V compared to WKY. After two (SHR-R-2wk) and four (SHR-R-4wk) weeks, rhRLX administration was able to reverse this expression to where it was not significantly different from WKY. *$P<0.01$ vs. WKY, $^{\#}P<0.01$ vs. SHR-R-2wk, $^{ł}P<0.01$ vs. SHR-R-4wk by single-factor ANOVA with Fisher's LSD *post hoc* analysis.

Both durations of rhRLX administration were able to significantly reverse LV fibrosis on the compositional level to a similar extent, therefore we assumed that functional effects resulting

from administration of rhRLX would be similar in these groups. We did not perform a full characterization of LV contractile and diastolic function. Instead, we performed non-invasive echocardiography to determine the parameters of end-diastolic volume and pressure which would suggest any further improvement to diastolic function than presented in **Appendix A** at the prolonged treatment duration (**Figure 38**). There was no conclusive evidence for functional improvements after four weeks of administration of rhRLX; while the end-diastolic pressure was modestly reduced in SHR-R-4wk compared to SHR-V and SHR-R-2wk, this finding corresponded with modestly reduced end-diastolic volume, so the LV passive stiffness (inferred loosely from this measurement) was unchanged.

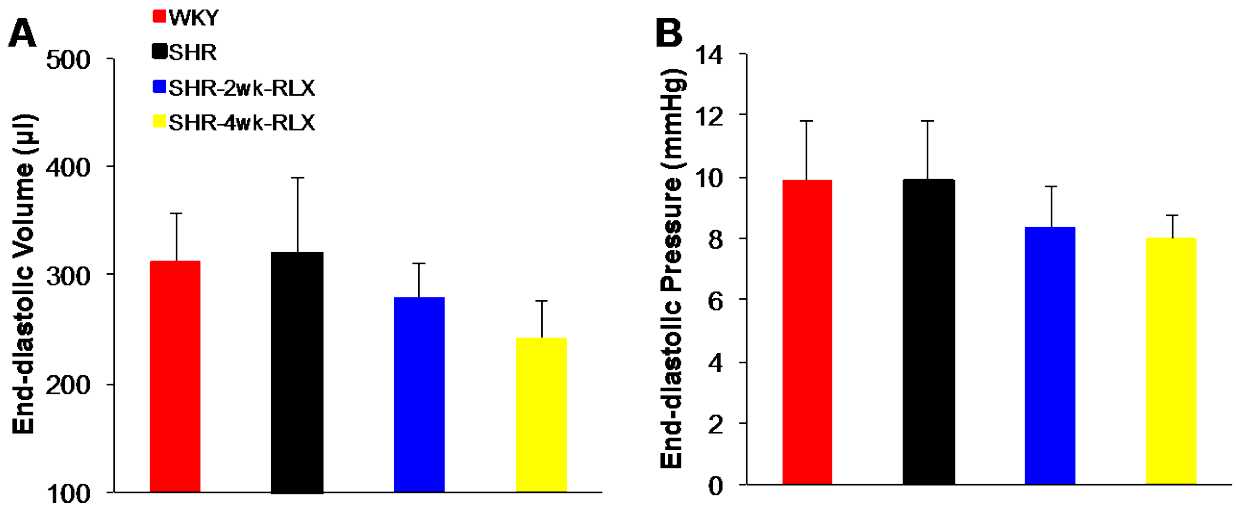

Figure 38. End-diastolic function in SHR after variable rhRLX treatment durations

End-diastolic volume (A) and pressure (B) were determined by non-invasive echocardiography for each of the experimental groups. There were no significant differences between all experimental groups by single-factor ANOVA.

The results from this study provided evidence that 14 days of administration of rhRLX is sufficient for the reversal of compositional-level LV fibrosis and extending this treatment

duration does not seem to further improve diastolic function nor damage healthy collagen deposition in the LV. This study provided the rationale for the dose and duration of exogenous relaxin used in **Aim 2**. A final pilot study was developed following the results presented here. In the study presented in **Appendix C**, we wanted to confirm that 14 days of administration of rhRLX had no unwanted treatment effects on the healthy deposition of collagen or the proper function of the LV in a normotensive animal model.

APPENDIX C

EXOGENOUS RELAXIN ADMINISTRATION IN A NORMOTENSIVE RAT MODEL

In previous work, it has been confirmed that exogenous rhRLX treatment is targeted to fibrosis and does not have an effect on hypertension, hypertrophy, collagen degradation, or functional parameters in healthy animal models [40, 75]. To validate that there were no significant effects of rhRLX administration in a non-fibrotic environment, we utilized the Wistar-Hannover (WHAN) normotensive rat as a treatment control group because of its availability and similarity to other outbred rats, such as SD and WKY [76]. Male, WHAN rats aged ~15 weeks were divided into two treatment groups: rhRLX-treated WHAN (WHAN-R, n=5) and VEH-treated WHAN (WHAN-V, n=4). Exogenous relaxin was administered by osmotic minipump at the same dose and duration as explained in **Section 4.2.2.**

Administration of rhRLX had no effect on blood pressure (as measured by noninvasive blood pressure tail-cuff, **Table 8**) nor heart weights (**Figure 39**) in normotensive WHAN rats.

Table 8. Blood pressures in the WHAN normotensive rat

		WHAN-R (n=5)	WHAN-V (n=4)	*P-value*
	AGE (w)	17.0 ± 0.1	16.9 ± 0.04	*NS*
	BODY WEIGHT (g)	570.2 ± 36.8	486.8 ± 11.2	*NS*
HYPERTENSION	DIASTOLIC BP (mmHg)	96 ± 1	102 ± 10	*NS*
	SYSTOLIC BP (mmHg)	141 ± 4	144 ± 9	*NS*
	MEAN BP (mmHg)	111 ± 2	115 ± 9	*NS*

Data are mean±SEM. Blood pressure was not affected by 14 days of rhRLX administration in age- and sex-matched normotensive WHAN rats (*P>0.05* by Student's t-test).

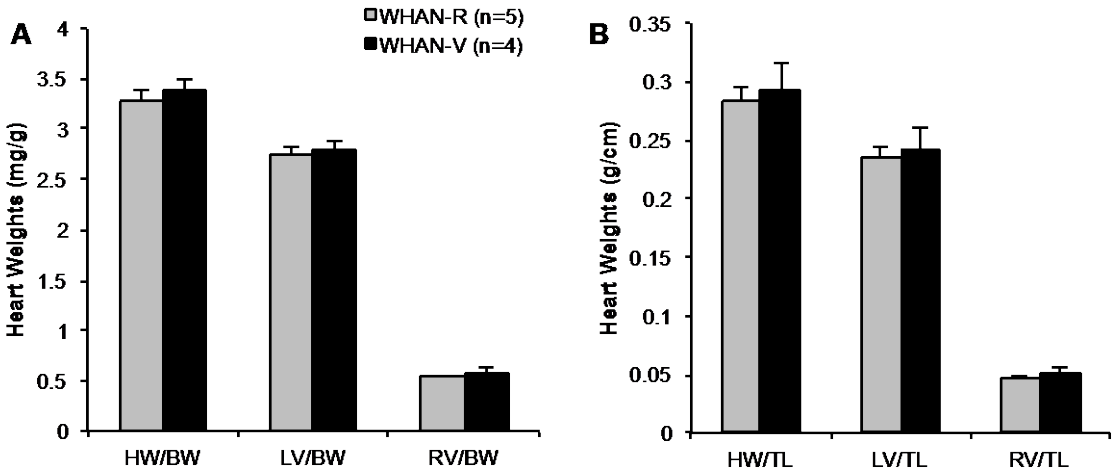

Figure 39. Heart weights in the normotensive WHAN rats

There were no significant effects of rhRLX administration on normalized heart weights (HW), LV, or RV weights in normotensive WHAN rats (*P>0.05* by Student's t-test).

Interstitial and perivascular LV fibrosis was determined by PSR staining on apical LV cross-sections for vehicle- and rhRLX-treated normotensive WHAN rats. There were no significant differences in interstitial collagen within either the epicardial or endocardial region,

and there was not heterogeneity between these regions (**Figure 40A**). Similarly, there were no differences in perivascular collagen between WHAN-V and WHAN-R (**Figure 40B**).

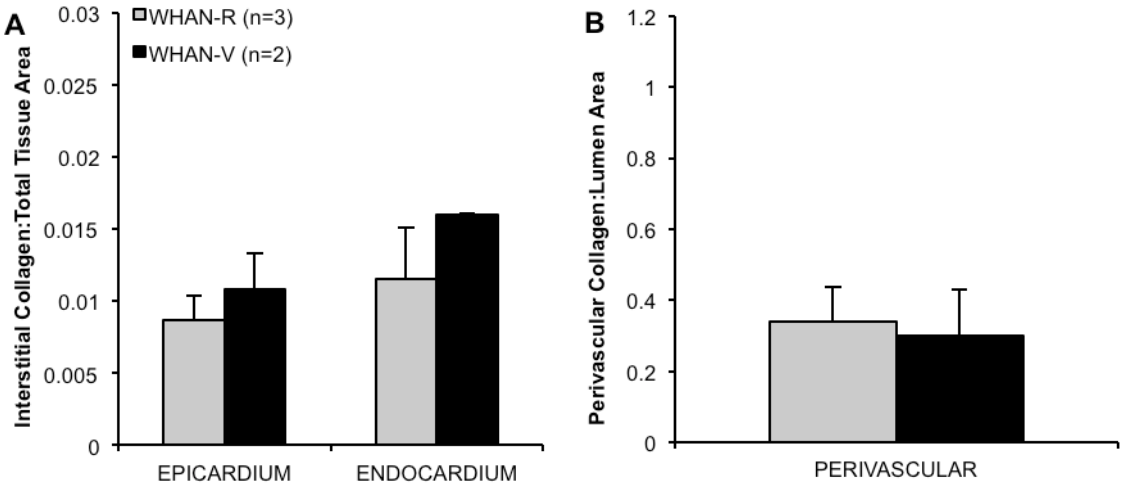

Figure 40. Regional collagen quantification in rhRLX-treated normotensive rats

Images were processed computationally and interstitial and perivascular collagen was quantified for each of normotensive WHAN groups. There were no statistical differences in interstitial or perivascular collagen at the levels of the LV epicardium or endocardium across the groups, regardless of rhRLX administration (*P>0.05* by Student's t-test).

LV function was assessed by the isolated perfused heart method and Frank-Starling protocol as explained previously. Exogenous relaxin administration had no significant effect on PPVR (**Figure 41**), DevPVR (**Figure 42**), or kinetic contractility parameters ($+dP/dt_{max}$ and rise time, **Figure 43**) in normotensive WHAN rats. Similarly, diastolic function was unaffected by rhRLX administration as evidenced by EDPVR (**Figure 44**), and relaxation properties ($-dP/dt_{min}$ and relaxation time, **Figure 45**) in WHAN rats. All pressure-volume relationships are displayed with normalized volume (V/V_0); however, there were no significant differences in LV chamber geometry as indicated by similar V_0 between WHAN-V and WHAN-R (**Figure 46**).

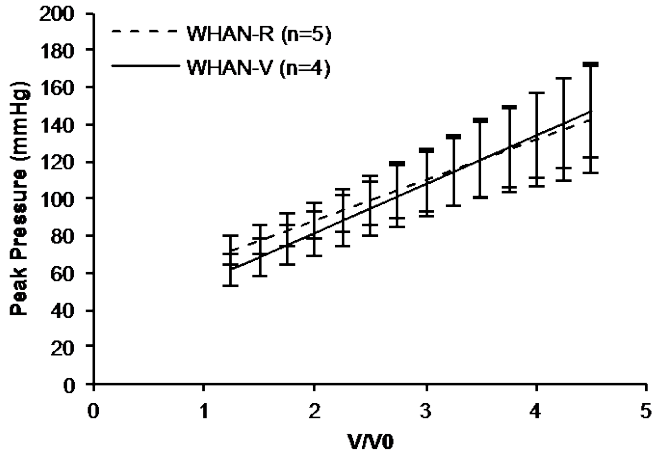

Figure 41. PPVR for rhRLX-treated normotensive rats

LV contractile function, determined by PPVR and plotted against normalized volume, was not significantly affected by rhRLX administration in WHAN rats (*P=0.912* by repeated-measures ANOVA).

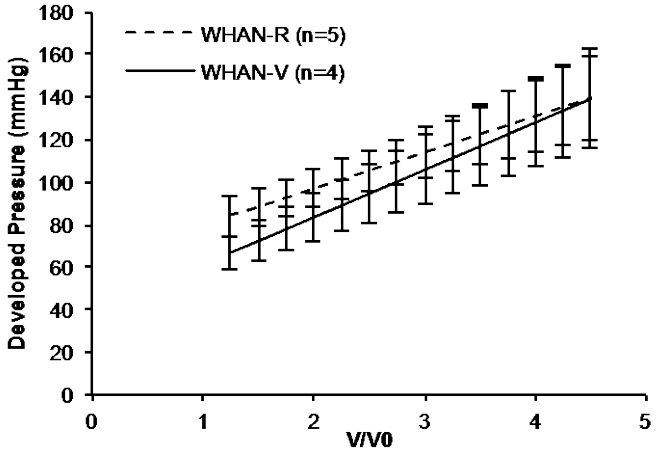

Figure 42. DevPVRs for rhRLX-treated normotensive rats

LV contractile function, determined by DevPVR and plotted against normalized volume, was not significantly affected by rhRLX administration in WHAN rats (*P=0.745* by repeated-measures ANOVA).

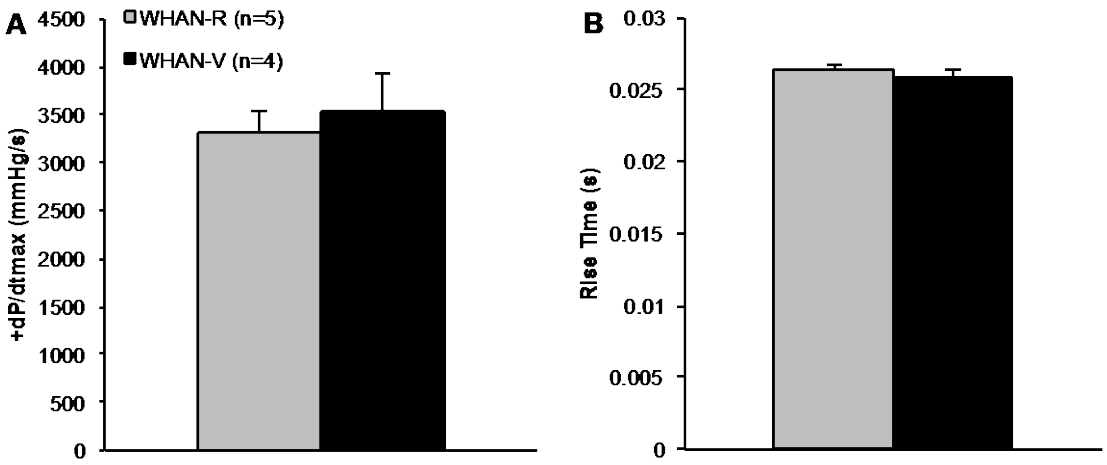

Figure 43. Kinetic properties of contraction for rhRLX-treated normotensive rats

Maximal rate of pressure development ($+dP/dt_{max}$, A) and rise time (B) were determined by the isolated perfused heart method and Frank-Starling protocol. There were no significant differences in either contractile property between the WHAN-V and WHAN-R (*P>0.05* by single-factor ANOVA).

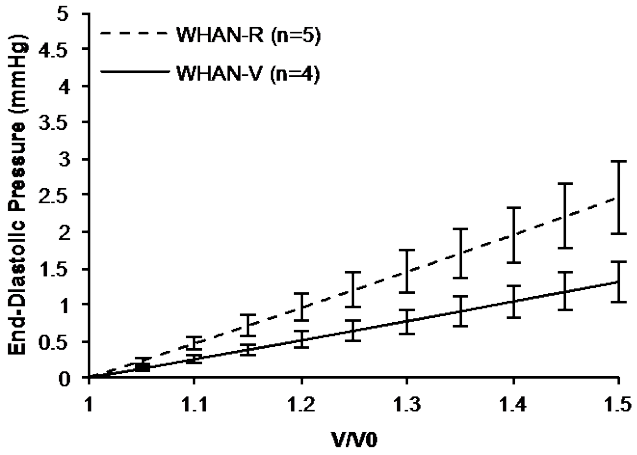

Figure 44. EDPVRs for rhRLX-treated normotensive rats

LV passive stiffness, determined by EDPVR and plotted against normalized volume, was not significantly affected by rhRLX administration in WHAN rats (*P=0.101* by repeated-measures ANOVA).

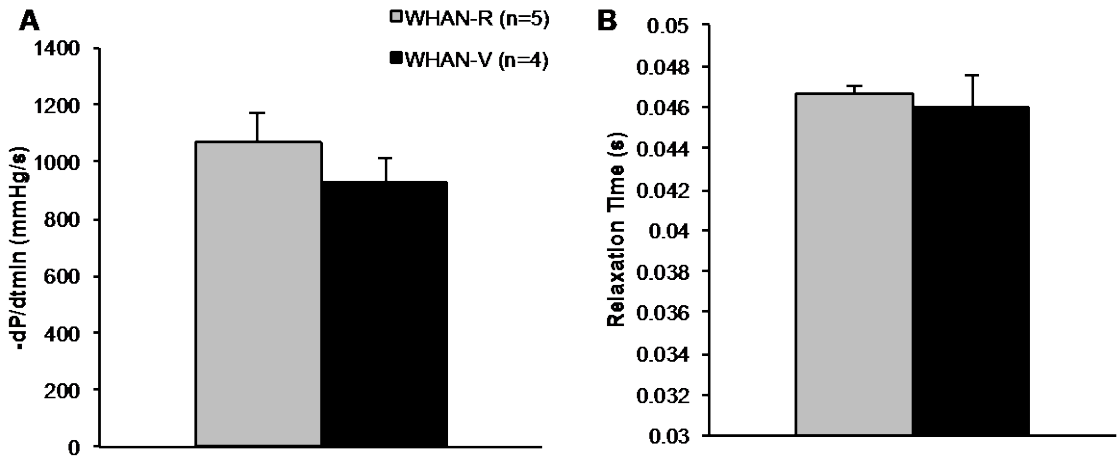

Figure 45. Kinetic properties of relaxation for rhRLX-treated normotensive rats

Maximal rate of pressure relaxation ($-dP/dt_{min}$, A) and relaxation time (B) were determined by the isolated perfused heart method and Frank-Starling protocol. There were no significant differences in either relaxation property between the WHAN-V and WHAN-R (*P>0.05* by single-factor ANOVA).

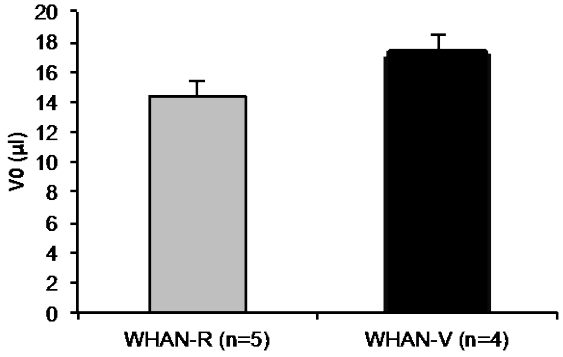

Figure 46. V_0 values for rhRLX-treated normotensive rats

Exogenous rhRLX administration had no effect on LV dilation as evidenced by similar initial chamber volumes corresponding to Ped=0 mmHg (V_0) between WHAN-V and WHAN-R (*P=0.51* by Student's t-test).

These studies in the WHAN rat model provide conclusive evidence that exogenous rhRLX administration does not negatively affect physiological LV structure and function in a normotensive, healthy environment.

APPENDIX D

DETAILED PROTOCOLS

D.1 PICROSIRIUS RED STAINING

This protocol was adapted from that used by Dr. Joseph Janicki at the University of South Carolina. The purpose of this stain is to detect interstitial and perivascular collagen in LV tissue based on the capacity for Sirius red dye to bind fibrillar collagen.

Reagent Preparation	
0.2% Phosphomolybdic Acid (PMA)	
Phosphomolybdic acid	1 g
ddH20	500 ml
1.2% Saturated Picric Acid (Sigma Aldrich)	
Picrosrius Red Dye (PSR)	
Sirius Red/Direct Red	0.4 g
Saturated Picric Acid	400 ml
0.01 N Hydrochloric Acid (HCl)	
6N Hydrochloric Acid	0.7 ml
ddH20	420 ml

Procedure	
Deparaffin	
Rehydration	
Staining:	
0.2% PMA	8 min
ddH20	5 min
PSR	60 min
0.01 HCl	4 min x 2
Dehydration	
ddH20	1 min
70% EtOH	30 s
90% EtOH	30 s
100% EtOH	30 s
100% EtOH	30 s
Mounting	
Xylenes	1 min
Xylenes	1 min
Xylenes	1 min
Mount with Cytoseal XYL and coverslip	

APPENDIX E

PREDICTED UNCERTAINTY IN CALCULATED VARIABLES DUE TO MEASUREMENT INACCURACIES

Several variables are calculated using two or more experimental measurements that are associated with individual measurement inaccuracies, which contribute to the uncertainty of the calculated variables. Let us assume that a calculated variable, Y, is a function of three experimental measurements, x_1, x_2, and x_3, (*Eqn. E1*). The propagated error in Y (ΔY) can be calculated from the individual measurement errors (Δx_1, Δx_2, Δx_3) as shown in *Eqn. E2*.

$$Y = f(x_1, x_2, x_3) \qquad (E1)$$

$$\Delta Y = \left|\frac{\partial Y}{\partial x_1}\right| |\Delta x_1| + \left|\frac{\partial Y}{\partial x_2}\right| |\Delta x_2| + \left|\frac{\partial Y}{\partial x_3}\right| |\Delta x_3| \qquad (E2)$$

where | | denotes absolute value. Two examples of the calculation of the propagated error are provided below: interstitial collagen:total tissue area ratio calculation (**Section E.1**) and gene expression calculation of $2^{-\Delta\Delta Ct}$ for RXFP-1 (**Section E.2**).

E.1 COLLAGEN:TOTAL TISSUE AREA RATIO CALCULATIONS

We used the ratio of interstitial collagen to total tissue area ratio (*Eqn. E3*) to quantify fibrosis in LV from the experimental groups.

$$A_{ratio} = \frac{A_{collagen}}{A_{tissue}} \qquad (E3)$$

Both collagen area and total tissue area were determined by quantifying the positively stained tissue by computational methods. The error associated with these computational methods was determined by running each analysis program three times and calculating the standard deviation of the mean. The ratio of collagen:total tissue area (A_{ratio}) is a function of two measured variables: collagen area ($A_{collagen}$) and total tissue area (A_{tissue}) and therefore the predicted uncertainty in A_{ratio} (ΔA_{ratio}) can be expressed in terms of the measurement inaccuracies of $A_{collagen}$ and A_{tissue} ($\Delta A_{collagen}$ and ΔA_{tissue}, respectively) as follows:

$$\Delta A_{ratio} = \left|\frac{\partial A_{ratio}}{\partial A_{collagen}}\right| \left|\Delta A_{collagen}\right| + \left|\frac{\partial A_{ratio}}{\partial A_{tissue}}\right| \left|\Delta A_{tissue}\right| \qquad (E4)$$

where $\delta A_{ratio}/\delta A_{collagen}$ and $\delta A_{ratio}/\delta A_{tissue}$ are partial derivatives given by (from *Eqn. E3*):

$$\frac{\partial A_{ratio}}{\partial A_{collagen}} = \frac{1}{A_{tissue}} \qquad (E5)$$

$$\frac{\partial A_{ratio}}{\partial A_{tissue}} = -\frac{A_{collagen}}{A_{tissue}^2} \qquad (E6)$$

Using *Eqns. E5-E6* the partial derivates can be calculated at nominal values of $A_{collagen}$ and A_{tissue} as shown in **Table 9**. These derivative values can then be substituted in to *Eqn. E4* to obtain the error in A_{ratio}. For this example, the uncertainty of the collagen:total tissue ratio is estimated to be 12.5%.

Table 9. Error Propagation in Interstitial Collagen:Total Tissue Area Ratio Calculation

	Nominal Value	Error	Error
Measured $A_{collagen}$	9721 pixels	725 pixels	7.5%
Measured A_{tissue}	1207907 pixels	60395 pixels	5.0%
Calculated A_{ratio}	0.008	**0.001**	**12.5%**

E.2 GENE EXPRESSION CALCULATIONS

To calculate the relative expression of genes of interest for **Aims 1 and 2,** we used representative measurements from qPCR experiments and the $2^{-\Delta\Delta CT}$ method. The calculation of $2^{-\Delta\Delta CT}$ depends on the C_T values of the gene of interest and the endogenous reference control gene GAPDH ($C_{T,GOI}$ and $C_{T,GAPDH}$) and this calculation is performed to compare two (or more) experimental groups (ie. C_{T1}, C_{T2}, $C_{T1,GAPDH}$, and $C_{T2,GAPDH}$).

$$2^{-\Delta\Delta C_T} = 2^{-\left((C_{T1}-C_{T1,GAPDH})-(C_{T2}-C_{T2,GAPDH})\right)} \qquad (E7)$$

Therefore, the predicted uncertainty in $2^{-\Delta\Delta CT}$ (Y) can be expressed in terms of the measurement inaccuracies of C_{T1}, C_{T2}, $C_{T1,GAPDH}$, and $C_{T2,GAPDH}$ (ie. ΔC_{T1}, ΔC_{T2}, $\Delta C_{T1,GAPDH}$, and $\Delta C_{T2,GAPDH}$) as follows:

$$\Delta(2^{-\Delta\Delta C_T}) = \Delta(Y) = \left|\frac{\partial(Y)}{\partial(C_{T1})}\right|\left|\Delta(C_{T1})\right| + \left|\frac{\partial(Y)}{\partial(C_{T2})}\right|\left|\Delta(C_{T2})\right| + \left|\frac{\partial(Y)}{\partial(C_{T1,GAPDH})}\right|\left|\Delta(C_{T1,GAPDH})\right| + \left|\frac{\partial(Y)}{\partial(C_{T2,GAPDH})}\right|\left|\Delta(C_{T2,GAPDH})\right| \qquad (E8)$$

The partial derivatives are given by (from *Eqn. E7*):

$$\frac{\partial(Y)}{\partial(C_{T1})} = -2^{-C_{T1}-C_{T2,GAPDH}+C_{T2}+C_{T1,GAPDH}}\ln(2) \qquad (E9)$$

$$\frac{\partial(Y)}{\partial(C_{T2})} = 2^{-C_{T1}-C_{T2,GAPDH}+C_{T2}+C_{T1,GAPDH}} \ln(2) \qquad (E10)$$

$$\frac{\partial(Y)}{\partial(C_{T1,GAPDH})} = 2^{-C_{T1}-C_{T2,GAPDH}+C_{T2}+C_{T1,GAPDH}} \ln(2) \qquad (E11)$$

$$\frac{\partial(Y)}{\partial(C_{T2,GAPDH})} = -2^{-C_{T1}-C_{T2,GAPDH}+C_{T2}+C_{T1,GAPDH}} \ln(2) \qquad (E12)$$

Using *Eqns. E9-E12* the partial derivatives can be calculated at nominal values of C_{T1}, C_{T2}, $C_{T1,GAPDH}$, and $C_{T2,GAPDH}$. These derivative values can then be substituted in to *Eqn. E8* to obtain the uncertainty in $2^{-\Delta\Delta CT}$.

To demonstrate the propagation of error in gene expression calculations from qPCR measurements, we analyzed RXFP-1 gene expression data from MREN-V compared to SD controls (where there is a large fold change in gene expression between groups) and MREN-R compared to SD controls (where there is a small, near 1, fold change in gene expression between groups). The nominal values used for the error analysis of this experiment are shown in **Table 10.** For this example, we assumed that the inaccuracies are the same for each of the four measured variables since they are collected using the same protocol and the same PCR cycler. The PCR cycler is capable of interpolating between cycles and it reports C_T values to the second decimal place. For illustration, we assumed two different accuracies of the PCR cycler: (1) the PCR cycler is capable of measuring accurately within 0.1 cycles (this is the pessimistic scenario) and (2) the PCR cycler is capable of measuring accurately within 0.05 cycles (this is the likely scenario). The uncertainty of the calculated variable, $2^{-\Delta\Delta CT}$, is 27.7% and 13.9% corresponding to the PCR cycler accuracy of 0.1 cycle and 0.05 cycle, respectively (**Table 10**).

Table 10. Error Propagation in RXFP-1 Gene Expression Calculation

	Nominal Value	Error-1 (pessimistic)	Error-1 (%) (pessimistic)	Error-2 (likely)	Error-2 (%) (likely)
Measured C_{T1}	21.5 cycles	0.1 cycles	0.5%	0.05 cycles	0.2%
Measured C_{T2}	23.4 cycles	0.1 cycles	0.4%	0.05 cycles	0.2%
Measured $C_{T1,GAPDH}$	18.0 cycles	0.1 cycles	0.6%	0.05 cycles	0.3%
Measured $C_{T2,GAPDH}$	16.9 cycles	0.1 cycles	0.6%	0.05 cycles	0.3%
Calculated $2^{-\Delta\Delta CT}$	**8.0**	**2.2**	**27.7%**	**1.1**	**13.9%**

APPENDIX F

MATLAB PROGRAMS

F.1 QUANTIFICATION OF INTERSTITIAL AND PERIVASCULAR COLLAGEN FROM PICROSIRIUS RED STAINED IMAGES

Two programs were used to compute the interstitial collagen:total tissue area and perivascular collage:lumen area ratios used for the quantification of protein-level fibrotic deposition in images for picrosirius red stained slides. The first program, ImageJ, was used to manually color threshold whole tissue images to determine total tissue area in pixels. A manual trace tool was used to measure the lumen area in pixels for perivascular tissue images. Both of these measurements were exported from ImageJ and used as the normalization factor for interstitial or perivascular collagen pixel measurements made from a custom MATLAB program. This program is used to computationally quantify positive collagen staining based on intensity thresholding at 3 user-designated representative sections of each image. The code for the program is as follows:

```
clear all
close all
clc

[datafile,pathname] = uigetfile('*.tif','Choose Data File');
```

```
addpath(pathname)
I=imread(datafile);

%Separating out the green filter from RGB and converting to grayscale
G=I(:,:,2);
G2=mat2gray(G);

%Eliminating uneven exposure background
G2inv=imcomplement(G2);
background=imopen(G2inv,strel('disk',15));
G3inv=G2inv-background;

%Selecting regions of collagen for intensity thresholding
G3inv_orig=G3inv;
figure;imshow(G3inv_orig)
title('Pick 3 areas that represents positive collagen stain')
selection=ginput(3);

x=round(selection(:,1));
y=round(selection(:,2));
for i=1:1:3
   colthresh(i)=G3inv(y(i),x(i));
   results(i)=colthresh(i);
end
i=i+1;
close all

%Defining, displaying, and saving collagen pixel area
meancolthresh=(mean(colthresh)-(mean(colthresh)*0.15));
G3inv(G3inv>=meancolthresh)=1;
figure;
H2=imshow(G3inv);
filename=['coll_',datafile];
saveas(H2,filename);

%Calculate collagen
collagen=length(find(G3inv==1));

results(i)=collagen;
G3inv=G3inv_orig;

fid1 = fopen('PSR Provis Results.txt', 'a');
fprintf(fid1,' %9.4f %9.4f %9.4f %9.4f',results);
fprintf(fid1,'%s\n','');
```

F.2 ANALYSIS OF FRANK-STARLING DATA FROM ISOLATED PERFUSED HEART SYSTEM

The purpose of this program is to analyze data collected from LabChart for isolated heart studies on the rat left ventricle. The code for the program is as follows:

```
clear
close all

current=cd;
[datafile,pathname] = uigetfile('*.txt','Choose Data File');
addpath(pathname)
data = textread(datafile,'','delimiter',' ','headerlines',9);
[rows,columns] = size(data);

Frank_time = data(:,1);            %unit: s
Frank_Pressure = data(:,3);        %unit: mmHg
Frank_trig = data(:,2);            %unit: n/a

%Changes Frank Starling trigger to digital (on/off) signal
for n = 1:length(Frank_trig)
   if Frank_trig(n) < 1            %Baseline trigger = ~0.155
      Frank_trig(n) = 0;
   else
      Frank_trig(n) = 1;           %Trigger spike = ~3.34
   end
end

%Cleaning up any noise in the trigger spikes
for n=length(Frank_trig):-1:2
   if Frank_trig(n-1)>0
      Frank_trig(n)=0;
   end
end

%            FRANK STARLING ANALYSIS            %

Do_Frank_Analysis = questdlg('Perform Frank Starling Analysis?',...
   'FS Analysis','Yes','No','???','Yes');

if Do_Frank_Analysis == 'Yes'

   islast = 'n';
```

```
counter = 1;

% Opens files for data export and writes datafile name
fid1 = fopen('Matlab Analysis Results.txt', 'a');
textheader = ['Pdev Pes Ped Volume relax_time rise_time sdev',...
   'dSdt_max dSdt_min dPdt_max dPdt_min'];
fprintf(fid1,'%s',datafile);
fprintf(fid1,'%s\n','');
fprintf(fid1,'%s %s %s %s %s %s %s %s %s %s %s',textheader);
fprintf(fid1,'%s\n','');

%User enters muscle mass (g) for Stress Calculation
prompstr = {'What is the LV mass (g)?        '};
titlestr = 'LV Mass';
initstr = {'1.0'};
n = inputdlg(prompstr,titlestr,1,initstr);
m = str2double(n);

%Insert Balloon Vol for Stress Calculation
prompstr = {'What is the balloon volume (ul)?        '};
titlestr = 'Balloon Vol';
%Determined by calculation 3/2014 (mass = 0.0123g, density = 0.93g/cm3)
initstr = {'13'};
n = inputdlg(prompstr,titlestr,1,initstr);
RefVol = str2double(n);
rho=1.05;   %MacGowan et al. (2004, Circ Res)

while islast == 'n' %Allows the user to enter iterative volumes

   %Sampling frequency *unit=1/s
   sample_freq=1/(data(2,1)-data(1,1));
   deltat = 1/sample_freq;
   section='y';

   %Allows the user to pick different sections on the pressure graph
   while section=='y'

      %Plots Frank Starling data
      figure(2)
      plot(Frank_time,Frank_Pressure);
      title('Pick starting and ending points of the pressure section')

      %Select section of graph to average
      [x,y]=ginput(2);
      find_point1=1;
      while abs(Frank_time(find_point1)-x(1,1)) > 0.1;
```

```
        find_point1=find_point1+1;
    end
    find_point2=find_point1+1;
    while abs(Frank_time(find_point2)-x(2,1)) > 0.01;
        find_point2=find_point2+1;
    end

    %Plot the selected section
    figure(3)
    subplot(2,1,1,'replace');
    plot(Frank_time(find_point1:find_point2), ...
        Frank_Pressure(find_point1:find_point2))
    ylabel('Pressure (mmHg)');
    xlabel('Time (sec)');

    %In case the section you chose was not clean waveforms
    prompstr = {'Do you want to pick a different section? (y/n)'};
    titlestr = 'Formatting Data ...';
    initstr = {'n'};
    n = inputdlg(prompstr,titlestr,1,initstr);
    section=(n{1});
end
clf

Frank_Pressure_segment = Frank_Pressure(find_point1:find_point2);
Frank_time_segment = Frank_time(find_point1:find_point2);
Frank_trig_segment = Frank_trig(find_point1:find_point2);

% Makes sure each segment is the same size (should match pacing, 250)
x = find(Frank_trig_segment>0);
xmin = min(diff(x));

%Compiles Pressure waveforms
for n = 1:length(x)-1
    Pres_compilation(:,n) = Frank_Pressure_segment(x(n):x(n)+xmin-1);
end

%Averages each pressure waveform
Avg_Pressure = mean(Pres_compilation')';
seg_time = [1/sample_freq:1/sample_freq:xmin/sample_freq];

%Added 3/2014: allows user to select point for calculation of EDP
figure
plot(Avg_Pressure,'*')
title('Select a point for EDP')
```

```
%Calculates indices of average pressure waveform
systolic(counter) = max(Avg_Pressure);
[diast_x(counter),diast_y(counter)] = ginput(1);
diast_x(counter) = round(diast_x(counter));
diastolic(counter) =
            mean(Avg_Pressure(diast_x(counter):diast_x(counter)+2));
Pdev(counter) = systolic(counter) - diastolic(counter);
min_dPdt(counter) = min(gradient(Avg_Pressure))/deltat;
max_dPdt(counter) = max(gradient(Avg_Pressure))/deltat;

%t25
count = 1;
Avg_Pressure2 = Avg_Pressure - diastolic(counter);

for n=1:find(Avg_Pressure2==max(Avg_Pressure2));
   if Avg_Pressure2(n)<0.25*(systolic(counter)-diastolic(counter))
      count = count+1;
   end
end
t25_rise = seg_time(count);

%t75
count = 1;
for n=1:find(Avg_Pressure2==max(Avg_Pressure2));
   if Avg_Pressure2(n)<0.75*(systolic(counter)-diastolic(counter))
      count = count+1;
   end
end
t75_rise = seg_time(count);

%Calculates Rise Time
rise_time(counter) = t75_rise - t25_rise;

%Calculates Relax Time
count = find(Avg_Pressure2==max(Avg_Pressure2));
for n=find(Avg_Pressure2==max(Avg_Pressure2)):xmin;
   if Avg_Pressure2(n)>0.75*(systolic(counter)-diastolic(counter))
      count = count+1;
   end
end
t75_relax = seg_time(count);

count = find(Avg_Pressure2==max(Avg_Pressure2));
for n=find(Avg_Pressure2==max(Avg_Pressure2)):xmin;
   if Avg_Pressure2(n)>0.25*(systolic(counter)-diastolic(counter))
      count = count+1;
```

```
    end
end
t25_relax = seg_time(count);
relax_time(counter) = t25_relax - t75_relax;

%Plots average waveform
figure
plot(seg_time,Avg_Pressure)
hold on
plot([0 xmin/sample_freq],[systolic(counter) systolic(counter)])
plot([0 xmin/sample_freq],[diastolic(counter) diastolic(counter)])
hold off

%Dialog box requesting volume and if this is the last volume run
prompstr = {'Current balloon volume (ul)?',...
    'Is this the final volume?        '};
titlestr = 'Frank Starling Protocol';
initstr = {'','n'};
n = inputdlg(prompstr,titlestr,1,initstr);

volume(counter) = str2num(n{1}) %in ul

     %Calculates developed stress for the specific pressure waveform
stressconstant(counter)=(1+(m./(rho.*...
    ((volume(counter)+RefVol)/1000)))).^(2/3)-1;
sdev(counter)=Pdev(counter)/stressconstant(counter)
stotal=Avg_Pressure/stressconstant(counter);
min_dSdt(counter) = min(gradient(stotal))/deltat;
max_dSdt(counter) = max(gradient(stotal))/deltat;
FinalVol(counter)=(RefVol+volume(counter));  %ul

%Writes to file
Rltnshps=[Pdev(counter);systolic(counter);diastolic(counter);...
    FinalVol(counter);...
    relax_time(counter);rise_time(counter);...
    sdev(counter);max_dSdt(counter);min_dSdt(counter);...
    max_dPdt(counter);min_dPdt(counter);];

if counter == 1
    AvePW(:,counter)=Avg_Pressure;
end

k=length(Avg_Pressure);
k1=length(AvePW);

if k>k1
```

```
        Avg_Pressure=Avg_Pressure(1:k1);
    elseif k1>k
        AvePW=AvePW(1:k,:);
    end

    AvePW(:,counter)=Avg_Pressure;
    Vol(:,counter)=linspace(volume(counter),volume(counter));

    fprintf(fid1,' %9.4f %9.4f %9.4f %9.4f %9.4f %9.4f %9.4f %9.4f',...
        '%9.4f %9.4f %9.4f %9.4f ',Rltnshps);
    fprintf(fid1,'%s\n','');

    islast=(n{2}); %check for last volume run
    counter = counter + 1;
    clear Pres_compilation;
    close all

  end %end of while loop

  %Finish writing data files and close
  border = ['------'];
  fprintf(fid1,'%s',border);
  fprintf(fid1,'%s\n','');
  fclose(fid1);

elseif Do_Frank_Analysis == '???'
  errordlg('Im going to assume that means no.')
  pause
end

%Creates graph of Frank Starling data and certain parameters
subplot(2,3,1)
plot((0:deltat:(deltat*length(AvePW))-deltat),AvePW,(diast_x/1000),diastolic,'r*')
xlabel('Time')
ylabel('Pressure (mmHg)')
title(datafile(1:end-4))
subplot(2,3,2)
plot(volume,Pdev,'bs','LineWidth',1,...
  'MarkerEdgeColor','k','MarkerFaceColor','g', 'MarkerSize',5)
xlabel('Volume (uL)')
ylabel('Developed Pressure (mmHg)')
title(date)
subplot(2,3,3)
plot(volume,rise_time,'bd','LineWidth',1,...
  'MarkerEdgeColor','b','MarkerFaceColor','b', 'MarkerSize',5)
xlabel('Volume (uL)')
```

```
ylabel('Rise Time (ms)')
axis([0 max(volume) 0 0.1])
subplot(2,3,4)
plot(Vol)
ylabel('Volume (uL)')
subplot(2,3,5)
plot(volume,diastolic,'bs','LineWidth',1,...
   'MarkerEdgeColor','k','MarkerFaceColor','g', 'MarkerSize',5)
xlabel('Volume (uL)')
ylabel('Diastolic Pressure (mmHg)')
subplot(2,3,6)
plot(volume,relax_time,'bd','LineWidth',1,...
   'MarkerEdgeColor','b','MarkerFaceColor','b', 'MarkerSize',5)
xlabel('Volume (uL)')
ylabel('Relax Time (ms)')
axis([0 max(volume) 0 0.1])
```

The output from the Isolated Heart Program produces raw end-diastolic pressures at increasing volume steps (in addition to other hemodynamic parameter outputs). These raw data are fitted to the equation for P_{ed} in **Section 4.2.7.5** by MATLAB iterative nonlinear regression using the following code:

```
clear all

global V0

[datafile,pathname] = uigetfile('*.txt','Choose Data File');
addpath(pathname)
data = textread(datafile,'','delimiter',' ');

[rows,cols] = size(data);

%Initial values
A0=1;
B0=0.001;
V0=10;

%Reading in end-diastolic pressure/volume data as .txt file
Vol=data(:,2);
```

```
Ped=data(:,1);

Newx=Vol;
Newy=Ped;

%Condition 1 - Check for initial negative pressures
if Ped(1)<0
   %Separating Ped into positive and negative segments
   j=1;
   k=1;
   for i=1:1:length(Ped)
      if Ped(i)<0
         NegPed(k)=Ped(i);
         VolSeg_Neg(k)=Vol(i);
         k=k+1;
      elseif Ped(i)>0
         PosPed(j)=Ped(i);
         VolSeg_Pos(j)=Vol(i);
         j=j+1;
      elseif Ped(i)==0
         PosPed(j)=0.00001;
         VolSeg_Pos(j)=Vol(i);
         j=j+1;
      end
   end

   %Finding the two points that flank Ped=zero to interpolate
   Ped1 = NegPed(end);
   Ped2 = PosPed(1);
   Vol1 = VolSeg_Neg(end);
   Vol2 = VolSeg_Pos(1);

   %Interpolation to find V0
   NewPed = linspace(Ped1,Ped2,10000);
   NewVol = linspace(Vol1,Vol2,10000);

   for i=1:length(NewPed)
      if NewPed(i) < 0
         NewPed(i) = 0;
      end
   end

   %Find the location where the first non-negative Ped occurs
   LocPed = find(NewPed);
   LocVol = LocPed(1);
```

```
    %Use that location to set the new first point of the dataset, where
    %Ped~=0 and the corresponding Volume
    Ped0 = NewPed(LocVol);
    V0 = NewVol(LocVol);

    %Reset the original datasets using the new initial points
    Newx = [V0 VolSeg_Pos];
    Newy = [Ped0 PosPed];

    %Condition 2 - Check if starting Ped is greater than 0
elseif Ped(1)>0

    %Use the first 3 data points to fit a linear line
    y = Ped(1:3);
    x = Vol(1:3);
    coeff = polyfit(x,y,1);

    %Determine the x-intercept to find a new V0
    V0 = (-coeff(2))/coeff(1);

end

%Exponential curve fitting for 2 coefficients with preset V0
beta0=[A0,B0];
beta=nlinfit(Newx,Newy,@edpvr,beta0);

A=beta(1);
b=beta(2);

%Determining the Volume where Ped=25 by linear extrapolation
if max(Newy)<25
    V25_x = Vol(length(Vol)-2:end);
    V25_y = Ped(length(Ped)-2:end);

    V25_coeff = polyfit(V25_x,V25_y,1);
    V25 = (25-V25_coeff(2))/V25_coeff(1);
else
    for i=1:length(Newy)
        if Newy(i)>20 && Newy(i)<30
            V25=Newx(i);
            break
        end
    end
end

if exist('V25')==1
```

```
   deltaV=V25-V0;
else
   deltaV=0;
   V25=0;
end

NewPed=beta(1)*(exp(beta(2)*(Newx-V0))-1);
figure;
plot(Vol,Ped,'k*',Newx,NewPed,'r')
xlabel('Volume(ul)')
ylabel('End-diastolic Pressure (mmHg)')
plot_res = [beta(1),beta(2),V0];

%Goodness of fit calculations
edpvr_resid=Newy-NewPed;
SS_edpvr_resid=sum(edpvr_resid.^2);
edpvr_resid_total=Newy-(mean(Newy));
SS_edpvr_resid_total=sum(edpvr_resid_total.^2);
edpvr_R2=1-SS_edpvr_resid/SS_edpvr_resid_total;
gtext(['R2 = ',num2str(edpvr_R2)])

% Opens file for data export and writes datafile name and column headers
fid1 = fopen('EDPVR Analysis Results.txt', 'a');
Rltnshps = [beta(1);beta(2);V0;V25;deltaV;edpvr_R2];

fprintf(fid1,' %9.4f %9.4f %9.4f %9.4f %9.4f %9.4f',Rltnshps);
fprintf(fid1,'%s\n','');
```

The code for the model fitting function call ‘edvpr’ is as follows:

```
function NewPed=edpvr(beta0,Newx)

global V0

NewPed=beta0(1)*(exp(beta0(2)*(Newx-V0))-1);
```

The output from the Isolated Heart Program produces raw end-diastolic stresses at increasing volume steps that can be transformed to end-diastolic midwall strain following the equations in

Section 4.2.7.5. To make this transformation, V_0 is required from the interpolation output from MATLAB end-diastolic pressure-volume relationship program (**Appendix F.2.2**). These end-diastolic stress and strain data are fitted to the model equation (**Section 4.2.7.5**) by MATLAB iterative nonlinear regression using the following code:

```
clear all

[datafile,pathname] = uigetfile('*.txt','Choose Data File');
addpath(pathname)
data = textread(datafile,'','delimiter',' ');

[rows,cols] = size(data);

%Initial starting values for curve fitting
A0=1;
B0=10;
beta0=[A0,B0];

%Reading in end-diastolic stress/strain data as .txt file
%Strain must be calculated using V0 from fitedpvr.m code
x=data(:,2);  %strain
y=data(:,1);  %stress

%Check for initial negative stresses
if y(1)<0
   %Separating stress into positive and negative sections
   j=1;
   k=1;
   for i=1:1:length(y)
      if y(i)<0
         Negy(k)=y(i);
         xSeg_Neg(k)=x(i);
         k=k+1;
      elseif y(i)>0
         Posy(j)=y(i);
         xSeg_Pos(j)=x(i);
         j=j+1;
      elseif y(i)==0
         Posy(j)=0.00001;
         xSeg_Pos(j)=x(i);
         j=j+1;
      end
   end
```

```
    %Finding the two points that flank y=zero to interpolate
    y1 = Negy(end);
    y2 = Posy(1);
    x1 = xSeg_Neg(end);
    x2 = xSeg_Pos(1);

    %Interpolation
    Newy = linspace(y1,y2,10000);
    Newx = linspace(x1,x2,10000);

    for i=1:length(Newy)
        if Newy(i) < 0
            Newy(i) = 0;
        end
    end

    %Find the location where the first non-negative stress occurs
    Locy = find(Newy);
    Locx = Locy(1);

    %Use that location to set the new first point of the dataset, where
    %stress~=0 and the corresponding strain
    y0 = Newy(Locx);
    x0 = Newx(Locx);

    %Reset the original datasets using the new initial points
    Newx = [x0 xSeg_Pos];
    Newy = [y0 Posy];

end

beta=nlinfit(Newx,Newy,@stressstrain,beta0);

NewStress=beta(1)*(exp(beta(2)*(Newx))-1);
figure;
plot(x,y,'k*',Newx,NewStress,'r')
xlabel('Strain')
ylabel('End-diastolic Stress (mmHg)')

%Goodness of fit calculation
stressstrain_resid=Newy-NewStress;
SS_stressstrain_resid=sum(stressstrain_resid.^2);
stressstrain_resid_total=Newy-(mean(Newy));
SS_stressstrain_resid_total=sum(stressstrain_resid_total.^2);
stressstrain_R2=1-SS_stressstrain_resid/SS_stressstrain_resid_total
```

```
gtext(['R2 = ',num2str(stressstrain_R2)])

% Opens file for data export and writes datafile name and column headers
fid1 = fopen('SS Analysis Results.txt', 'a');
Rltnshps = [beta(1);beta(2);stressstrain_R2];

fprintf(fid1,' %9.4f %9.4f %9.4f',Rltnshps);
fprintf(fid1,'%s\n','');
```

The code for the model fitting function call 'stressstrain' is as follows:

```
function NewStress=stressstrain(beta0,Newx)

NewStress=beta0(1)*(exp(beta0(2)*(Newx))-1);
```

The output from the Isolated Heart Program produces raw peak and developed pressures at increasing volume steps (in addition to other hemodynamic parameter outputs). These raw data are fitted to the equation in **Section 4.2.7.5** by MATLAB iterative first-order polynomial linear regression using the following code:

```
clear all

[datafile,pathname] = uigetfile('*.txt','Choose Data File');
addpath(pathname)
data = textread(datafile,'','delimiter',' ');

[rows,cols] = size(data);

%Reading in peak (PP) and developed (Pdev) pressure/volume data as .txt file
Vol=data(:,3);
Pdev=data(:,1);
PP=data(:,2);

PP_grad=gradient(PP);
PP_cutoff=PP_grad(1)*0.1;

%Trim PP data at point where pressures plateau (Vmax)
for i=1:length(PP_grad)
```

```
    if PP_grad(i) > PP_cutoff
        NewPP(i)=PP(i);
        NewPdev(i)=Pdev(i);
        NewVol(i)=Vol(i);
        i=i+1;
    else
        break
    end
end

%1st order polynomial fit for PPVR
PP_coeff=polyfit(NewVol,NewPP,1);

E=PP_coeff(1);
Vd=PP_coeff(2)/E;

FitPP=polyval(PP_coeff,NewVol);

figure;
plot(NewVol,NewPP,'k*',NewVol,FitPP,'r')
xlabel('Volume(ul)')
ylabel('Peak Pressure (mmHg)')

%Goodness of fit calculations
espvr_resid=NewPP-FitPP;
SS_espvr_resid=sum(espvr_resid.^2);
espvr_resid_total=NewPP-(mean(NewPP));
SS_espvr_resid_total=sum(espvr_resid_total.^2);
espvr_R2=1-SS_espvr_resid/SS_espvr_resid_total;
gtext(['R2 = ',num2str(espvr_R2)])

%1st order polynomial fit for Developed PVR
Pdev_coeff=polyfit(NewVol,NewPdev,1);

E_dev=Pdev_coeff(1);
Vd_dev=Pdev_coeff(2)/E_dev;

FitPdev=polyval(Pdev_coeff,NewVol);

figure;
plot(NewVol,NewPdev,'k*',NewVol,FitPdev,'r')
xlabel('Volume(ul)')
ylabel('Developed Pressure (mmHg)')

%Goodness of fit calculations
devpvr_resid=NewPdev-FitPdev;
```

```
SS_devpvr_resid=sum(devpvr_resid.^2);
devpvr_resid_total=NewPdev-(mean(NewPdev));
SS_devpvr_resid_total=sum(devpvr_resid_total.^2);
devpvr_R2=1-SS_devpvr_resid/SS_devpvr_resid_total;
gtext(['R2 = ',num2str(devpvr_R2)])

fid1 = fopen('ESPVR Analysis Results.txt', 'a');
Rltnshps = [PP_coeff(1);PP_coeff(2);Vd;espvr_R2;Pdev_coeff(1);...
   Pdev_coeff(2);Vd_dev;devpvr_R2];

fprintf(fid1,' %9.4f %9.4f %9.4f %9.4f %9.4f %9.4f %9.4f %9.4f ',Rltnshps);
fprintf(fid1,'%s\n','');
```

The output from the Isolated Heart Program produces raw developed stress at increasing volume steps that can be transformed to end-diastolic midwall strain following the equations in **Section 4.2.7.5**. To make this transformation, V_0 is required. These developed stress and midwall strain data are fitted to the model equation (**Section 4.2.7.5**) by MATLAB iterative nonlinear regression using the following code:

```
clear all

[datafile,pathname] = uigetfile('*.txt','Choose Data File');
addpath(pathname)
data = textread(datafile,'','delimiter',' ');

[rows,cols] = size(data);

%Reading in developed stress/strain data as .txt file
x=data(:,2);
y=data(:,1);

P=polyfit(x,y,1);
NewStress=polyval(P,x);

figure;
plot(x,y,'k*',x,NewStress,'r')
```

```
xlabel('Strain')
ylabel('Developed Stress (mmHg)')

%Goodness of fit calculations
stressstrain_resid=y-NewStress;
SS_stressstrain_resid=sum(stressstrain_resid.^2);
stressstrain_resid_total=y-(mean(y));
SS_stressstrain_resid_total=sum(stressstrain_resid_total.^2);
stressstrain_R2=1-SS_stressstrain_resid/SS_stressstrain_resid_total
gtext(num2str(stressstrain_R2))

% Opens file for data export and writes datafile name and column headers
fid1 = fopen('SS Analysis Results.txt', 'a');
Rltnshps = [P(1);P(2);stressstrain_R2];
fprintf(fid1,' %9.4f %9.4f %9.4f',Rltnshps);
fprintf(fid1,'%s\n','');
```

BIBLIOGRAPHY

1. Go, A.S., et al., *Heart disease and stroke statistics--2013 update: a report from the American Heart Association.* Circulation, 2013. **127**(1): p. e6-e245.

2. Udelson, J.E., *Heart failure with preserved ejection fraction.* Circulation, 2011. **124**(21): p. e540-3.

3. Filippatos, G., et al., *Serelaxin in acute heart failure patients with preserved left ventricular ejection fraction: results from the RELAX-AHF trial.* Eur Heart J, 2014. **35**(16): p. 1041-50.

4. Martos, R., et al., *Diastolic heart failure: evidence of increased myocardial collagen turnover linked to diastolic dysfunction.* Circulation, 2007. **115**(7): p. 888-95.

5. Berk, B.C., K. Fujiwara, and S. Lehoux, *ECM remodeling in hypertensive heart disease.* J Clin Invest, 2007. **117**(3): p. 568-75.

6. Brilla, C.G., R.C. Funck, and H. Rupp, *Lisinopril-mediated regression of myocardial fibrosis in patients with hypertensive heart disease.* Circulation, 2000. **102**(12): p. 1388-93.

7. Diez, J., *Losartan-Dependent Regression of Myocardial Fibrosis Is Associated With Reduction of Left Ventricular Chamber Stiffness in Hypertensive Patients.* Circulation, 2002. **105**(21): p. 2512-2517.

8. Kai, H., et al., *Diastolic dysfunction in hypertensive hearts: roles of perivascular inflammation and reactive myocardial fibrosis.* Hypertens Res, 2005. **28**(6): p. 483-90.

9. Paulus, W.J. and C. Tschope, *A novel paradigm for heart failure with preserved ejection fraction: comorbidities drive myocardial dysfunction and remodeling through coronary microvascular endothelial inflammation.* J Am Coll Cardiol, 2013. **62**(4): p. 263-71.

10. Ferreira-Martins, J. and A.F. Leite-Moreira, *Physiologic basis and pathophysiologic implications of the diastolic properties of the cardiac muscle.* J Biomed Biotechnol, 2010. **2010**: p. 807084.

11. Westermann, D., et al., *Cardiac inflammation contributes to changes in the extracellular matrix in patients with heart failure and normal ejection fraction.* Circ Heart Fail, 2011. **4**(1): p. 44-52.

12. Mullins, J.J., J. Peters, and D. Ganten, *Fulminant hypertension in transgenic rats harbouring the mouse Ren-2 gene.* Nature, 1990. **344**(6266): p. 541-4.

13. Pinto, Y.M., et al., *Cardiovascular end-organ damage in Ren-2 transgenic rats compared to spontaneously hypertensive rats.* J Mol Med (Berl), 1997. **75**(5): p. 371-7.

14. Langheinrich, M., et al., *The hypertensive Ren-2 transgenic rat TGR (mREN2)27 in hypertension research. Characteristics and functional aspects.* Am J Hypertens, 1996. **9**(5): p. 506-12.

15. Doggrell, S.A. and L. Brown, *Rat models of hypertension, cardiac hypertrophy and failure.* Cardiovasc Res, 1998. **39**(1): p. 89-105.

16. Bing, O.H., et al., *The spontaneously hypertensive rat as a model of the transition from compensated left ventricular hypertrophy to failure.* J Mol Cell Cardiol, 1995. **27**(1): p. 383-96.

17. Cingolani, O.H., et al., *Increased systolic performance with diastolic dysfunction in adult spontaneously hypertensive rats.* Hypertension, 2003. **41**(2): p. 249-54.

18. LeGrice, I.J., et al., *Progression of myocardial remodeling and mechanical dysfunction in the spontaneously hypertensive rat.* Am J Physiol Heart Circ Physiol, 2012. **303**(11): p. H1353-65.

19. Engler, S., M. Paul, and Y.M. Pinto, *The TGR(mRen2)27 transgenic rat model of hypertension.* Regul Pept, 1998. **77**(1-3): p. 3-8.

20. McGuane, J.T. and L.J. Parry, *Relaxin and the extracellular matrix: molecular mechanisms of action and implications for cardiovascular disease.* Expert Rev Mol Med, 2005. **7**(21): p. 1-18.

21. Samuel, C.S., *Relaxin: antifibrotic properties and effects in models of disease.* Clin Med Res, 2005. **3**(4): p. 241-9.

22. Debrah, D.O., et al., *Relaxin regulates vascular wall remodeling and passive mechanical properties in mice.* J Appl Physiol, 2011. **111**(1): p. 260-71.

23. Samuel, C.S., et al., *Relaxin modulates cardiac fibroblast proliferation, differentiation, and collagen production and reverses cardiac fibrosis in vivo.* Endocrinology, 2004. **145**(9): p. 4125-33.

24. Williams, E.J., et al., *Relaxin inhibits effective collagen deposition by cultured hepatic stellate cells and decreases rat liver fibrosis in vivo.* Gut, 2001. **49**(4): p. 577-83.

25. Garber, S.L., et al., *Relaxin decreases renal interstitial fibrosis and slows progression of renal disease.* Kidney Int, 2001. **59**(3): p. 876-82.

26. Unemori, E.N., et al., *Relaxin induces an extracellular matrix-degrading phenotype in human lung fibroblasts in vitro and inhibits lung fibrosis in a murine model in vivo.* J Clin Invest, 1996. **98**(12): p. 2739-45.

27. Bathgate, R.A., et al., *Relaxin family peptides and their receptors.* Physiol Rev, 2013. **93**: p. 405-480.

28. Sherwood, O.D., *Relaxin's physiological roles and other diverse actions.* Endocr Rev, 2004. **25**(2): p. 205-34.

29. Dschietzig, T., et al., *The pregnancy hormone relaxin is a player in human heart failure.* FASEB J, 2001. **15**(12): p. 2187-95.

30. Kong, R.C., et al., *Membrane receptors: structure and function of the relaxin family peptide receptors.* Mol Cell Endocrinol, 2010. **320**(1-2): p. 1-15.

31. Samuel, C.S., et al., *Relaxin deficiency in mice is associated with an age-related progression of pulmonary fibrosis.* Faseb J, 2003. **17**(1): p. 121-3.

32. Samuel, C.S., et al., *Relaxin-1-deficient mice develop an age-related progression of renal fibrosis.* Kidney Int, 2004. **65**(6): p. 2054-64.

33. Du, X.J., et al., *Increased myocardial collagen and ventricular diastolic dysfunction in relaxin deficient mice: a gender-specific phenotype.* Cardiovasc Res, 2003. **57**(2): p. 395-404.

34. Halls, M.L., et al., *Relaxin activates multiple cAMP signaling pathway profiles in different target cells.* Ann N Y Acad Sci, 2009. **1160**: p. 108-11.

35. Moore, X.L., et al., *Relaxin antagonizes hypertrophy and apoptosis in neonatal rat cardiomyocytes.* Endocrinology, 2007. **148**(4): p. 1582-9.

36. Mookerjee, I., et al., *Relaxin inhibits renal myofibroblast differentiation via RXFP1, the nitric oxide pathway, and Smad2.* FASEB J, 2009. **23**(4): p. 1219-29.

37. Nistri, S. and D. Bani, *Relaxin receptors and nitric oxide synthases: search for the missing link.* Reprod Biol Endocrinol, 2003. **1**: p. 5.

38. Ho, T.Y., W. Yan, and C.A. Bagnell, *Relaxin-induced matrix metalloproteinase-9 expression is associated with activation of the NF-kappaB pathway in human THP-1 cells.* J Leukoc Biol, 2007. **81**(5): p. 1303-10.

39. Ahmad, N., et al., *Relaxin induces matrix-metalloproteinases-9 and -13 via RXFP1: induction of MMP-9 involves the PI3K, ERK, Akt and PKC-zeta pathways.* Mol Cell Endocrinol, 2012. **363**(1-2): p. 46-61.

40. Du, X.J., et al., *Reversal of cardiac fibrosis and related dysfunction by relaxin.* Ann N Y Acad Sci, 2009. **1160**: p. 278-84.

41. Lekgabe, E.D., et al., *Relaxin reverses cardiac and renal fibrosis in spontaneously hypertensive rats.* Hypertension, 2005. **46**(2): p. 412-8.

42. Samuel, C.S., et al., *Relaxin ameliorates fibrosis in experimental diabetic cardiomyopathy.* Endocrinology, 2008. **149**(7): p. 3286-93.

43. Hossain, M.A., et al., *H3 relaxin demonstrates antifibrotic properties via the RXFP1 receptor.* Biochemistry, 2011. **50**(8): p. 1368-75.

44. Zhang, J., et al., *Effect of relaxin on myocardial ischemia injury induced by isoproterenol.* Peptides, 2005. **26**(9): p. 1632-9.

45. Glasel, J.A., *Validity of nucleic acid purities monitored by 260nm/280nm absorbance ratios.* Biotechniques, 1995. **18**(1): p. 62-3.

46. Schmittgen, T.D. and K.J. Livak, *Analyzing real-time PCR data by the comparative C(T) method.* Nat Protoc, 2008. **3**(6): p. 1101-8.

47. Whittaker, P., et al., *Quantitative assessment of myocardial collagen with picrosirius red staining and circularly polarized light.* Basic Res Cardiol, 1994. **89**(5): p. 397-410.

48. Hartig, S.M., *Basic image analysis and manipulation in ImageJ.* Curr Protoc Mol Biol, 2013. **Chapter 14**: p. Unit14 15.

49. Feng, M., et al., *Validation of volume-pressure recording tail-cuff blood pressure measurements.* Am J Hypertens, 2008. **21**(12): p. 1288-91.

50. Skrzypiec-Spring, M., et al., *Isolated heart perfusion according to Langendorff---still viable in the new millennium.* J Pharmacol Toxicol Methods, 2007. **55**(2): p. 113-26.

51. de Leiris, J., D.P. Harding, and S. Pestre, *The isolated perfused rat heart: a model for studying myocardial hypoxia or ischemia.* Basic Res Cardiol, 1984. **79**: p. 313-321.

52. Burkhoff, D., I. Mirsky, and H. Suga, *Assessment of systolic and diastolic ventricular properties via pressure-volume analysis: a guide for clinical, translational, and basic researchers.* Am J Physiol Heart Circ Physiol, 2005. **289**(2): p. H501-12.

53. Berger, D.S., et al., *Ejection has both positive and negative effects on left ventricular isovolumic relaxation.* Am J Physiol, 1997. **273**(6 Pt 2): p. H2696-707.

54. MacGowan, G.A., et al., *Troponin I protein kinase C phosphorylation sites and ventricular function.* Cardiovasc Res, 2004. **63**(2): p. 245-55.

55. MacGowan, G.A., et al., *Pressure-calcium relationships in perfused mouse hearts.* Am J Physiol Heart Circ Physiol, 2006. **290**: p. H2614-H2624.

56. Du, X.J., et al., *Increased myocardial collagen and ventricular diastolic dysfunction in relaxin deficient mice: a gender-specific phenotype.* Cardiovascular Research, 2003. **57**: p. 395-404.

57. Kompa, A.R., C.S. Samuel, and R.J. Summers, *Inotropic responses to human gene 2 (B29) relaxin in a rat model of myocardial infarction (MI): effect of pertussis toxin.* British Journal of Pharmacology, 2002. **137**: p. 710-718.

58. Gunnersen, J.M., R.J. Crawford, and G.W. Tregear, *Expression of the relaxin gene in rat tissues.* Mol Cell Endocrinol, 1995. **110**(1-2): p. 55-64.

59. Esler, M., et al., *Adrenergic nervous system in heart failure.* Am J Cardiol, 1997. **80**(11A): p. 7L-14L.

60. Moore, X.L., et al., *Diverse Regulation of Cardiac Expression of Relaxin Receptor by alpha- and beta -Adrenoceptors.* Cardiovasc Drugs Ther, 2014.

61. Pinto, Y.M., et al., *Reduction in Left Ventricular Messenger RNA for Transforming Growth Factor 1 Attenuates Left Ventricular Fibrosis and Improves Survival Without Lowering Blood Pressure in the Hypertensive TGR(mRen2)27 Rat.* Hypertension, 2000. **36**(5): p. 747-754.

62. Parikh, A., et al., *Relaxin suppresses atrial fibrillation by reversing fibrosis and myocyte hypertrophy and increasing conduction velocity and sodium current in spontaneously hypertensive rat hearts.* Circ Res, 2013. **113**(3): p. 313-21.

63. Tsuruda, T., et al., *Brain natriuretic Peptide is produced in cardiac fibroblasts and induces matrix metalloproteinases.* Circ Res, 2002. **91**(12): p. 1127-34.

64. Trask, A.J., et al., *Inhibition of angiotensin-converting enzyme 2 exacerbates cardiac hypertrophy and fibrosis in Ren-2 hypertensive rats.* Am J Hypertens, 2010. **23**(6): p. 687-93.

65. Zolk, O., et al., *Activation of the cardiac endothelin system in left ventricular hypertrophy before onset of heart failure in TG(mREN2)27 rats.* Cardiovascular Research, 2001. **53**: p. 363-371.

66. Villarreal, F.J., et al., *Myocardial remodeling in hypertensive Ren-2 transgenic rats.* Hypertension, 1995. **25**(1): p. 98-104.

67. Kang, T., J.D. Humphrey, and F.C. Yin, *Comparison of biaxial mechanical properties of excised endocardium and epicardium.* Am J Physiol, 1996. **270**(6 Pt 2): p. H2169-76.

68. Du, X.J., et al., *Cardiovascular effects of relaxin: from basic science to clinical therapy.* Nat Rev Cardiol, 2010. **7**(1): p. 48-58.

69. Chen, S.A., et al., *The pharmacokinetics and absorption of recombinant human relaxin in nonpregnant rabbits and rhesus monkeys after intravenous and intravaginal administration.* Pharm Res, 1993. **10**(2): p. 223-7.

70. Conrad, C.H., et al., *Myocardial fibrosis and stiffness with hypertrophy and heart failure in the spontaneously hypertensive rat.* Circulation, 1995. **91**(1): p. 161-70.

71. Redfield, M.M., et al., *Effect of phosphodiesterase-5 inhibition on exercise capacity and clinical status in heart failure with preserved ejection fraction: a randomized clinical trial.* JAMA, 2013. **309**(12): p. 1268-77.

72. Iribe, G., M. Helmes, and P. Kohl, *Force-length relations in isolated intact cardiomyocytes subjected to dynamic changes in mechanical load.* Am J Physiol Heart Circ Physiol, 2007. **292**(3): p. H1487-97.

73. Hamdani, N. and W.J. Paulus, *Myocardial titin and collagen in cardiac diastolic dysfunction: partners in crime.* Circulation, 2013. **128**(1): p. 5-8.

74. Chung, C.S., et al., *Shortening of the elastic tandem immunoglobulin segment of titin leads to diastolic dysfunction.* Circulation, 2013. **128**(1): p. 19-28.

75. Samuel, C.S., E.D. Lekgabe, and I. Mookerjee, *The effects of relaxin on extracellular matrix remodeling in health and fibrotic disease.* Adv Exp Med Biol, 2007. **612**: p. 88-103.

76. Richmond, W., et al., *Interstrain differences of in vitro metabolic stability and impact on early drug discovery.* J Pharm Sci, 2010. **99**(11): p. 4463-8.